

**SPECTRUM-SLICED INCOHERENT LIGHT SOURCE
FOR
OPTICAL ACCESS NETWORKS**

HU QIKAI

NATIONAL UNIVERSITY OF SINGAPORE

2016

**SPECTRUM-SLICED INCOHERENT LIGHT SOURCE
FOR
OPTICAL ACCESS NETWORKS**

HU QIKAI

(B.Eng., Zhejiang University, China)


A THESIS SUBMITTED
FOR THE DEGREE OF DOCTOR OF PHILOSOPHY
DEPARTMENT OF ELECTRICAL & COMPUTER ENGINEERING
NATIONAL UNIVERSITY OF SINGAPORE

2016

Declaration

I hereby declare that this thesis is my original work, and it has been written by me in its entirety. I have duly acknowledged all the sources of information which have been used in the thesis.

This thesis has also not been submitted for any degree in any university previously.

A handwritten signature in black ink, appearing to read 'Hu Qikai', written over a horizontal line.

Hu Qikai

5 August 2016

Acknowledgments

The work described in this thesis was conducted with the kind help and support of many people to whom I would like to express my thanks.

Firstly, I would like to express my deep appreciation and sincere gratitude to my supervisors, Dr. Mohan Gurusamy, Prof. Kam Pooi-Yuen, Dr. Yu Changyuan and Dr. Kim Hoon, for their infinite patience, continuous guidance, high-quality advice, immense knowledge and generous support throughout my Ph.D. research. I could not imagine having better advisors and mentors for my Ph.D. study.

I also feel grateful for the support I have received from the National University of Singapore through NUS Research Scholarship and the President's Graduate Fellowship. Many thanks also go to my colleagues and staffs of the optical communication lab at the National University of Singapore for providing a friendly work environment.

On the personal level, I would like to acknowledge my parents and my sister, Hu Yuyang, Xu Mifen and Hu Qiwei for their support, encouragement, help, and sacrifice throughout my entire life. Special thanks also to my wife Ma Yijia for her unfailing support and encouragement throughout my Ph.D. research and my life in general. Last but not least, I would like to thank my friends for their support and love all the while, which gives me the strength to carry on.

Content

Summary	IX
List of Figures	XV
List of Tables	XX
List of Acronyms	XXII
Chapter 1	1
Introduction	1
1.1 Overview.....	1
1.2 Literature review.....	2
1.3 Objectives of the thesis.....	5
1.4 Contributions of this thesis.....	6
1.5 Thesis outline.....	8
Chapter 2	11
Fundamental Theory of SSIL Source	11
2.1 Overview.....	11
2.2 EIN of the SSIL source.....	14
2.3 Techniques for EIN reduction.....	17
2.3.1 Using feedforward noise reduction circuit for EIN suppression.....	17
2.3.2 Using four-wave mixing technique for EIN reduction.....	20

2.3.3	Using gain-saturated SOAs for EIN suppression.....	22
2.3.4	Summary	28
2.4	Ultra-narrow SSIL source	29
2.5	Conclusion	30
Chapter 3	31
Optimum Linewidth of SSIL Source Using a Gain-Saturated SOA	31
3.1	Introduction.....	31
3.2	Experiment and simulation setup.....	33
3.3	Optimum linewidth of SSIL source for capacity and transmission distance	39
3.3.1	Optimum linewidth of the SSIL for BER performance	39
3.3.2	Optimum linewidth of SSIL for transmission distance over SSMF	42
3.3.3	Optimum linewidth of SSIL for capacity.....	43
3.4	Drawbacks of the ultra-narrow SSIL source.....	44
3.4.1	Spectrum-slicing loss	45
3.4.2	SOA injection power for EIN suppression	46
3.4.3	Tolerance to in-band crosstalk	48
3.5	Conclusion	50
Chapter 4	54
Performance Improvement of Ultra-narrow SSIL Using Offset Filtering	54

4.1	Introduction.....	54
4.2	The correlation between amplitude and frequency of SSIL	55
4.3	Impact of offset optical filtering on the performance of ultra-narrow SSIL.....	59
4.4	Conclusion	66
Chapter 5		68
Upstream Transmission Using Ultra-narrow SSIL in WDM-PON Systems		68
5.1	Introduction.....	68
5.2	10 Gb/s/channel upstream transmission using ultra-narrow SSIL source	69
5.2.1	Introduction.....	69
5.2.2	Experimental setup.....	69
5.2.3	Results and discussion	72
5.2.4	Summary	74
5.3	5-Gb/S Upstream Transmission Using an RSOA Seeded by Ultra-narrow SSIL	74
5.3.1	Introduction.....	74
5.3.2	Experimental setup.....	76
5.3.3	Results and discussion	82
5.3.4	Summary	84
5.4	Conclusion	85

Chapter 6	88
Downstream Transmission Using Ultra-narrow SSIL in WDM-PON Systems	88
6.1 Introduction.....	88
6.2 50-km Transmission of 10-Gb/s SSIL signals using EDC	90
6.2.1 Introduction.....	90
6.2.2 Experimental setup.....	91
6.2.3 Results and discussion	92
6.2.4 Summary	97
6.3 25-Gb/s/per-channel WDM-PON Using SSIL sources	98
6.3.1 Introduction.....	98
6.3.2 Experimental setup.....	99
6.3.3 Results and discussion	101
6.3.4 FEC selection	106
6.3.5 Summary	109
6.4 Conclusion	109
Chapter 7	110
Conclusions and Future Works	110
7.1 Conclusions.....	110
7.2 Future works	113

7.2.1	FEC	113
7.2.2	Feedforward noise reduction with ultra-narrow SSIL source.....	114
Appendix A:		116
SNR of Optical Signal Using SSIL		116
Appendix B:		122
Electronic Equalization		122
Bibliography		126

Summary

Spectrum-sliced incoherent light (SSIL) sources have been considered as a promising candidate for wavelength-division-multiplexed (WDM) passive optical networks (PONs) owing to its advantages of low implementation cost, excellent wavelength stability, and considerable flexibility. In these light sources, a broadband thermal-like light (e.g., amplified spontaneous emission (ASE)) is spectrally sliced into numerous lights at different wavelengths. Then these wavelength-specific spectrum-sliced lights are used as continuous-wave light sources and fed into optical modulators in each channel of the WDM PON.

However, the widespread implementation of SSIL sources is restricted by its predominant excess intensity noise (EIN). This high-intensity noise is induced through the spontaneous-spontaneous beating between numerous SSIL components at different wavelengths. It is shown that the signal-to-noise ratio (SNR) of the unpolarized SSIL source is governed by B_o/B_e , where B_o is the optical linewidth of the SSIL source and B_e is the electrical bandwidth of the receiver.

To cope with the large EIN, various techniques have been investigated. These techniques include all-optical methods such as using a gain-saturated (GS) semiconductor optical amplifier (SOA) or intra-channel four-wave mixing (FWM) technique, and optic-electronic method such as feedforward noise cancellation technique. Nevertheless, in the previous studies, a large B_o is a common practice to accommodate high-speed signals (typically wider than 0.4 nm to accommodate 10-Gb/s signals). This is because that a larger

B_o could result in better SNR regardless of whether the EIN-suppression techniques are utilized or not. On the other side, a large B_o reduces the spectral efficiency of the WDM-PON systems and eventually, does not help to improve the system capacity. Additionally, a large B_o also makes the optical signal susceptible to frequency-related effect (e.g. fiber chromatic dispersion and optical filtering effect).

In this thesis, an ultra-narrow SSIL source is to dramatically improve the system capacity and boost the tolerance to fiber dispersion and optical filtering effect. In the transmitter, a wideband ASE emitted from an erbium-doped fiber amplifier (EDFA) is spectrally sliced through a fiber Fabry-Perot (FFP) filter. This FFP filter has 700-MHz bandwidth and 102 GHz free spectral range. Then the ultra-narrow SSIL sources are selected by an array waveguide grating for multiple channels at different wavelengths. In each channel, a GS-SOA was utilized to suppress the inherent EIN inside the SSIL. After the EIN-suppression, these EIN-smoothed SSIL sources could be utilized as continuous-wave light sources in the WDM transmitters.

In Chapter 3 of this thesis, the optimum linewidth of the SSIL source is investigated. Both experimental and simulation studies have been carried out on using the SSIL sources, which have the optical linewidth over a wide range. The simulation results demonstrate that there exist two windows of the linewidth for high-speed transmission using SSIL sources: ultra-narrow (i.e., the linewidth is much narrower than the receiver bandwidth) and ultra-wide (i.e., the linewidth is much wider than the receiver bandwidth). However, in the ultra-wide window, the 10-Gb/s signal suffers severely from the degradation induced by the fiber chromatic dispersion and optical filtering effect. These results are also confirmed by the experimental results, where an FFP filter having an ultra-narrow

bandwidth (bandwidth is 700 MHz) and a bandwidth-tunable optical filter (bandwidth ranges from 20 to 53 GHz) are utilized to change the SSIL linewidth over a wide range. Considering the system capacity and the longest transmission distance (without dispersion compensation), the optimal linewidth of the SSIL source is in the ultra-narrow window (less than 700 MHz). To provide comprehensive analysis, this section also investigates the drawbacks of the ultra-narrow SSIL source, compared to the SSIL with linewidth larger than 20 GHz. For instance, the spectrum-slicing loss is discussed, the tolerance to in-band crosstalk and the requirement of the SOA input power for sufficient EIN suppression in this chapter.

In Chapter 4 of this thesis, a novel technique is reported to reduce the EIN further and improve the bit-error-rate (BER) performance of the signals using ultra-narrow SSIL source. This method is realized by using the offset optical filtering. This chapter first shows that a gain-saturated SOA introduces a negative correlation between amplitude and frequency (or chirp) of the ultra-narrow SSIL signal. Through the offset optical filtering, the filter edge at longer wavelength side can convert the SOA-induced chirp into amplitude variation, produce the destructive interference with the existing EIN and eventually, reduce the EIN further. For 10-Gb/s signals, this simple offset filtering can reduce the EIN-induced BER floor by a factor of 2. As the BER is near the forward-error correction (FEC) threshold, this BER improvement could be considerably enhanced after FEC decoding.

Chapter 5 investigated the performance of upstream transmission using ultra-narrow SSIL in WDM-PON systems. In this chapter, I firstly demonstrated the upstream transmission of 10-Gb/s signal, which is generated by a 700-MHz SSIL source, in a loopback configured 20-km SSMF link. To show the feasibility of 320-Gb/s capacity using

this SSIL source, this chapter also studied 25-nm wavelength operation of the 10-Gb/s/channel upstream transmission. Second, to further improve the cost-effectiveness and simplify the system architecture, the possibility of using an RSOA is also explored at the transmitter, which exhibits color-free operation, direct modulation, optical amplification as well as EIN suppression capability. Finally, the 5-Gb/s/channel upstream transmission using an RSOA is experimentally demonstrated over a 20-km standard single-mode fiber (SSMF).

In Chapter 6, the highest data rate of downstream transmission is experimentally investigated using the ultra-narrow SSIL. This is the first time that SSIL could provide service greater than 10-Gb/s/channel. The ultra-narrow spectrally pre-slicing, electronic dispersion compensation technique, as well as the simple offset optical filtering, are exploited to achieve 25-Gb/s/channel transmission. To investigate the remarkable dispersion tolerance of ultra-narrow SSIL, this chapter also experimentally demonstrated the longest transmission distance for the 10-Gb/s/channel signals without additional optical techniques to compensate the chromatic dispersion. It has been shown that the transmission distance can be longer than 50 km using the 700-MHz SSIL source with the help of electronic equalization. This experimental result confirms that the SSIL having ultra-narrow linewidth makes the signal less susceptible to fiber dispersion than the wideband SSIL (linewidth larger than 20 GHz). The chromatic dispersion not only induces inter-symbol interference but also breaks down the correlation between the SSIL components at different wavelengths and eventually, restores the EIN. Due to the restored EIN, the simple electronics equalization can only extend the reach by 25% for 10 Gb/s/channel signals.

The findings of this thesis can help to implement high-speed (data rate higher than 10Gb/s/channel) WDM-PONs with high cost-effectiveness by exploiting the ultra-narrow SSIL sources. The ultra-narrow SSIL sources can provide color-free operation, low-cost implementation, strong tolerance against optical dispersion, and the capability of simultaneously generating multiple sources at different wavelengths. To reduce the EIN, the gain-saturated SOA/ROSA can be exploited with the offset optical filtering.

List of Figures

Figure 2.1 A schematic diagram of using spectrum-sliced incoherent light sources as multichannel WDM light sources. Reprinted with permission from reference [11].	13
Figure 2.2 A spectrum-sliced transmitter with feedforward noise reduction circuit [24]. The SSMF is the standard single-mode fiber.	18
Figure 2.3 Experimental setup of the spectrum-sliced transmitter with four-wave mixing noise reduction technique. Reprinted with permission from reference [48] ..	21
Figure 2.4 The principle of the noise suppression using the gain-saturated SOA [33].	22
Figure 2.5 SOA modulator with gain saturation [33].	24
Figure 3.1 The experimental setup to analyze the optimum linewidth of the SSIL at 10.7 Gb/s/channel. The PRBS length is $2^{31}-1$ in the experiment.	33
Figure 3.2 The optical spectra of the SSIL measured at the input of SOA when (a) the FFP and (b) the bandwidth-tunable optical filter are used as the spectrum-slicing filter. Also shown in the figures are the Lorentzian and 2 nd -order Gaussian function in dashed line.	34
Figure 3.3 SOA characteristics when the SOA is biased at 200 mA at 1542 nm.	35
Figure 3.4 Measured SOA carrier response when the bias current and the operation wavelength are 200 mA and 1542nm, respectively.	36
Figure 3.5 BER performance of the 10-Gb/s OOK signal as a function of the linewidth of the SSIL source when the SSIL has (a) 2 nd -order Gaussian and (b) Lorentzian	

spectral profiles. The solid and dotted lines indicate the BERs estimated by using the Gaussian and Chi ² , respectively.....	39
Figure 3.6 Maximum transmission length over dispersion-uncompensated SSMF versus linewidth of the SSIL source to achieve the FEC BER threshold of 1.2×10^{-3} . The solid and dotted lines indicate the transmission distance estimated by using the Gaussian and Chi ² approximations, respectively. The symbols are the experimental values.....	42
Figure 3.7 The minimum 3-dB bandwidth of OBPF2 to achieve the FEC threshold of 1.2×10^{-3} for the 10-Gb/s signal generated by using the Lorentzian-shaped SSIL.....	43
Figure 3.8 Spectrum-slicing loss as a function of the linewidth of the Lorentzian-shaped SSIL.....	43
Figure 3.9 SOA input power required to achieve the FEC threshold for the 10-Gbs signal versus the linewidth of the SSIL source when the SSIL has (a) 2 nd -order Gaussian and (b) Lorentzian spectral profiles. The solid and dotted lines indicate the SOA input power estimated by using the Gaussian and Chi ² approximations, respectively. The symbols are the experimental values.....	47
Figure 3.10 Experimental setup to measure the power penalty caused by in-band crosstalk.....	48
Figure 3.11 Power penalty of the 10-Gb/s SSIL signal induced by the in-band crosstalk.....	49
Figure 4.1 The experimental setup to measure the correlation between amplitude and frequency of the ultra-narrow SSIL source.	55

Figure 4.2 Measured correlation coefficient between the amplitude and frequency of the ultra-narrow SSIL as a function of SSMF length.	57
Figure 4.3 Captured amplitude and instantaneous frequency waveforms of the ultra-narrow SSIL after (a) 0-, (b) 10-, (c) 20-, and (d) 30-km transmission over SSMF...	58
Figure 4.4 Experimental setup to investigate the impact of offset optical filtering on the BER performance of the ultra-narrow SSIL. EAM: Electro-absorption modulator, (b) Transmittance of OBPF2 and the optical spectrum of the signal at SOA output with 0.12-nm optical offset.....	61
Figure 4.5 Optical spectra of the ultra-narrow SSIL.....	61
Figure 4.6 Measured EIN variance of the ultra-narrow SSIL as a function of SSMF length. For 0.12-nm offset filtering, a 0.12-nm detuning of the SSIL source is applied to OBPF2 longer wavelength edge.....	62
Figure 4.7 Measured RIN spectra of the ultra-narrow SSIL. Data modulation is not applied to this measurement.	64
Figure 4.8 Measured BER performance of 12.5-Gb/s ultra-narrow SSIL signals versus the offset filtering. The received signal power is set to be -15dBm.....	64
Figure 5.1 Experimental setup of (a) scheme 1 (upstream transmission), (b) scheme 2 (without in-band crosstalk), and (c) scheme 3 (without dispersion). The inset shows the optical spectra of the signal at the SOA input, SOA output, and EAM output.....	72
Figure 5.2 Measured BER as a function of the optical received power in three different configurations when the data rate is (a) 10.7 and (b) 12.5 Gb/s.....	72

Figure 5.3 (a) Measured eye diagrams of the signals in three schemes at different data rates. The receiver signal power is -15dBm. (b) BER performance versus the center wavelength of the SSIL source. 73

Figure 5.4 Experimental setup of 5-Gb/s RSOA-based upstream transmission..... 73

Figure 5.5 Measured E/O response of the RSOA used in the demonstration..... 78

Figure 5.6 Measured BERs (a) as a function of the de-emphasis ratio, and (b) as a function of filter offset. The RSOA injection power and the signal received power are kept to be -10.3 and -15dBm, respectively. 79

Figure 5.7 The eye diagrams measured at the receiver with (a) no de-emphasis and -0.18-nm offset filtering (b) no de-emphasis and no offset filtering, (c) no de-emphasis and 0.17-nm offset filtering, (d) 6-dB de-emphasis and -0.18-nm offset filtering, (e) 6-dB de-emphasis and no offset filtering, (f) 6-dB de-emphasis and 0.17-nm offset filtering. The RSOA injection power and received power are kept to be -10.3 and -15dBm, respectively. 80

Figure 5.8 (a) BER curves measured at the back-to-back and after 20-km transmission with 0.17-nm offset filtering. (b) Measured BER as a function of the RSOA injection power at the back-to-back and after 20-km transmission. The optical power at the receiver is set to be -15dBm. The de-emphasis of 6dB is employed for both measurements. 82

Figure 6.1 Experimental setup of 12.5-Gb/s SSIL-based transmission. Electronic equalizer is utilized to extend the transmission distance..... 91

Figure 6.2 Eye diagrams constructed from averaged waveforms of the signal at (a) 0 km, (b) 20 km, and (c) 50 km. 93

Figure 6.3 Q-factor of the isolated mark in ‘00001000’ pattern versus the transmission distance over SSMF.....	94
Figure 6.4 Measured BER curves after 0-, 20-, and 50-km transmission.....	95
Figure 6.5 BER performance versus transmission distance.....	96
Figure 6.6 (a) Experimental setup of 25-Gb/s/channel SSIL-seeded transmission (b) The optical spectrum of the 25-Gb/s OOK signal measured at the output of the modulator.....	100
Figure 6.7 RIN of the SSIL sources with two different linewidths measured at the output of the SOA.....	101
Figure 6.8 Measured BER performance of the 25-Gb/s OOK signal as a function of the optical filtering offset. Also plotted is the power loss incurred by offset filtering.	102
Figure 6.9 Measured sensitivity (BER is 10^{-3}) versus the transmission distance.	104
Figure 6.10 Measured BER as a function of received power. The inset is the eye diagram of the signal at the output of the EDC.	105
Figure 6.11 (a) Measured PMF of the number of consecutive errors in the back-to-back operation (BER is 10^{-4}) (b) The PMF of the number of consecutive errors of the signal with Gaussian noise.	106
Figure 6.12 Measured receiver sensitivity versus code rate (without FEC overhead) for various FEC codes.....	107
Figure B.1 Structure of symbol-spaced FFE [93].....	123
Figure B.2 Structure of half-symbol-spaced DFE [93].....	123

List of Tables

Table 3.1 SOA PARAMETERS USED IN THE SIMULATION	38
---	----

List of Acronyms

Acronyms	Description
ASE	Amplified spontaneous emission
AM	Amplitude modulation
AWG	Arrayed waveguide grating
BCH Code	Bose-Chaudhuri-Hocquenghem Code
BER	Bit-error-rate
CD	Chromatic dispersion
COs	Central offices
CW	Continuous wave
DC	Direct current
DCF	Dispersion-compensation fiber
DCM	Dispersion compensation module
DFE	Decision-feedback equalizer
DGD	Differential group delay
DI	Delay interferometer
EAM	Electro-absorption modulator

EDC	Electronic dispersion compensation
EDFA	Erbium-doped fiber amplifier
EIN	Excess intensity noise
ER	Extinction ratio
FEC	Forward-error correction
FFE	Feedforward equalizer
FFNR	Feedforward noise reduction
FFNS	Feedforward noise suppression
FFP	Fiber Fabry-Perot
FM	Frequency modulation
FP-LD	Fabry-Perot laser diode
FSR	Free-spectral range
FWM	Four-wave mixing
GS	Gain-saturated
HDTV	High-definition television
ITU-T	International telecommunication union- telecommunication standardization sector
LDPC	Low-density parity check

LED	Light-emitting diode
MMSE	Minimum mean-square error
NRZ	Non-return-to-zero
OBPF	Optical bandpass filter
ONU	Optical network unit
OOK	On-off keying
PD	Photo-detector
PDF	Probability density function
PMD	Polarization-mode dispersion
PMF	Probability mass function
PON	Passive optical network
PRBS	Pseudo-random binary sequence
RIN	Relative intensity noise
RMS	Root mean square
RN	Remote node
RSOA	Reflective semiconductor optical amplifier
RS Code	Reed-Solomon Code
SLD	Super-luminescent diode

SNR	Signal-to-noise ratio
SOA	Semiconductor optical amplifier
SSIL	Spectrum-sliced incoherent light
SSMF	Standard single-mode fiber
WDM	Wavelength-division multiplexing

List of Publications

Journal Papers:

1. **Qikai Hu**, Hoon Kim and Chul Han Kim, “Receiver impact on in-band crosstalk-induced penalties in differentially phase-modulated signals,” Journal of Optical Society of Korea, vol. 20 no. 2, pp. 223-227, Apr. 2016
2. **Qikai Hu**, Changyuan Yu, Pooi-yuan Kam and Hoon Kim, “Optimal linewidth of spectrum-sliced incoherent light with a gain-saturated semiconductor optical amplifier,” IEEE/OSA Journal of Lightwave Technology, vol. 33, no. 17, pp. 3744-3750, Sep. 2015
3. **Qikai Hu**, Changyuan Yu and Hoon Kim, “5-Gb/s upstream transmission using an RSOA seeded by ultra-narrow spectrum-sliced incoherent light,” Optical Fiber Technology, vol. 21, pp. 137-140, Jan. 2015
4. **Qikai Hu** and Hoon Kim, “Performance improvement of ultra-narrow spectrum sliced incoherent light using offset filtering,” IEEE Photonics Technology Letters, vol. 26, no. 9, pp. 870 -873, Mar. 2014

Conference Papers

5. **Qikai Hu**, Changyuan Yu, Pooi-yuan Kam and Hoon Kim, “25-Gb/s SSIL-seeded WDM PON,” OptoElectronics and Communications Conference (OECC), Japan, 2016, Oral Presentation

6. Jing Zhang, **Qikai Hu** and Changyuan Yu, “Elastic-bandwidth Access with Spectrum-Sliced Incoherent Light Source in WDM-PON,” OptoElectronics and Communications Conference (OECC), Japan, 2016, Post Presentation
7. **Qikai Hu** and Changyuan Yu, “Analysis of SOA optimization in spectrum-sliced WDM systems for EIN reduction and dispersion effect,” Signal Processing in Photonics Communications (SPPCom) 2015, SpS4D.5, Boston, USA, 2015, Oral Presentation
8. **Qikai Hu** and Hoon Kim, “Upstream transmission of 5.35-Gb/s spectrum-sliced incoherent light signal using RSOA,” International Conference on Optical Internet (COIN), pp. 1-2, Korea, 2014, Oral Presentation
9. **Qikai Hu** and Hoon Kim, 10-Gbps upstream transmission of ultra-narrow spectrum-sliced incoherent light signal,” OptoElectronics and Communications Conference (OECC) 2014, pp. 293-295, Melbourne, Australia, 2014, Oral Presentation
10. **Qikai Hu** and Hoon Kim, “50-km transmission of 10-Gb/s spectrum-sliced incoherent light signals using electronic dispersion compensation,” OptoElectronics and Communications Conference (OECC) 2014, pp. 431-433, Melbourne, Australia, 2014, Post Presentation

Chapter 1

Introduction

1.1 Overview

Within the last ten years, the Internet traffic grows rapidly with the high-bandwidth applications such as high-definition television (HDTV), social networking, IP videos and Internet telephony [1-3]. However, the access networks, which connect the service provider's central offices (COs) to the residential and businesses subscribers, have not scaled up commensurately and eventually become the principal limitation for broadband services [3-7]. Unlike long-haul networks where enormous cost can be affordable by the volume, optical access networks require low costs and economically viable network management. Wavelength-division multiplexing passive optical network (WDM-PON), exhibiting large capacity, excellent security, and considerable flexibility, has thereby been considered as a promising candidate for meeting the booming demand for the access networks [3-10].

However, the widespread deployment of WDM-PONs has been hindered mainly by the relatively expensive implementation and maintenance costs of wavelength-specific light sources [3]. To reduce the implementation cost, the spectrum-sliced WDM-PON have been proposed [11-12]. In the spectrum-sliced WDM-PON, a single broadband thermal-like light is spectrum-sliced into numerous incoherent lights, each having a distinct center

wavelength. Then these spectrum-sliced incoherent lights (SSILs) are divided into multiple channels by a demultiplexer, and employed as continuous-wave light sources for WDM-PON. Besides the low cost of the transmitter side, the colorless operation significantly reduces the replacement stock inventory requirements. Thus, the WDM-PON utilizing SSIL sources has been approved as an international standard for the optical access network at 1.25 Gb/s-per-channel data rate [13].

Nevertheless, the performance of the system using SSILs is significantly limited by its inherent excess intensity noise (EIN). This high-intensity EIN is generated from the spontaneous-spontaneous beating between the SSIL components at different wavelengths. According to the square-root law, the achievable signal-to-noise ratio (SNR) of an unpolarized SSIL is governed by B_o/B_e , where B_o is the linewidth of the unpolarized SSIL and B_e is the electrical bandwidth of the receiver [11, 14, 15]. As a result, the SSILs were mainly used for the demonstration of WDM-PONs operating at speed lower than 10 Gb/s/channel.

The remaining sections in this chapter address the motivations, objectives, and organization of this thesis

1.2 Literature review

The operation of SSILs at 10 Gb/s/channel and higher data rate is challenging [14-19] and faces several problems: the large inherent EIN [14-19], the limited bandwidth capacity and the low tolerance to chromatic dispersion [20] and optical filtering effect [21-23]. In

particular, the large EIN primarily limits the performance of the WDM-PONs utilizing SSIL sources [14-15].

To address this inherent EIN, various EIN-suppression schemes have been proposed. In the optoelectronic compensation system [24], a radio-frequency circuit is used to detect the forward propagating light and subtract out the intensity fluctuation from the light source. However, this associated circuitry requires precise gain and phase matching which intensively increases the system complexity and implementation cost.

One of the all-optical schemes [25] is using the intra-channel four-wave mixing (FWM) effect, which could significantly broaden the bandwidth of the received optical signal, and thus reduces the EIN. This FWM effect was produced through a high-power EDFA associated with 20-km dispersion-shifted fiber.

Another all-optical scheme [17, 26-34] is based on the nonlinear amplification of a semiconductor optical amplifier (SOA). The intensity fluctuation of the transmitted light signal could be suppressed through the nonlinear amplification of a gain-saturated SOA, especially at the frequency lower than the SOA bandwidth [28, 29]. Compared to other two schemes, this scheme is more cost-effective and compact in size. Furthermore, the SOA could be utilized simultaneously for both amplification and modulation, and thus provide further cost saving [33, 35].

Nevertheless, at the outset of my Ph.D. study (July 2012), a large B_o (typically wider than 0.4 nm) is a common practice to accommodate the high-speed signals in the WDM PONs, where the SSILs are utilized as light sources regardless whether the EIN-suppression techniques are employed or not [36, 37, 18, 19]. The use of large B_o not only limits the capacity of the WDM-PON systems but also makes the signal susceptible to fiber

chromatic dispersion and narrow optical filtering [20-23]. Due to the limited bandwidth of the SOAs (typically less than 3 GHz [17, 29]), the SOA-assisted system cannot sufficiently suppress the EIN at high frequency. Moreover, large optical linewidth of the SSIL also results in poor spectral efficiency and eventually limits the capacity of WDM-PON. Except for the preliminary experiments of spectrum-slicing WDM-PON, there still exist open questions such as the optimum linewidth of the SSIL for WDM-PON systems, more effective EIN suppression and so on.

This thesis first presents a comprehensive study on the optimum linewidth of the SSIL used for WDM-PON systems [32], considering the efficiency of EIN-suppression as well as the tolerance to optical filtering effect, chromatic dispersion, and in-band crosstalk. Regarding these factors, an SSIL source with an ultra-narrow linewidth (less than 600 MHz) shows tremendous advantages: strong dispersion tolerance, excellent bandwidth efficiency and high cost effectiveness. Based on the SSIL having ultra-narrow linewidth, a novel technique is also investigated to reduce the EIN of the ultra-narrow SSIL. The system experiments reveal that the nonlinear operation of the SOA could introduce a negative correlation between the intensity and phase of the SSIL light [38]. Using offset optical filtering could help to reduce the EIN at the expense of extra insertion loss (about 1 dB) of an optical filter. Thus, this scheme can improve the performance of the SSIL source cost-effectively without requiring additional components. Finally, this thesis presents the experimental demonstrations of high-speed WDM PON systems using the ultra-narrow SSIL and offset filtering technique in the following two chapters. In the upstream and downstream experimental demonstration, the highest data rate has been achieved for the optical signals using SSIL sources.

1.3 Objectives of the thesis

The SSIL sources has long been recognized as a promising solution for the light sources of WDM-PONs owing to their high cost-effectiveness and capability of generating multiple wavelength lights simultaneously. However, the widespread deployment of such systems has been hindered mainly by the high-intensity EIN. To solve this issue and improve the performance of this light source, the technical objectives have been listed as below.

First of all, the optimal linewidth of the SSIL is investigated in this thesis. Although the SNR of the signal using SSIL is proportional to the optical linewidth of the SSIL, large SSIL linewidth would make the signal susceptible to the chromatic dispersion and reduce the available system capacity. Therefore, it is required to evaluate the optimal spectral-slicing linewidth for the WDM-PONs. The optimum optical linewidth of the SSIL should be able to obtain the most efficient EIN suppression, highest bandwidth efficiency, strong tolerance to the in-band crosstalk, and reasonable power consumption.

Secondly, novel techniques are required to reduce the EIN of SSIL. Although a couple of techniques have been reported to reduce the EIN of SSIL, both of these techniques cannot suppress the EIN sufficiently for the transmission at the rate higher than 10 Gb/s/channel. Therefore, it is required to discuss the novel technical schemes to suppress the EIN further for higher speed transmission using SSIL.

Finally, it is preferred to experimentally analyze the performance and limitations of the WDM-PONs using SSIL sources both in downstream transmission and upstream

transmission. Through the experiments, this thesis could investigate the highest available capacity as well as the limitations in the WDM-PONs using SSIL sources.

1.4 Contributions of this thesis

First of all, this thesis successfully introduces the principles and restrictions of using the SSILs as the light sources in WDM-PONs. The key features and essential characteristics of SSILs are presented with specific emphasis on the relationship between the noise intensity level and the spectral profile of the SSIL. The main hurdle of the SSIL is its inherent large EIN. Thus, the EIN-suppression schemes are also reviewed including the principles, advantages as well as the limitations.

Then, the optimum linewidth of the SSIL for WDM-PONs are also investigated. To obtain the best SSIL linewidth for the maximum capacity and longest transmission distance, various characteristics have been evaluated. For example, this thesis has evaluated the EIN-suppression efficiency as well as the tolerance to chromatic dispersion, optical filtering effect, and in-band crosstalk. Both experiments and simulations have been studied on the transmission performance of a 10-Gb/s on-off keying (OOK) signal in the system using SSIL, which has linewidth over a wide range. These results show that there are two available windows of linewidth for high-speed transmission using SSIL source: very broad (i.e., the linewidth is much wider than the receiver electrical bandwidth) and ultra-narrow (i.e., the linewidth is much narrower than the receiver electrical bandwidth). However, the SSIL source with extreme wide linewidth would render the signal extremely susceptible to the chromatic dispersion and optical filtering effect. On the other side, the SSIL having ultra-narrow linewidth shows advantages on the system capacity and transmission distance.

Compared to the conventional wide-linewidth SSIL, ultra-narrow SSIL source also presents a couple of drawbacks, such as a large spectrum-slicing loss, a relatively high SOA input power requirement for sufficiently EIN suppression, and the susceptibility to in-band crosstalk.

To further alleviate the EIN of ultra-narrow SSIL signals, a novel technique has been proposed and experimentally demonstrated. According to the measured experimental data, a gain-saturated SOA creates a negative correlation between amplitude variation and frequency (or chirp) of the ultra-narrow SSIL signals. Based on this correlation, using offset optical filtering could convert the frequency variations into amplitude variations, which are the destructive interferences with existing EIN in the ultra-narrow SSIL signals. This offset optical filtering scheme provides benefits on the cost effectiveness as well as the implementation complexity while the error floor is reduced by a factor of 2. Since the error level is close to the forward-error correction (FEC) threshold, this performance benefits offered by offset optical filtering could be greatly enhanced after FEC decoding.

Last but not the least, this thesis have experimentally demonstrated the upstream transmission and downstream transmission using the ultra-narrow SSIL and investigated the limitations. In the upstream transmission, 10-Gb/s/channel signals have been transmitted over 25-nm wavelength range to show an available capacity of 320-Gb/s in C-band window. Then to further improve the system cost advantages and low-complexity benefits, reflective semiconductor optical amplifiers (RSOAs) is also utilized as a modulator as well as an EIN suppressor in the transmitter side to transmit 5.35-Gb/s/channel upstream signal. In the downstream transmission, the 10-Gb/s ultra-narrow SSIL signal has been experimentally transmitted over 50-km SSMF link with the assistance

of an electronic equalization. This is the first time that the electronic equalizer is utilized for the incoherent signal. Then a 25-Gb/s/channel spectrum-sliced WDM-PON is demonstrated with the help of offset optical filtering and electronic equalization. This is the first time, to the best of our knowledge, SSIL could provide service at the rate greater than 10-Gb/s/channel.

1.5 Thesis outline

This thesis consists of seven chapters which are organized in a logical structure as follows:

Chapter 1 presents an overview of this thesis including the research objectives and the contributions.

Chapter 2 reviews the relevant literatures on SSIL-based WDM-PON systems. First, Section 2.1 presents the key features and essential characteristics of SSILs, with particular emphasis on inherent EIN in SSIL. Second, Section 2.2 reviews the EIN-suppression schemes including the principles. The following parts discuss the limitations of the EIN-suppression schemes.

In Chapter 3, the optimal linewidth of the SSIL source using a gain-saturated SOA is investigated. This optimal linewidth of the SSIL is analyzed according to the available capacity and the transmission distance. Various characteristics have been evaluated, including EIN-suppression efficiency as well as the tolerance to chromatic dispersion, optical filtering effect, and in-band crosstalk.

In Chapter 4, a novel technique has been discussed, which can alleviate the EIN and improve BER performance of the system using ultra-narrow SSIL source. A gain-saturated SOA could create a negative correlation between amplitude modulation and frequency modulation of the ultra-narrow SSIL signals. Based on this unique characteristic, the offset optical filtering could convert the frequency variations into amplitude variations. Thus, this offset optical filtering could create the destructive interferences with existing EIN in the ultra-narrow SIL signals and reduce the existing EIN.

In Chapter 5, the upstream transmission with ultra-narrow SSIL in WDM-PON systems is experimentally investigated in this chapter. 10-Gb/s upstream signals are generated by using an ultra-narrow SSIL source, and transmitted over 20-km standard single-mode fiber (SSMF) in a loopback configuration. To further enhance the system cost advantages and low-complexity benefits, an RSOA is also utilized as a modulator and an EIN suppressor in the transmitter side for the 5-Gb/s upstream transmission.

In Chapter 6, the downstream transmission using ultra-narrow SSIL is demonstrated. To demonstrate the strong dispersion tolerance of the ultra-narrow SSIL, the 10-Gb/s ultra-narrow SSIL signal has been experimentally transmitted over 50-km SSMF link with the assistance of an electronic equalization. Then, a 25-Gb/s/channel spectrum-sliced WDM-PON is demonstrated with the benefits of the ultra-narrow linewidth of SSIL, offset optical filtering, and electrical equalization. This is the first time, to the best of our knowledge, the WDM-PON utilizing SSIL source could provide service at the rate greater than 10-Gb/s/channel.

The Chapter 7 summarizes the research findings of this thesis and suggests future works.

Chapter 2

Fundamental Theory of SSIL Source

In this chapter, an overview of the SSIL source is presented in details, including the basic principles of the SSILs, the inherent EIN limitation, the EIN-suppression techniques and the related restrictions of these techniques.

The following content is organized as below: Section 2.1 introduces the fundamental principles of the SSIL sources. Moreover, section 2.2 illustrates the main constraint to the SSIL source. In section 2.3, the EIN-suppression techniques have been studied, including using the intra-channel FWM, gain-saturated SOA as well as the feedforward noise reduction (FFNR) techniques. Section 2.4 mainly studies the influence of optical dispersion on the EIN-suppression using gain-saturated SOA, separately. Finally, some conclusions are drawn in section 2.5, and some possible future problems are identified

2.1 Overview

Recent achievements in optical amplifiers result in the attraction of wavelength-division-multiplexed (WDM) systems for both long-distance transmission and local-loop applications [3, 5, 6]. However, WDM systems require multiple numbers of transmitter light sources, which operate at individual wavelengths. The transmitter light sources should be controlled to operate at specific wavelengths during the system's lifetime. Therefore,

these wavelength-selected laser sources would significantly increase the system cost and complexity. For cost-sensitive WDM-PON applications, using wavelength-selected transmitter lasers for each channel is not practical. So the issue is how to implement the light sources in a cost-effective manner.

There have been a few attempts to overcome this problem by using broadband light sources. In the early stages, light-emitting diodes (LEDs) were utilized for the SSIL sources [39-41]. For example, the broadband light from 1.3- μm LEDs or super-luminescent diodes (SLD's) was spectrum-sliced by using grating-based demultiplexers and was employed in WDM systems. However, the transmission rates were limited to 2 Mb/s-150 Mb/s over distances less than 7 km because of the insufficient power inherent in LEDs [11].

However, optical fiber amplifiers (e.g. EDFAs) have been a promising solution, which could emit high-power amplified spontaneous emission (ASE) output [42] without any input. Hence, spectrum slicing through an erbium-doped fiber amplifier (EDFA) becomes more attractive. It can simultaneously generate multiple-channel light sources. Compared to the spectrum-sliced coherent light source, it requires neither a short pulse generator nor a high-power optical amplifier [42]. As SSILs have a large optical linewidth, they are robust against optical reflections as well as the fiber nonlinearity [43]. As a result, the SSILs have long been considered as a promising solution for transmitter sources of WDM-PONs. Despite these considerable advantages of SSILs, only recently have they been considered for WDM-PONs.

While many details of an SSIL source are complex, the basic concept of the SSIL source is quite simple. In such a scheme, a wideband ASE originates from an optical amplifier and is then sliced into multiple channels at different wavelengths by utilizing an arrayed

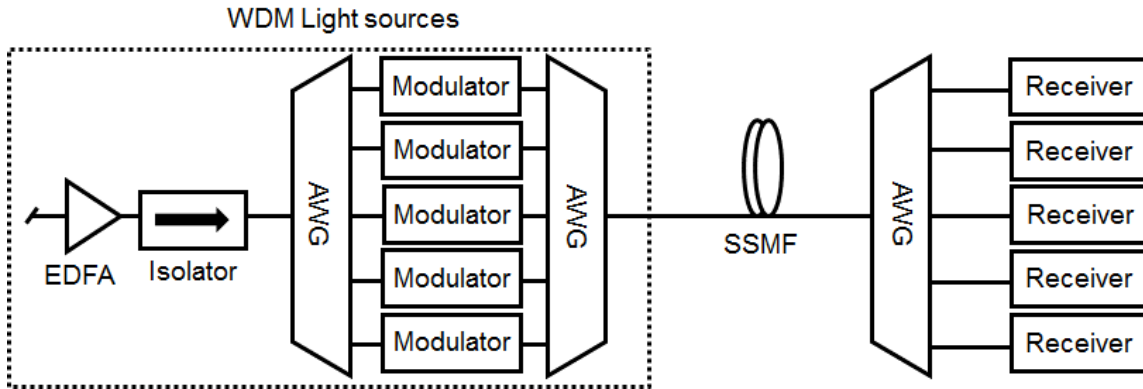


Figure 2.1 A schematic diagram of using spectrum-sliced incoherent light sources as multichannel WDM light sources. Reprinted with permission from reference [11].

waveguide grating (AWG). In each channel, the SSIL can be used as an optical source for data modulation. Compared to the wavelength-selected laser sources for each channel, these SSIL sources significantly enhance the cost effectiveness of the WDM PONs [11, 12].

Figure 2.1 shows the schematic diagram of the spectrum-sliced WDM light sources. The EDFA emits high-power (e.g. about 40mW [11]) ASE light as a broadband light source. The following isolator is employed to prevent lasing. Then an AWG operates as a $1 \times N$ WDM demultiplexer to split the broadband ASE into numerous SSIL sources and inject these light sources into multiple WDM channels at individual wavelengths. In each channel, the SSIL is modulated individually and eventually, multiplexed back into the SSMF via the second AWG, which is operated as an $N \times 1$ WDM multiplexer. After passing through the AWG at the optical network unit (ONU), the SSIL signals are split into different channels and detected by the photodetector in each channel.

2.2 EIN of the SSIL source

In spite of the advantages of the SSIL source, the system performance is severely limited by its significant EIN, which arises from the spontaneous-spontaneous beating between the SSIL components at different wavelengths during the direct detection processing.

According to [44, 45], the beating signals consist of two types of terms: an average term and a variance term. The average term comes from the sum of the beating between the components at the same wavelength while the variance part arises from the beating between the light components at different wavelengths. When the SSIL source is employed as a WDM light source, the average term is always considered as a carrier (non-time varying) and the time-varying variance part is the inherent EIN of SSIL. These two terms can be expressed as the following equations [44]:

$$I_{ASE}^2 = (e\eta mn_{sp}(G - 1)B_o)^2 \quad (1)$$

$$I_{sp-sp}^2 = \frac{2I_{ASE}^2 B_e}{mB_o} \quad (2)$$

Here, the term I_{ASE}^2 is the average signal and I_{sp-sp}^2 is the noise variance, η is the quantum detection efficiency, m is the number of polarization modes, G is the amplifier gain, n_{sp} is the spontaneous emission factor, B_o is the optical linewidth of the SSIL source, and B_e is the electrical bandwidth, e is the electron charge. Thus, the SNR of ASE light at the receiver can be calculated by the equation below [11]:

$$SNR = \frac{I_{ASE}^2}{I_{sp-sp}^2 + I_{shot}^2 + I_{th}^2} \quad (3)$$

The I_{shot}^2 and I_{th}^2 are the noise power produced by the ASE shot noise and the receiver electronics, respectively. In WDM systems utilizing SSIL sources, the spontaneous-spontaneous beating noise becomes pre-dominant over electrical shot noise and thermal noise and eventually, limits the total transmission capacity [11]. Neglecting the shot noise and thermal noise, the equation becomes

$$SNR \approx \frac{mB_o}{2B_e} \quad (4)$$

Where m is the amount of polarization statements, B_o is the optical linewidth of an SSIL and B_e is the bandwidth of the electrical receiver. The detailed derivation of (4) is illustrated in Appendix A.

Since the electrical noise is neglected, the Q -parameter at the receiver can be expressed as below [11]

$$Q \approx \sqrt{\frac{I_{ASE}^2}{I_{sp-sp}^2}} = \sqrt{SNR} \quad (5)$$

Here, the term I_{ASE}^2 is the signal power of the average term and I_{sp-sp}^2 is the noise power of the variance term. For Gaussian noise approximation, Q should be greater than 7.65 to achieve the bit-error-rate (BER) lower than 10^{-14} . Thus, the corresponding SNR is about 60.

As previously discussed, the limitation of the inherent EIN could be overcome at the expense of the system capacity, i.e., by reducing the bit rate of each channel or by increasing the optical linewidth of the SSIL source (i.e. reducing the amount of available

channels). As illustrated in [11], the B_e is assumed to be 0.7 times the transmission rate.

Then the system capacity T is given by the following equation:

$$T = NB \approx \frac{B_{BLS}}{42M} \quad (6)$$

Here, the term B is the data rate in each channel, the term N is the number of available channels in WDM system, and equals to $\frac{B_{BLS}}{MB_o}$; B_{BLS} is the linewidth of the ASE emitted from the EDFA, whose value is around 40 nm, and M is the multiplication factor given by the WDM channel spacing divided by B_o . According to (4), (5), and (6), the system capacity is not dependent on the transmission rate of each channel (i.e. B_e). The ultimate value of T could be about 120 Gb/s if the channel spacing is allowed to be as narrow as B_o (i.e. M is 1). However, the realistic estimation of T would be about 40 Gb/s because the channel spacing should be at least three times the B_o (i.e. M is not less than 3) to avoid inter-channel crosstalk.

Increasing the optical linewidth of the SSIL improves the signal quality at the expense of the reduction of the amount of available channels in WDM system and hence, cannot help to improve the system capacity. Moreover, the wideband SSIL would make the signal susceptible to the frequency-related effects such as chromatic dispersion and optical filtering effect.

Since the SNR expression is derived from the case using continuous wave (CW), the optically-modulated scheme cannot be expected correctly [46]. Both of the electrical receiver filter and the optical pulse shape have serious impact on the signal SNR [46]. For the single-pole filter, the SNR increases monotonically for the most of the electrical signal. Thus, when the EIN is pre-dominant, the optimum decision threshold should be well behind

the signal peak. Therefore, to obtain the best SNR, it is better to make the mark duration long enough. Thus, in this SSIL communications, small rise and fall times are required, and the non-return-to-zero modulation format is recommended

2.3 Techniques for EIN reduction

Multiple techniques have been proposed to cope with the high-intensity EIN and improve the capacity of WDM PONs. For instance, the optic-electronic method uses the FFNR scheme [24] and all-optical methods utilize a gain-saturated SOA [17, 26, 31-34] or the intra-channel FWM technique [25].

In the FFNR technique, the noise is reduced by detecting and subtracting out the fluctuations of the SSIL signals. In the scheme of using gain-saturated SOA, the nonlinear amplification of the gain-saturated SOA could help to amplify the SSIL intensity signal nonlinearly, and smooth the intensity waveform. On the other side, the intra-channel FWM method can reduce EIN by significantly broadening the bandwidth of the received optical signal and hence, improve the SNR of the received signal.

2.3.1 Using feedforward noise reduction circuit for EIN suppression

Feedforward noise reduction circuit has been proposed as an optic-electronic method to reduce the EIN within the SSIL. The noise is reduced by detecting and subtracting out the fluctuations of the SSIL signals.

2.3.1.1 Principle of the feedforward noise reduction

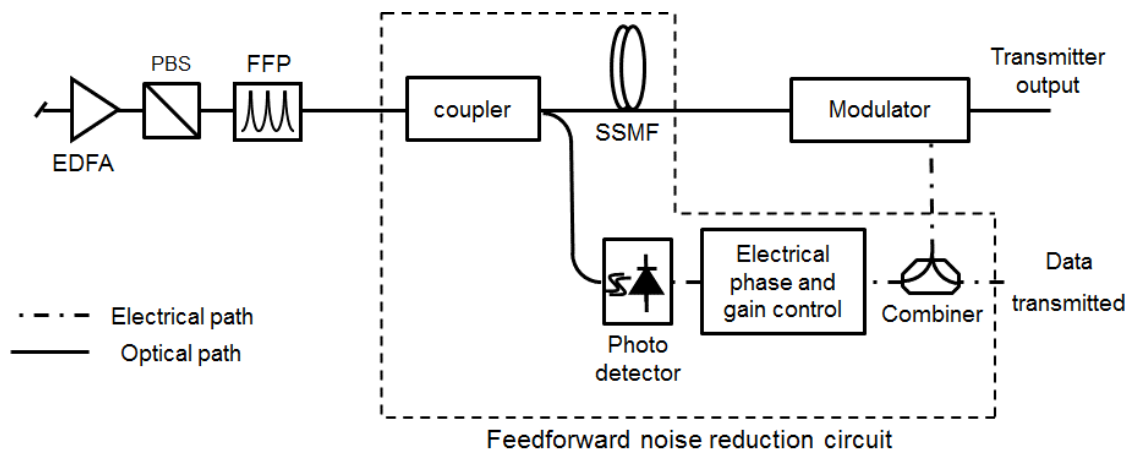


Figure 2.2 A spectrum-sliced transmitter with feedforward noise reduction circuit [24]. The SSMF is the standard single-mode fiber. Reprinted with permission from reference [24].

Figure 2.2 shows the schematic diagram of a spectrum-sliced transmitter incorporating FFNR. The FFNR circuit is depicted in the dashed region, which consists of a 90:10 fiber coupler, a tunable optical attenuator, a photodetector, an electrical gain controller and a phase matching module. Firstly, a fiber coupler is used to tap off a fraction of the optical incoherent light signal before modulation. Then EIN is detected by measuring the excursions in the optical power above (overshoots) and below (drop-outs) the average power within the FFNR circuit results. On the other hand, the remaining light is considered as the primary signal, which propagates through the intensity modulator. Based on the EIN detection, the FFNR circuit could revise the modulated data, which can be imposed on the primary signal through the intensity modulator. This FFNR circuit could help to suppress the primary signal at signal overshoots and enhance the primary signal at signal drop-outs

and eventually, flatten the primary waveform. Since the average power is unaffected [24] and the signal variance has been flattened, the SNR of the primary signal at modulator output can be improved.

It is assumed that FFNR could ideally detect the SSIL fluctuation and subtract the fluctuation. However, only subtraction of fields cannot be performed optically (through interference) whereas subtraction of intensity is required for FFNR. To approximate the intensity subtraction, an electro-optic modulator could be utilized, which multiplies the modulated RF signal of the optical power. In [24], a LiNbO₃ Mach-Zehnder intensity modulator is employed, which has the sinusoidal power-to-voltage characteristic. The sinusoidal PN characteristic could be linear for small applied RF signals while the modulator is biased at its 3-dB point. To analyze the process of noise cancellation quantitatively, the SSIL is considered as a signal with Gaussian noise $n(t)$. After signal modulation and FFNR, the optical signal is expressed as [24]:

$$P_{out}(t) = P[1 + n(t)] \frac{1 - \sin[\Delta(t)]}{2} \approx P[1 + n(t)] \frac{1 - \Delta(t)}{2} \quad (7)$$

Here $\Delta(t)$ is the linear noise correction signal induced by FFNR circuit. The EIN is minimized when $\Delta(t)$ equals $n(t)$; However, there still exist noise remained, which is second-order noise terms as described below

$$P_{out}(t) = P[1 - n^2(t)]/2 \quad (8).$$

The SNR of the photocurrent with FFNR (i.e. SNR_{out}) can be derived from (7) :

$$SNR_{out}(t) = SNR_{in}(t)^2/2 \quad (9)$$

The SNR_{in} denotes the SNR of the signal detected at the modulator input, and the approximation holds when the SNR is much larger than the 1 (linear). Without any EIN-

suppression techniques, the SNR is proportional to the ratio of the optical to the electrical bandwidth [11]. Thus, (2) indicates that FFNR could help to enhance the system capacity by reducing the bandwidth of the spectrum-slicing and maintain the SNR. It is worth to note that the actual improvement induced by FFNR depends on the noise statistics of the input light [47].

2.3.1.2 Drawbacks of the Feedforward noise reduction

However, the performance of the FFNR depends on the critical control of the delay time and gain in the FFNR circuit. Deviation from the optimum value of the delay time and gain would obviously degrade EIN suppression [47].

Moreover, the FFNR circuits are bit-rate-dependent, which dramatically increases the system cost for the high-speed transmission. Both of these practical limitations intensely rise the system complexity as well as the implementation cost [47].

Last but not least, if the FFNR circuit is utilized to reduce the existing noise after the gain-saturated SOA, the efficiency of FFNR technique would be degraded by the ASE background noise generated by the SOA as well as the filtering effect [47]

2.3.2 Using four-wave mixing technique for EIN reduction

2.3.2.1 Principles of using FWM for EIN reduction

As demonstrated in Figure 2.3[48], the modulated optical signal was amplified by a booster amplifier and transmit over a dispersion-shifted fiber (DSF). At the receiver side,

a high-power EDFA associated with 20-km dispersion-shifted fiber could produce the FWM effect, which significantly broadens the bandwidth of the received optical signal.

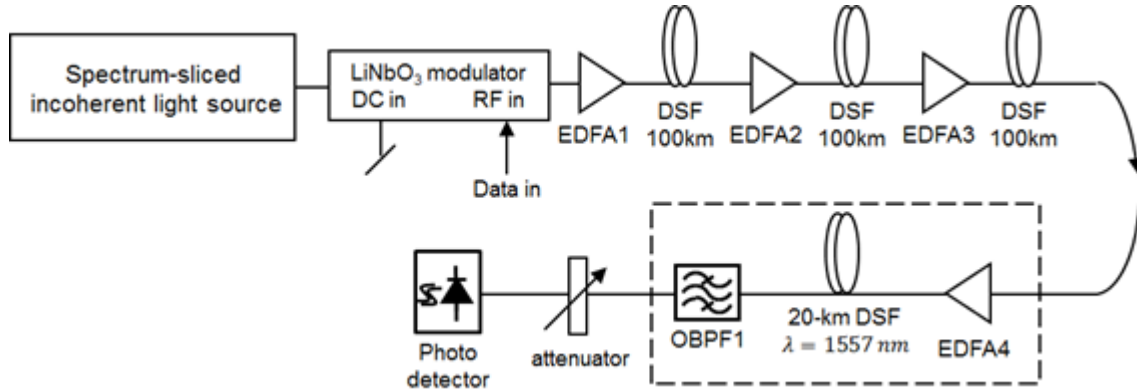


Figure 2.3 Experimental setup of the spectrum-sliced transmitter with four-wave mixing noise reduction technique. Reprinted with permission from reference [48].

Since the SNR of SSIL signal is proportional to the bandwidth of the received optical signal, the SNR of SSIL signal can be improved after the intra-channel FWM. Then a 2.7-nm optical filter (i.e. OBPF1) is utilized to filter out the noise components.

2.3.2.2 Drawbacks of the FWM for EIN suppression

Although the FWM technique relaxes the requirement of the optical bandwidth of the SSIL at the transmitter side, the bandwidth of the optical signal at the receiver is extremely extended. Thus, this technique also makes the signal susceptible to the inter-channel crosstalk and eventually, reduces the channel amount in the WDM systems.

Moreover, the FWM requires dispersion-shifted fiber as well as the extra optical amplifiers on the receiver side (i.e. each ONU requires the extra optical amplifiers), which dramatically increase the cost of system implementation and maintenance.

2.3.3 Using gain-saturated SOAs for EIN suppression

The gain-saturated SOA could help to amplify the SSIL intensity signal nonlinearly, and smooth the intensity waveform. Compared to other noise suppression techniques [17, 26-34], SOA-based EIN suppression is more attractive due to its higher efficiency, ease of implementation and the potential of optical integration. The gain-saturated SOA has also been used as a 2R regenerator (i.e. the regenerator does re-amplification and pulse

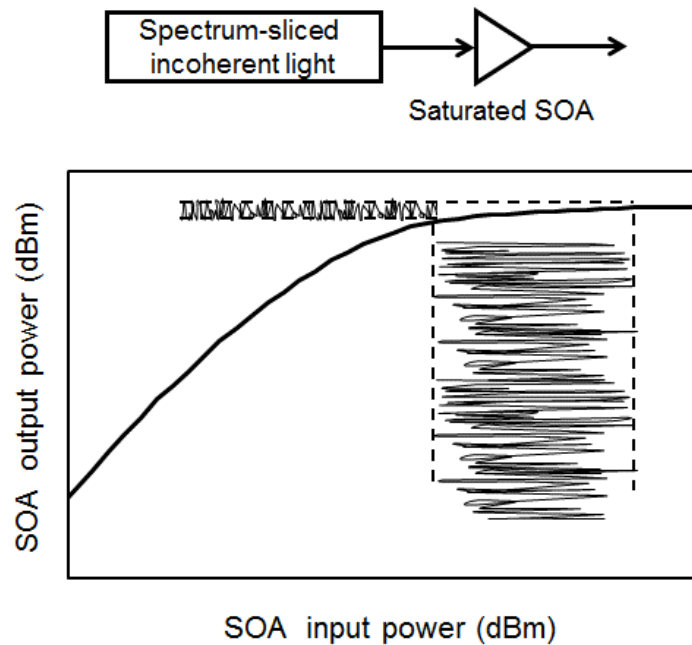


Figure 2.4 The principle of the noise suppression using the gain-saturated SOA. Reprinted with permission from reference [33].

reshaping) for long-haul transmission systems [49, 50] as well as reducing the mode-partition noise of the semiconductor lasers [51].

2.3.3.1 Principles of using gain-saturated SOA for EIN suppression

Figure 2.4 depicts the principle of noise suppression through a gain-saturated SOA. A high-power broadband light (i.e. ASE) is emitted from an EDFA and then, coupled into a wavelength demultiplexer (e.g. AWG) for spectrum-slicing. In each channel, a gain-saturated SOA is utilized to suppress the high-intensity EIN of the SSIL source. The nonlinear amplification characteristic of gain-saturated SOAs can be helpful to suppress the EIN of spectrum-sliced light as shown in Figure 2.4: the weak signal could be boosted while the strong signal is suppressed by the nonlinear amplification. The traveling equations can be used to calculate the noise suppression of the SSIL, which is benefited from nonlinear amplification of the gain-saturated SOA. The spontaneous emission generated from this SOA is neglected in this calculation. [33] derived the relative noise power suppression P_f as below.

$$P_f = \frac{(P_{in} + 1)^2 + (2\pi f \tau_s)^2}{(P_{out} + 1)^2 + (2\pi f \tau_s)^2} \quad (10)$$

Here, f is the frequency, τ_s is the effective carrier lifetime of the SOA, P_{in} and P_{out} denote the input and the output optical power normalized by the saturation output power of the SOA, respectively. Thus, P_f (i.e. the relative noise power suppressed by the nonlinear amplification) could be larger at deeper saturation level (i.e. the larger difference between the saturation input power and saturation output power), especially at low frequency.

Therefore, to enhance the saturation effect, it is possible to use the cascaded SOAs. Moreover, due to the limited carrier lifetime of the SOA (i.e. τ_s), the noise power suppression would be mitigated as the frequency increases

This technique is more compact than the FWM method and has lower cost and

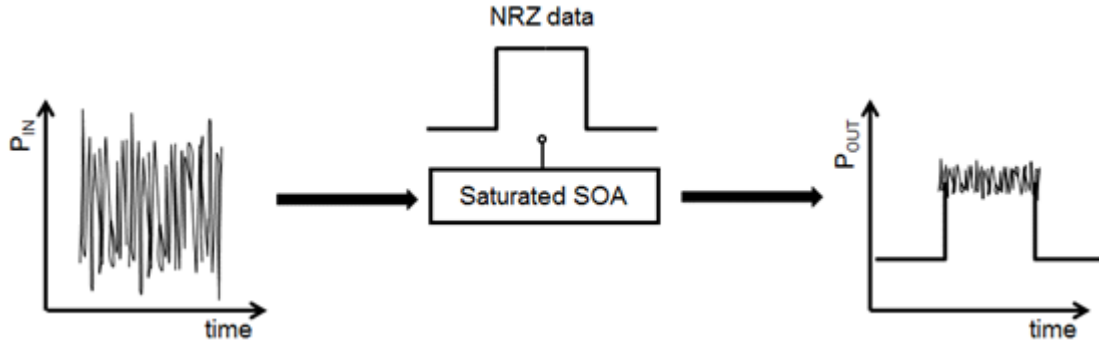


Figure 2.5 SOA modulator with gain saturation. Reprinted with permission from reference [33].

complexity compared to the FFNR technique. Furthermore, SOA can be used simultaneously for both signal modulation as well as the EIN suppression [33] as showed in Figure 2.5.

2.3.3.2 Drawbacks of the use of a GS SOA for EIN suppression

The noise suppression of a gain-saturated SOA is dependent on the noise frequency f and the effective carrier lifetime of the SOA [28, 29, 33]. Due to the limited carrier lifetime of the SOA, the noise reduction is typically effective at frequency less than 3 GHz [17, 29]. Thus, it is challenging to provide the transmission service at rate higher than 10-Gb/s/channel through the SSILs and gain-saturated SOAs [17, 26-34].

In the frequency domain, this EIN suppression is realized by achieving an elaborate balancing between SSIL components at different wavelengths or polarization statements and eventually, introducing a strong correlation between them [17]. Thus, this EIN suppression is vulnerable to wavelength- or polarization-dependent optical phenomena such as optical filtering effect [21-23], chromatic dispersion [20] and polarization-mode dispersion (PMD) [20]. In the following section, the optical filtering effect and optical dispersion effect are discussed in details.

2.3.3.2.1 Optical filtering effect on the EIN-suppression of the GS-SOA

As previously discussed, the GS-SOA induced EIN-suppression is sensitive to the optical filtering effect, hence, the spectral filtering of the SOA output would moderate the EIN-suppression benefit offered by the SOA and degrade the signal quality. As shown in [43, 21, 22], the EIN suppressed by the GS SOA is restored after the optical filtering, even when the optical filter has the 0.8-nm bandwidth. As a result, the BER performance is obviously degraded.

On the other side, the narrow spectrum filtering is required on the receiver side to diminish the inter-channel crosstalk within the WDM system. Thus, there exists a trade-off between the intra-channel crosstalk and the restored EIN. As studied in [21], regarding the signal quality, the optimum optical bandwidth is larger than the channel spacing. Thus, the EIN is still the major limitation of the system having the optical bandwidth less than the WDM channel spacing.

2.3.3.2.2 Chromatic dispersion effect on the EIN-suppression of the GS-SOA

The [20] shows that the suppressed EIN would be increased with the increasing chromatic dispersion (CD). This is in contrast to the case without the GS-SOA, where the EIN can be reduced by increasing the CD owing to the broadened optical bandwidth. This is because that the gain-saturated SOA creates a strong correlation between the SSIL components at different wavelength and obtains an elaborate balancing between different wavelength components of the SSIL. Thanks to these correlations, the intensity waveform of the SOA output would be relatively constant, while the intensity of SSIL components at each wavelength still fluctuates over time [20, 52].

However, the chromatic dispersion, which arises from the different group velocity of light components at different wavelengths, results a temporal walk-off between the light components at different wavelengths. In the system using GS-SOA, this temporal walk-off effect would break the correlation induced by the SOA and eventually, degrades the EIN suppression. After propagating through a dispersive medium, the temporal walk-off between different wavelength components causes the EIN recovered. Hence, for the same amount of walk-off, the components at higher frequency suffer a larger phase difference, which makes the EIN-restoration more efficient. For this reason, SSIL having wider linewidth suffers a larger amount of walk-off and hence, is more sensitive to the chromatic dispersion of components. Moreover, the suppressed EIN would be fully restored while the chromatic dispersion is large enough and totally breaks the correlation between the wavelength components within the SSIL signal.

2.3.3.2.3 Polarization-mode dispersion effect on the EIN-suppression of the GS-SOA

On the other side, PMD breaks the correlation of different polarization components rather than wavelength components of SSIL signal [20]. While the EIN is well suppressed through the gain-saturated SOA, not only the wavelength components of the SSIL signals have a strong correlation between one another, but also the orthogonal polarization components become correlated [20]. The reason is that at the SOA output, the orthogonally-polarized components, which are 180 degrees out of phase with each other, have similar intensity waveforms. Although the intensity of each polarization component fluctuates over time, the combined signal is relatively constant. After passing through a PMD element, the orthogonally-polarized components have different time delays. Thus, the out-of-phase correlation between the orthogonally-polarized components is broken by this temporal walk-off between the polarization components and hence, the EIN has been resorted.

According to [20], 0.2-dB power penalty is observed at 0.25-ns DGD in the presence of a gain-saturated SOA over a wide range of SSIL linewidth. On the other side, while the gain-saturated SOA is not used, the sensitivity penalty caused by a $DGD \leq 0.25\text{ns}$ is negligible.

Therefore, the noise-suppression benefits can be degraded by these wavelength-or polarization-related optical effects, which break the correlation between the SSIL components at different wavelength or polarizations.

2.3.4 Summary

In conclusion, both of these techniques could help to reduce the EIN with different limitations.

In the FFNR circuit, it utilizes the additional optic-electronic circuit to extract the EIN. With the benefits of FEC code and gain-saturated SOA, this technique could help to achieve 10-Gb/s/channel transmission [47]. However, the performance of this technique strictly depends on the critical control of the delay time and gain in the FFNR circuit. Moreover, this circuit is bit-rate dependent, and would intensively increase the system cost for the high-speed transmission.

In the FWM technique, it is implemented through the long DSF and additional optical amplifier at the receiver. It successfully reduces the requirement of optical linewidth of the SSIL source at the transmitter side to achieve the same signal quality. However, the long DSF and the extra optical amplifier not only greatly increase the system cost but also make it hard to be optically integrated. Moreover, the feasibility of using the FWM technique for the high-speed transmission (e.g. transmission rate is larger than 10 Gb/s/channel) is still an open question.

The gain-saturated SOA smooths the intensity fluctuation in SSIL by its nonlinear amplification (i.e. weak signal obtain high amplification while intense signal gets low amplification). Compared to previous two techniques, this method exhibits higher EIN-suppression efficiency, ease of implementation and the potential of optical integration. However, the gain-saturated SOA suppresses the EIN by creating a strong correlation between the different wavelength components of the SSIL and makes the signal sensitive

to optical filtering, chromatic dispersion, PMD and other frequency-related phenomena [20-22]. Moreover, to obtain better signal quality, SSIL having linewidth larger than 0.4 nm [36, 37, 18, 19] is always utilized with the GS-SOA. Due to the FWM and self-phase modulation effects within the GS-SOA, the optical signal spectrum would be further broadened. Therefore, the benefit of EIN suppression is severely susceptible to the frequency-dependent phenomena (e.g. optical filtering, CD, and PMD)

2.4 Ultra-narrow SSIL source

To accommodate the higher requirement of data rate (i.e., B_e), proportionally increasing B_o is a conventional method to maintain the SNR of the optical signal. However, the WDM PON using this approach suffers from vital problems especially at data rate larger than 12.5 Gb/s. For instance, the large B_o makes the optical signals susceptible to the fiber dispersion effect [20]. The possible transmission distance is inversely proportional to the square of data rate without dispersion compensation assuming the channel spacing is much larger than the B_o [95].

Moreover, larger optical linewidth results the signal vulnerable to the optical filtering effect. Since the gain-saturated SOA suppresses the EIN by creating a strong correlation between different wavelength components of the SSIL light, tight optical filtering disturbs this correlation and reduces the EIN suppression benefits.

Last but not least, large B_o decreases the system capacity. Although wide B_o could accommodate high-speed transmission at each channel, large channel spacing is required

to adapt the B_o and alleviate the inter-channel crosstalk in WDM system. As a result, the amount of feasible channels is reduced and thus, the system capacity cannot be improved.

As [43] demonstrated, the ultra-narrow SSIL source could achieve the transmission of 10-Gb/s NRZ signals over 20-km SSMF and 0.2-nm-bandwidth optical filter. Owing to the ultra-narrow linewidth of the SSIL source, this system is robust to fiber dispersion effect and optical filtering effect. In [43], the ultra-narrow SSIL source has been experimentally demonstrated to transmit 10-Gb/s signals over a 20-km SSMF without any dispersion compensation.

2.5 Conclusion

This review presents an introduction to the SSIL source. A typical spectrum-slicing system is illustrated, and the characteristics of the spectrum-slicing system are described. It shows that the main limitation of the spectrum-slicing system is the significant EIN. To solve this issue, the details of three of the EIN reduction techniques have been illustrated. Additionally, the effect of chromatic dispersion and PMD have been explained. Finally, the ultra-narrow spectrum-sliced incoherent source is also introduced, which can overcome the defects of the SSIL having large optical linewidth, and be adapted to higher data rate (e.g. 2.5 Gb/s and beyond). In conclusion, the SSIL is a very promising technology for WDM-PONs, but the different constraints introduced open up many new interesting avenues for research.

Chapter 3

Optimum Linewidth of SSIL Source Using a Gain-Saturated SOA

3.1 Introduction

SSIL sources have been considered as one of the most cost-effective multiple-wavelength light sources for WDM-PONs [11-19]. In these light sources, wideband thermal light (e.g., ASE from an EDFA) is spectrum-sliced into numerous incoherent lights, each having a specific center wavelength. Then these spectrum-sliced lights are fed to optical modulators to be used as continuous-wave light sources for WDM transmitters.

As Chapter 2 illustrated, the capacity of the system utilizing SSILS is mainly limited by the inherent EIN. Various techniques have been proposed to mitigate the EIN, including feedforward noise cancellation [24, 52] and the use of a gain-saturated SOA [30, 54]. Nevertheless, when the SSIL is used as a light source for a WDM-PON system, it is common practice to choose a large B_o (typically wider than 0.4 nm) to accommodate high-speed signals [55-57], [36, 37]. Nevertheless, the use of large B_o does not help to increase the capacity of the WDM-PON system based on SSIL sources [43]. Furthermore, it also makes the signal generated by using this light source susceptible to fiber chromatic dispersion and narrow optical filtering [20, 21].

Recently, the ultra-narrow SSIL source has proposed and demonstrated to increase the system capacity as well as the tolerance of the signal to fiber dispersion and narrow optical filtering [43]. Nevertheless, there still remains an open question about the optimum linewidth of the SSIL source for the capacity and dispersion-uncompensated reach of high-speed (i.e., faster than 10 Gb/s/channel) WDM-PON systems. Hence, this chapter investigates the transmission performances of a 10-Gb/s OOK signal generated by using an SSIL source using a GS-SOA (as an EIN suppressor) over a wide range of SSIL's linewidth. Through the computer simulation, this chapter evaluates the maximum dispersion-uncompensated transmission distance, the minimum passband of optical filtering, SOA input power required for EIN suppression, and the tolerance to in-band crosstalk, while varying the linewidth of the SSIL source. The simulation results are confirmed by experiment data. As shown in the simulation analysis and experimental results, good BER performance of the 10-Gb/s OOK signal could be achieved when the SSIL source linewidth is either ultra-narrow (i.e., the linewidth is much narrower than the receiver bandwidth) or very broad (i.e., the linewidth is much wider than the receiver bandwidth). However, the 10-Gb/s signal generated by using wide-linewidth SSIL suffers severely from fiber dispersion and optical filtering. On the other hand, by using the ultra-narrow SSIL source, it is available to minimize the channel spacing in WDM systems and make the signal tolerant to fiber dispersion even though the ultra-narrow spectrum slicing increases the slicing loss, the SOA input power required for EIN suppression, and the susceptibility to in-band crosstalk.

The following parts of this chapter are organized as below. Section 3.2 presents the experimental and simulation setup to investigate the effects of the linewidth of SSIL source

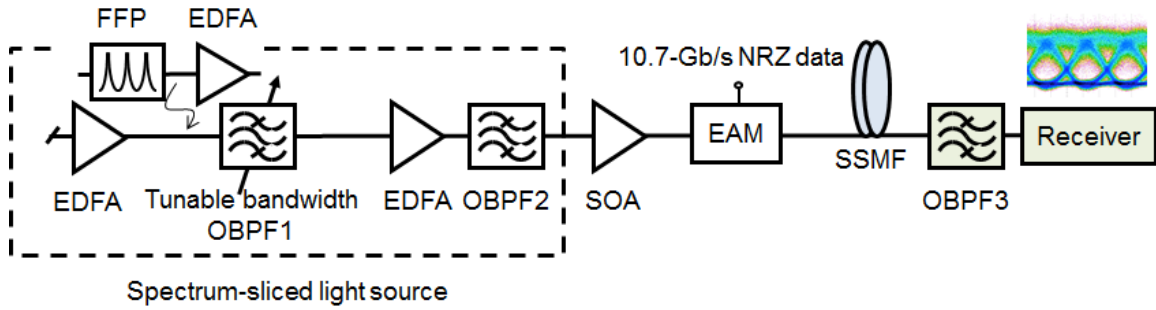


Figure 3.1 The experimental setup to analyze the optimum linewidth of the SSIL at 10.7 Gb/s/channel. The PRBS length is $2^{31}-1$ in the experiment.

on the performance of 10-Gb/s OOK signal. Two windows of linewidth for high-speed (e.g. faster than 10 Gb/s) operation of SSIL source are presented in Section 3.3. Also presented in this section is the optimum linewidth for capacity and transmission distance of WDM-PON system. This chapter shows that ultra-narrow SSIL source can provide the maximum capacity and longest transmission distance. Compared to the conventional SSIL having a wide linewidth, this ultra-narrow SSIL has a couple of drawbacks, which are discussed in Section 3.4. Finally, this chapter is summarized in Section 3.5.

3.2 Experiment and simulation setup

Figure 3.1 shows the experimental setup. A wideband ASE light generated from an EDFA is first sent to an optical bandpass filter (OBPF) for spectrum-slicing. Either a fiber Fabry-Perot (FFP) or a bandwidth-tunable optical filter is utilized as a spectrum-slicing filter. The FFP is employed to generate the ultra-narrow SSIL since its 3-dB bandwidth is

measured to be merely 700 MHz. It has periodic passbands at every 102 GHz, each having a Lorentzian profile. Thus, one of its passbands at 1542.14 nm is utilized by using an OBPF

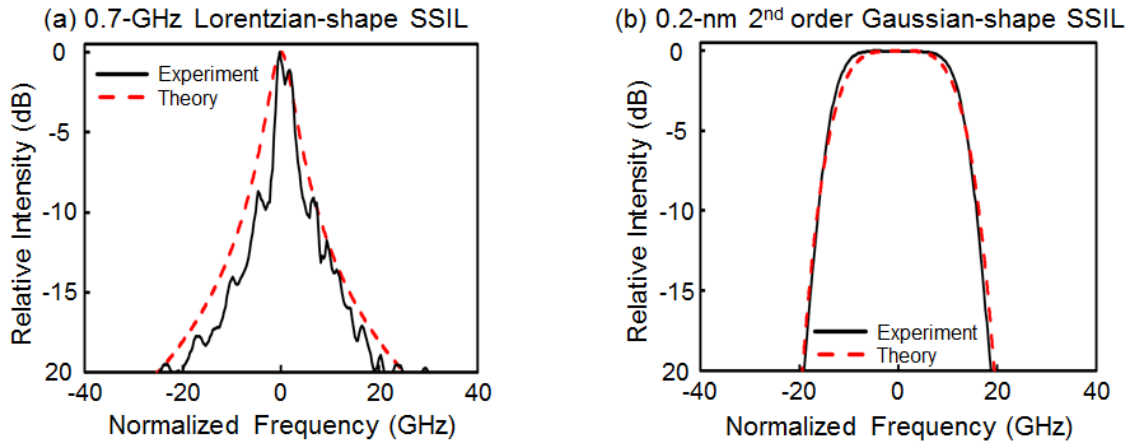


Figure 3.2 The optical spectra of the SSIL measured at the input of SOA when (a) the FFP and (b) the bandwidth-tunable optical filter are used as the spectrum-slicing filter. Also shown in the figures are the Lorentzian and 2nd-order Gaussian function in dashed line.

having a 3-dB bandwidth of 0.64 nm (i.e., OBPF1 in Figure 3.1).

Figure 3.2 shows the optical spectrum of the ultra-narrow SSIL measured at the output of OBPF2. Also shown in this figure is the Lorentzian function with a 3-dB bandwidth of 700 MHz. On the other hand, the bandwidth-tunable optical filter (i.e. OBPF1) has a 2nd-order Gaussian profile in its transmittance curve. The bandwidth of the filter can be varied from 0.16 to 0.42 nm. Figure 3.2 (b) shows the optical spectrum of the SSIL when the 3-dB bandwidth of the bandwidth-tunable filter is set to be 0.2 nm. The spectral profile of the measured spectrum agrees well with the 2nd-order Gaussian function. The SSIL is then sent to a GS-SOA for EIN suppression. The SOA used in the experiment has a small signal gain of 26 dB and the saturation input power of -15 dBm when the bias current is 200 mA

as shown in Figure 3.3. The SOA input power of the SSIL is set to be 3 dBm. Thus, the SOA operates in a deep-saturation region. To confirm the carrier lifetime of the GS-SOA at this operation condition, I first experimentally measured the carrier response of the SOA according to [96]. The measured results are indicated as solid dots in Figure 3.4. To obtain the carrier lifetime of this SOA, a revised frequency-dependent Lorentzian function [97] (i.e. the line in Figure 3.4) is utilized to fit the measured carrier response of SOA (i.e. the dots in Figure 3.4). Based on this fitting, the carrier lifetime of the GS-SOA is measured to be 57ps. The EIN-smoothed SSIL is then fed to a polarization-insensitive electro-absorption modulator (EAM) for data modulation. The EAM is driven by a 10.7-Gb/s non-return-to-zero (NRZ) pseudo-random binary sequence (pattern length is $2^{31}-1$). The Reed-Solomon codes with 7% overhead i(e.g. RS(2720, 2550)) is assumed to be utilized [22].

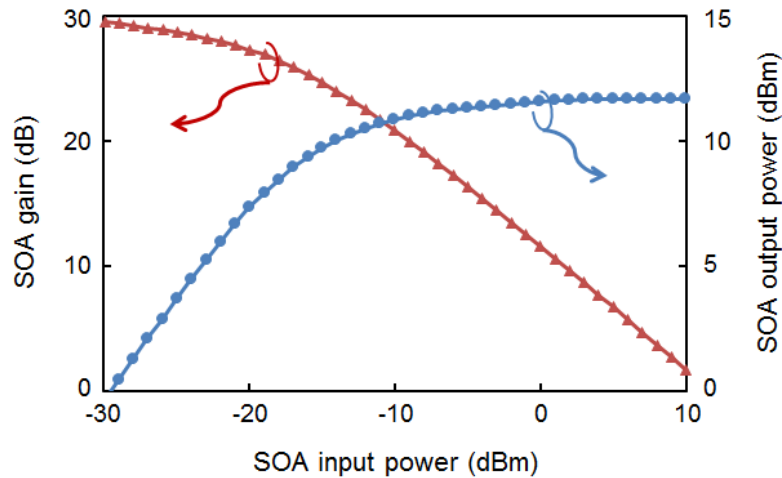


Figure 3.3 SOA characteristics when the SOA is biased at 200 mA at 1542 nm.

The extinction ratio of the signal is measured to be 10 dB. After transmission over SSMF, the 10-Gb/s signal passes through OBPF3 (3-dB bandwidth equals 0.64 nm) and is detected by a PIN detector. This optical filter emulates an AWG located at the remote node (RN). The received optical power of the signal is set to be -12 dBm.

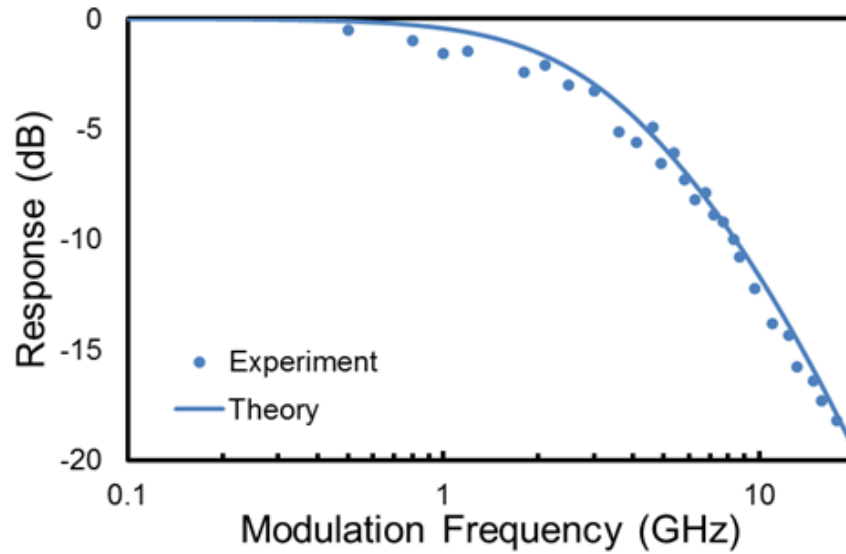


Figure 3.4 Measured SOA carrier response when the bias current and the operation wavelength are 200 mA and 1542nm, respectively. The theory line is based on revised frequency-dependent Lorentzian function in [97]

To investigate the effects of SSIL linewidth on the performance of the 10-Gb/s OOK signal, the computer simulation is also carried out by using a commercial program (VPI transmissionMaker). The simulation setup is the same as the experimental setup shown in Figure 3.1. Since the SOA parameters are vital to the EIN suppression and eventually the simulation performance, the SOA parameters employed in the simulation are listed in Table 3.1. Based on these parameters, the carrier lifetime is calculated as 45 ps, which agrees well with the measured value (i.e., 57 ps). As illustrated in [58, 59], the probability density

function (PDF) of the EIN follows the Chi^2 distribution. However, when the EIN is suppressed by using a GS-SOA, the PDF of the noise is changed and could be approximated as Gaussian when the SOA operates in the deep-saturation region [60, 61]. Thus, the BER performance of the signal is evaluated by using the semi-classical model based on both the Gaussian and Chi^2 approximations. Moreover, the receiver bandwidth is set to be 8 GHz, which is the same as the receiver used in the experiment. And the noise distribution estimation in the BER calculation is set to be Gaussian and Chi^2 Approximations [58,59].

Table 3.1 SOA PARAMETERS USED IN THE SIMULATION

Symbol	Description	Value
L (m)	Length of active region	7×10^{-4}
S (m ²)	Area of active region	1.76×10^{-13}
Γ	Confinement factor	0.6
α_{INT} (1/m)	Internal loss	5.7×10^3
a (m ²)	Differential gain coefficient	3.2×10^{-20}
N_{tr} (1/m ³)	Carrier density at transparency	1×10^{24}
A	Linewidth enhancement factor	4
A_{nr} (1/s)	Non-radiative recombination factor	3.8×10^9
B_{sp} (m ³ /s)	Spontaneous emission recombination factor	8×10^{-16}
C_{aug} (m ⁶ /s)	Auger recombination factor	2×10^{-40}
I (A)	Injection current	0.2

3.3 Optimum linewidth of SSIL source for capacity and transmission distance

3.3.1 Optimum linewidth of the SSIL for BER performance

The BER performance of the 10-Gb/s signal is first investigated while varying the linewidth of the SSIL from 0.1 to 70 GHz. Figure 3.5 (a) shows the BERs as a function of the linewidth when the SSIL has a 2nd-order Gaussian spectral profile. The linewidth of the SSIL source is the 3-dB linewidth of the SSIL before the EIN suppression. The solid and dotted lines indicate the BERs obtained by using the Gaussian and Chi² Approximations,

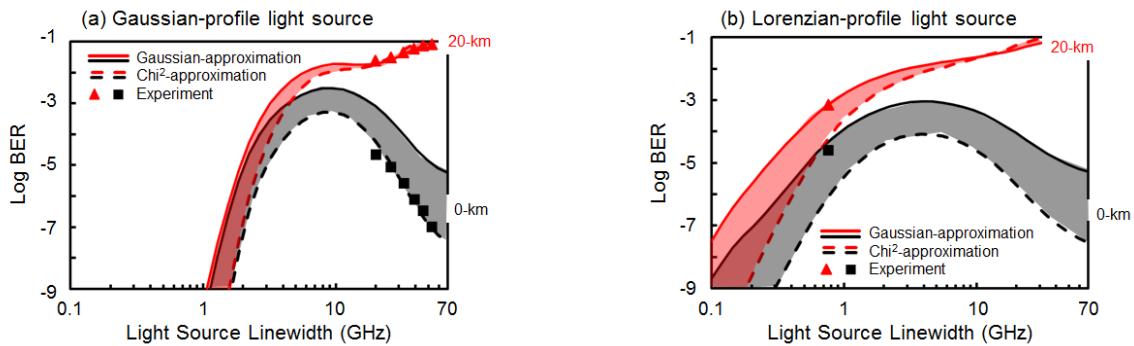


Figure 3.5 BER performance of the 10-Gb/s OOK signal as a function of the linewidth of the SSIL source when the SSIL has (a) 2nd-order Gaussian and (b) Lorentzian spectral profiles. The solid and dotted lines indicate the BERs estimated by using the Gaussian and Chi², respectively.

respectively. Since the optimal threshold of Gaussian approximation is lower than the one of Chi² approximation [59], the BERs obtained by using the Gaussian approximation are more conservative than those by using the Chi² approximation [58, 59]. Since these two

approximations represent the two extreme cases where the SOA operates in highly linear and deep saturation regions, the actual BER performance of the 10-Gb/s signal would fall in between them. Thus, the shaded areas in the figure indicate ranges of BER of the 10-Gb/s signal, depending upon the operation region of the SOA. Figure 3.5 (a) shows that the BER performance in the back-to-back condition is the worst at around 10 GHz of linewidth, but is improved when the linewidth of the SSIL source is either very narrow or very broad. For example, a BER lower than 10^{-7} (in the Chi^2 approximation) can be achieved when the linewidth is narrower than 2 GHz or wider than 50 GHz. It is not surprising that the BER performance is improved as the linewidth becomes broader (than 10 GHz). As expected, this is because the SNR is increased with the linewidth of the SSIL source. However, it is also found out that there is another window of linewidth where the high-speed operation of the SSIL is possible. This new window can be explained as follows: the bandwidth of the EIN at the receiver is determined by the linewidth of the SSIL source. Thus, when the linewidth is narrower than the receiver bandwidth, all the EIN components would fall within the receiver bandwidth. Then as the linewidth is further reduced, the total EIN power (within the receiver bandwidth) remains unchanged. However, when the GS-SOA is used as an EIN suppressor for the SSIL source, it suppresses the low-frequency components of the EIN (typically lower than a couple of GHz). This is because, due to the finite carrier lifetime, the GS-SOA exhibits high-pass-filter like characteristics in its intensity transfer function [29]. Since the EIN components mainly reside in the low-frequency region when the SSIL linewidth is ultra-narrow, this low-frequency EIN is effectively suppressed by the GS-SOA and consequently the total EIN power is reduced.

Even though there exist two windows of linewidth for the high-speed operation of the SSIL source in the back-to-back condition, one of the windows disappears after 20-km transmission over SSMF. Figure 3.5(a) shows that the 10-Gb/s signal generated by using wide-linewidth SSIL sources suffers from fiber chromatic dispersion. It has been demonstrated that the GS-SOA suppresses the EIN of the SSIL by creating strong intensity correlation between the different wavelength components of SSIL [17]. However, fiber chromatic dispersion not only distorts the signal waveforms, but it also breaks the intensity correlation created by the GS-SOA and thus negates the EIN suppression [20]. Therefore, the bad transmission performance of the wide-linewidth SSIL signal should be attributed to the dispersion-induced pulse distortion and EIN increase (caused by the restoration of the EIN inherent in the SSIL). However, when the linewidth of the SSIL is ultra-narrow (e.g., less than 2 GHz), decent BER values still could be achieved after 20-km transmission over SSMF. For example, a BER lower than 10^{-9} is estimated after the transmission when the linewidth is 1 GHz.

Figure 3.5(b) shows the BER performance of the 10-Gb/s signal when the Lorentzian-shaped SSIL is employed. Due to the gentle slope of the Lorentzian function in comparison with the 2nd-order Gaussian one, the BER values exhibit gradual changes on the linewidth of the SSIL source. Nevertheless, a similar tendency of the BER performance is observed. For example, there exist two windows of linewidth for high-speed operation of the SSIL source. The simulation results are partly confirmed by the experimental data. Figure 3.5(a) and (b) show that the experimental results agree well with the simulation results.

3.3.2 Optimum linewidth of SSIL for transmission distance over SSMF

This section evaluates the maximum transmission distance of the 10-Gb/s OOK signal to achieve the FEC threshold of 1.2×10^{-3} without any dispersion compensation. Figure 3.6 shows the results. It indicates that the maximum transmission distance is increased as the linewidth of the SSIL source is reduced. However, the transmission distance levels off at about 90 km even when the linewidth is ultra-narrow. This is because when the linewidth is much smaller than the modulation speed, the spectral width of the signal is determined by the data modulation itself instead of the linewidth of the SSIL. The results also show that the Lorentzian-shaped SSIL has poorer dispersion tolerance than the 2nd-order Gaussian-shaped one since the Lorentzian function has slowly decaying tails. The

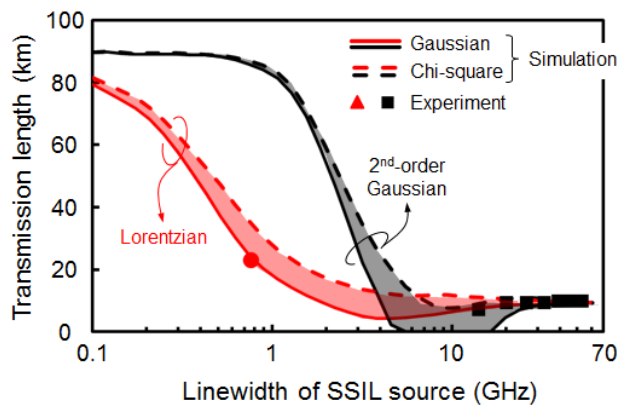


Figure 3.6 Maximum transmission length over dispersion-uncompensated SSMF versus linewidth of the SSIL source to achieve the FEC BER threshold of 1.2×10^{-3} . The solid and dotted lines indicate the transmission distance estimated by using the Gaussian and Chi^2 approximations, respectively. The symbols are the experimental values.

experimental data agree well with the simulation results. The 10-Gb/s OOK signal generated by using the ultra-narrow SSIL source can be transmitted over 23-km long dispersion-uncompensated SSMF.

3.3.3 Optimum linewidth of SSIL for capacity

To maximize the capacity of WDM systems utilizing the SSIL sources, it is imperative to minimize the spectral width of the high-speed signal so that adjacent channels can be placed compactly in wavelength, minimize the channel spacing and thus, maximize the available channel capacity. In WDM-PON systems, the minimum channel spacing can be determined by the passband of the AWGs located at the central office and remote node since the passband bandwidth of the AWGs should not exceed the channel spacing. Thus, the performance of the 10-Gb/s signal in the presence of narrow optical filtering is investigated. Figure 3.7 shows the minimum 3-dB bandwidth of OBPF2 to achieve the

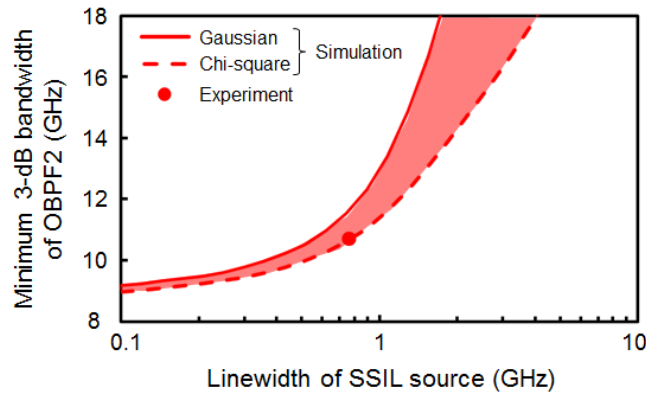


Figure 3.7 The minimum 3-dB bandwidth of OBPF2 to achieve the FEC threshold of 1.2×10^{-3} for the 10-Gb/s signal generated by using the Lorentzian-shaped SSIL.

FEC threshold (i.e., uncorrected BER is 1.2×10^{-3}) for the 10-Gb/s OOK signal generated by using the Lorentzian-shaped SSIL. OBPF2 represents the concatenated AWGs in WDM-PON systems. In the simulation, the 3rd-order Gaussian filter for OBPF2 is utilized. The results show that, as expected, the minimum bandwidth of OBPF2 increases with the linewidth of the SSIL. When the linewidth of the SSIL is very broad, the signal suffers severely from the narrow optical filtering. This is because the narrow optical filtering breaks the intensity correlation between the different wavelength components of SSIL, just like the fiber chromatic dispersion does to the signal [21]. Therefore, to maximize the capacity of WDM-PON systems based on SSIL sources (by minimizing the channel spacing), the ultra-narrow SSIL source is utilized. It should be noted that when the linewidth is as narrow as 200 MHz, the minimum 3-dB bandwidth of OBPF2 is estimated to be 9.5 GHz. In this case, the 20-dB spectral width of the 10-Gb/s OOK signal after the narrow optical filtering is measured to be 13.2 GHz. This implies that the channel spacing can be reduced as narrow as 13.2 GHz, considering that the 20-dB crosstalk from adjacent channels would incur a negligible power penalty (see Figure 3.11). Then it would be possible to achieve a spectral efficiency of 0.75 b/s/Hz (which is calculated from 10 Gb/s over 13.2 GHz) by using the ultra-narrow SSIL source.

3.4 Drawbacks of the ultra-narrow SSIL source

The previous section shows that there are two windows of linewidth for high-speed operation of the SSIL source utilizing GS-SOA. However, the SSIL source having a very broad linewidth (i.e., the linewidth is much wider than the receiver bandwidth) highly

susceptible to fiber chromatic dispersion and optical filtering. Thus, the optimal linewidth of the SSIL source for capacity and transmission distance should be ultra-narrow (i.e., the linewidth is much narrower than the receiver bandwidth). Nevertheless, the ultra-narrow SSIL source has some drawbacks, such as a large spectrum-slicing loss, a high required optical power at the input of the GS-SOA, and increased sensitivity to in-band crosstalk. This section discusses these drawbacks of the ultra-narrow SSIL in comparison with the conventional wide-linewidth SSIL.

3.4.1 Spectrum-slicing loss

For the generation of ultra-narrow SSIL for multi-channel WDM systems, it is highly desirable to utilize a periodic optical filter such as high-finesse FFP and Fabry-Perot etalon

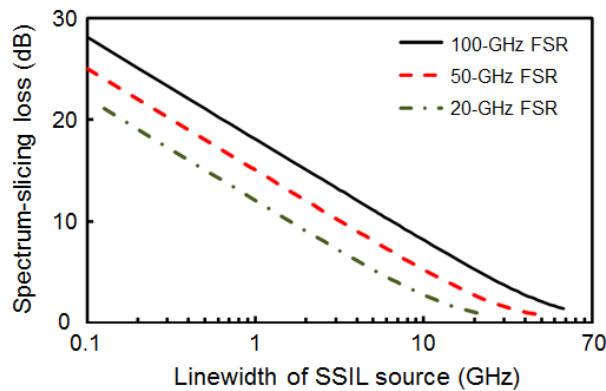


Figure 3.8 Spectrum-slicing loss as a function of the linewidth of the Lorentzian-shaped SSIL.

filters. However, as the linewidth decreases, the spectrum-slicing loss is increased since only a small portion of the wideband ASE is utilized as a light source. Figure 3.8 shows

the spectrum-slicing loss as a function of the linewidth of the SSIL source when a Fabry-Perot optical filter is used for spectrum-slicing. The spectrum-slicing loss is defined as the power ratio between the wideband ASE and SSIL at the output of the slicing filter. The insertion loss of the slicing filter is not included. The results show that the slicing loss is decreased at a rate of -10 dB/decade, regardless of the free-spectral range (FSR) of the Fabry-Perot filter. For example, when a Fabry-Perot filter having an FSR of 100 GHz is used, the slicing loss is 15 dB for SSIL with 2-GHz linewidth. However, it is increased to 25 dB when the linewidth decreases to 200 MHz. The slicing loss is reduced in proportion to the FSR of the filter. Thus, the slicing loss becomes less than 18 dB when the bandwidth and FSR of the Fabry-Perot filter are 200 MHz and 20 GHz, respectively. This loss can be readily compensated by using an optical amplifier at the CO. For example, a two-stage EDFA having the slicing filter as an inter-stage element can be used to generate multi-channel ultra-narrow SSIL [62]. The first-stage optical amplifier generates a wideband ASE, and the second-stage one compensates for the slicing loss.

3.4.2 SOA injection power for EIN suppression

The GS-SOA considerably improves the BER performance of the high-speed signal generated by using the SSIL by suppressing low-frequency EIN components. Regarding the implementation, it is important to have a low SOA input power since the SOA could be placed at the customer's premises for the upstream transmission but the spectrum-Sliced incoherent light is provided from the CO [63, 64]. The high optical power into the SOA required to achieve a target performance would limit the link budget of the upstream

transmission. Thus, this section investigates the SOA input power needed to meet the FEC threshold as a function of the linewidth of SSIL source. The results are plotted in Figure

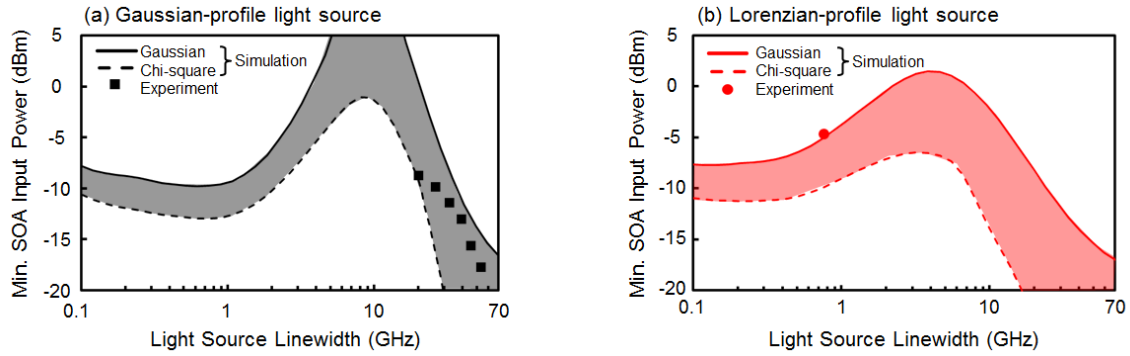


Figure 3.9 SOA input power required to achieve the FEC threshold for the 10-Gbs signal versus the linewidth of the SSIL source when the SSIL has (a) 2nd-order Gaussian and (b) Lorentzian spectral profiles. The solid and dotted lines indicate the SOA input power estimated by using the Gaussian and Chi² approximations, respectively. The symbols are the experimental values.

3.9 When the linewidth of the SSIL is very broad, the requirement of SOA input power is relaxed as the linewidth increases. The required SOA input power could be even less than the saturation input power of SOA (i.e., -15 dBm). For example, when the SSIL linewidth is 53 GHz, the BER of 1.2×10^{-3} can be achieved at an SOA input power of -17.7 dBm. This is because the SNR (i.e. B_o/B_e) is sufficiently high enough to achieve the FEC threshold without any EIN suppression. On the other hand, when the linewidth of the SSIL source is very narrow (e.g. less than 2 GHz), the minimum input power to the SOA is nearly independent of the linewidth. This should be attributed to the bandwidth of the EIN suppression, which is the inverse of the SOA carrier lifetime [65]. When the linewidth is very narrow, all the EIN components fall within the bandwidth of the EIN suppression. In

this range of linewidth, the amount of EIN suppression would not be affected by the linewidth.

3.4.3 Tolerance to in-band crosstalk

Optical access networks including WDM-PON should be robust against optical reflections caused by Rayleigh back-scattering and bad connectors. Those optical reflections would be unavoidable in WDM-PON systems utilizing loop-back configuration [66, 67]. Since the optical reflections have the same spectral components as the signal, they create in-band crosstalk to the signal. It has been shown that this crosstalk not only induces the signal crosstalk interference but also serves to break the intensity correlation produced by the GS-SOA [67]. However, there has been no study on the sensitivity of the SSIL

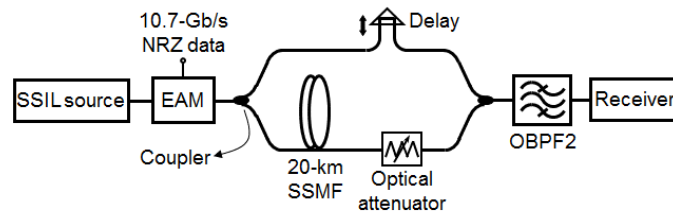


Figure 3.10 Experimental setup to measure the power penalty caused by in-band crosstalk.

source to in-band crosstalk for various linewidths of the SSIL source. Figure 3.10 shows the experimental setup to measure this sensitivity. The output of the SSIL is split into two ways; one is for the signal path and the other for the interferer. In the interferer path, a 20-km long SSMF is inserted to decorrelate the interferer with the signal. The optical power

of the interferer is adjusted by using an optical attenuator to control the signal-to-interference ratio. A tunable optical delay is utilized in the signal path to maximize the penalty at the receiver. The signal and interferer are recombined by using a 3-dB coupler and then sent to the receiver.

Figure 3.11 shows the measured power penalty as a function of the signal-to-interference ratio for two different linewidths, 700 MHz, and 0.4 nm. Also shown in this figure are the simulation results depicted in the solid and dotted lines to indicate the penalties estimated by using the Gaussian and Chi² approximations, respectively. The results show that the experimental data agree very well with the simulation results. They also show that the wide-linewidth signal (i.e., the linewidth is 0.4nm) outperforms the ultra-narrow linewidth one (i.e., the linewidth is 700 MHz) regarding tolerance to in-band

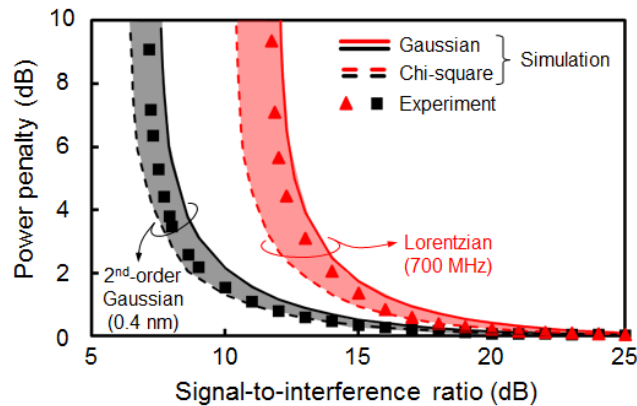


Figure 3.11 Power penalty of the 10-Gb/s SSIL signal induced by the in-band crosstalk.

crosstalk. For example, when the linewidth of the SSIL is 0.4 nm, the 10-Gb/s signal can tolerate the signal-to-interference ratio of up to 9.3 dB at 2-dB power penalty. However,

when the linewidth is reduced to 700 MHz, the tolerance is measured to be 14 dB at the same power penalty. This weak tolerance of ultra-narrow SSIL is ascribed to the fact that the in-band crosstalk components of the ultra-narrow SSIL signal fall within the receiver bandwidth whereas only a portion of the crosstalk components are captured by the receiver if the linewidth is very wide. This explanation is also confirmed by the simulation. The simulation results show that when the linewidth of SSIL source is very wide, the minimum allowable signal-to-interference ratio is increased as the linewidth decreases. However, the required signal-to-interference ratio becomes nearly constant at around 15 dB when the linewidth is very narrow (i.e. less than 2 GHz). Nevertheless, considering that a bad fiber connector could cause optical reflections of up to -14 dB, thus the ultra-narrow SSIL has sufficient tolerance to in-band crosstalk for the use in WDM-PON systems.

It should be noted that the experimental and simulation results presented in this chapter are obtained from the 10-Gb/s OOK signal. As a result, the BER performance is the worst when the linewidth of SSIL source is about 10 GHz (approximate to B_e). Therefore, as the data rate increases, the linewidth which brings us the worst BER performance should be shifted accordingly to a larger value.

3.5 Conclusion

The experimental and simulation studies are conducted on the optimum linewidth of SSIL source using a GS-SOA (as an EIN suppressor) for the maximum capacity and longest transmission distance. The BER performances of the 10-Gb/s OOK signal generated by using the SSIL source are evaluated over a wide range of source linewidth.

The studies show that there are two windows of linewidth for high-speed operation of the SSIL source: very broad (i.e., linewidth is much wider than the receiver bandwidth) and ultra-narrow (i.e., linewidth is much narrower than the receiver bandwidth). However, when the SSIL linewidth is very broad, the fiber chromatic dispersion and narrow optical filtering serve to break the intensity correlation created by the GS-SOA, and consequently, the BER performances of the 10-Gb/s signal are considerably deteriorated after transmission. Thus, the optimum linewidth for capacity and transmission distance is found to be ultra-narrow. For example, the simulation results show that, by using ultra-narrow SSIL sources with a 200-MHz linewidth, it is possible to transmit the 10-Gb/s OOK signal over 60-km long dispersion-uncompensated SSMF. Moreover, the channel spacing can be reduced as narrow as 13.2 GHz for the 10-Gb/s signals. Thus, it is feasible to implement an ultra-dense WDM system with the spectral efficiency of 0.75 b/s/Hz. However, these benefits come at the expense of large spectrum-slicing loss and high optical input power into the SOA. This chapter has shown that the ultra-narrow optical filtering of a wideband ASE induces a significant spectrum-slicing loss. The SOA input power of the SSIL required to suppress the EIN sufficiently is also increased when the linewidth of the SSIL is ultra-narrow. Nevertheless, these enhanced requirements of optical power could be readily satisfied by using high-gain and/or high-power optical amplifiers. The cost of these optical amplifiers can be shared by multiple channels and thus becomes insignificant as the number of WDM channels increases. It has shown that the employment of ultra-narrow SSIL sources makes the signal susceptible to in-band crosstalk possibly caused by Rayleigh backscattering and optical reflection in WDM-PON systems. Nevertheless, the experimental and simulation results show that the 10-Gb/s OOK signal generated by using

the ultra-narrow SSIL source with a 700-MHz linewidth is robust against in-band crosstalk as large as -14 dB on the signal. Therefore, the ultra-narrow SSIL sources could be used to implement high-capacity WDM-PON systems cost-effectively.

Chapter 4

Performance Improvement of Ultra-narrow SSIL Using Offset Filtering

4.1 Introduction

Recently, Z. Al-Qazwini and H. Kim have proposed and demonstrated the ultra-narrow spectrum to improve the capacity and the dispersion tolerance of WDM-PON systems based on SSIL [43]. In this scheme, a broadband ASE emitted from an EDFA is spectrally sliced through an ultra-narrow optical filter (i.e. an FFP filter having bandwidth $< 0.01\text{nm}$). The SSILs are sent to a gain-saturated SOA for the suppression of EIN. With the benefits of the narrow linewidth of the source, the signals demonstrate stronger tolerance against the fiber dispersion and optical filtering than the conventional SSIL signals [11, 55, 36, 37].

Even though the EIN is considerably suppressed by the SOA, the performance of the ultra-narrow SSIL signals is still limited by the EIN [43]. For example, an error floor is observed at a BER around 10^{-6} in a 10.7-Gb/s back-to-back experiment, and it is raised near the FEC threshold of 10^{-3} after transmission over 20-km SSMF.

This chapter demonstrates a simple technique to lower the error floors of the ultra-narrow SSIL signals by suppressing the EIN using offset optical filtering. To explain the

physical mechanism behind this simple technique, the correlation between amplitude and instantaneous frequency of the ultra-narrow SSIL signals is measured using the coherent receiver. To the best of our knowledge, it is the first time that a relationship between amplitude and frequency is reported and measured for incoherent light. This chapter show that frequency modulation-to-amplitude modulation conversion undertaken by offset optical filtering produces destructive interference with the EIN, and consequently suppresses the EIN. Error floors near FEC threshold are lowered by a factor of 2, which can greatly improve the corrected BER by several orders of magnitude after FEC decoding.

4.2 The correlation between amplitude and frequency of SSIL

The correlation between amplitude fluctuation and instantaneous frequency of the ultra-narrow SSIL is first measured. Figure 4.1 illustrates the setup for this measurement.

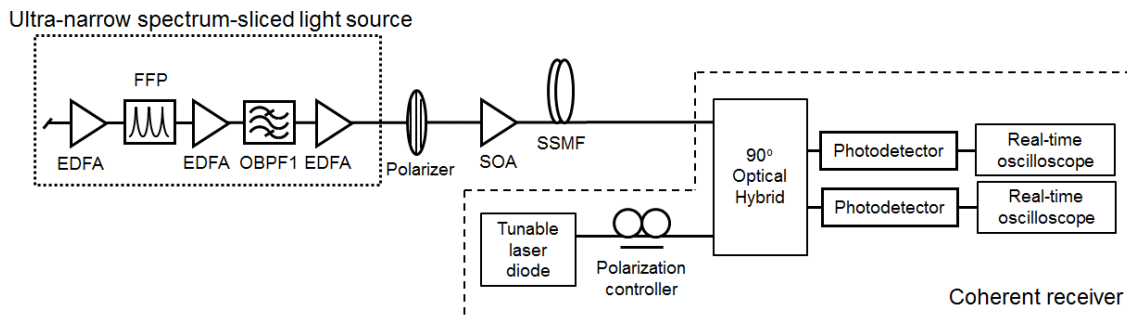


Figure 4.1 The experimental setup to measure the correlation between amplitude and frequency of the ultra-narrow SSIL source.

A wideband ASE is generated by an EDFA and spectrum-sliced by an FFP filter, which has a 3-dB bandwidth of 700 MHz and a finesse of 250. After optical amplification, one mode at 1542.14 nm is selected using a flat-top optical bandpass filter (OBPF, OBPF1 in Figure 4.1) having a 0.6-nm bandwidth. The light signal is then sent to a polarizer followed by a gain-saturated SOA to suppress the EIN. The SOA is biased at 200 mA and provides an optical gain of 6.4 dB when the optical power of the input light is 5 dBm. Since the saturation input power of the SOA is measured to be -2 dBm, the device operates in the saturation region. To analyze the amplitude and instantaneous frequency profiles, the light signal is finally fed to the coherent receiver, which is composed of a tunable laser diode, a polarization controller, a 90-degree optical hybrid, two photo-detectors (PDs), and a 100-Gsample/s real-time scope. The frequency of the tunable laser diode is set to be around 4 GHz off the center frequency of the SSIL. This is to avoid the direct-detected EIN falling on the beating frequency of the local oscillator and the signal. Due to the limited apparatus availability, the polarized incoherent light is analyzed in this measurement.

The electrical field of the ultra-narrow SSIL signal can be expressed as

$$E(t) = A(t) \exp \left[j \left\{ \omega t + 2\pi \int_{-\infty}^t \Delta f(\tau) d\tau \right\} \right] \quad (11)$$

The $A(t)$ is the signal amplitude, ω is the angular frequency of the signal, and $\Delta f(\tau)$ is the instantaneous frequency of the signal. Two million samples are captured, down-convert the signal to baseband, extract the waveforms of the amplitude and instantaneous frequency, and calculate the correlation between them. The correlation coefficient is given as

$$\rho = \frac{cov\{A(t), \Delta f(t)\}}{\sqrt{var\{A(t)\} \cdot var\{\Delta f(t)\}}} \quad (12)$$

The term of $cov(x, y)$ implies the covariance of the two waveforms x and y and $var(x)$ is the variance of x . Figure 4.2 shows the measured correlation coefficient as a function of the transmission distance over SSMF. Also shown in the dotted line is the correlation coefficient measured without using the SOA. In the absence of the SOA, there is no correlation between amplitude and frequency of the incoherent light. The correlation

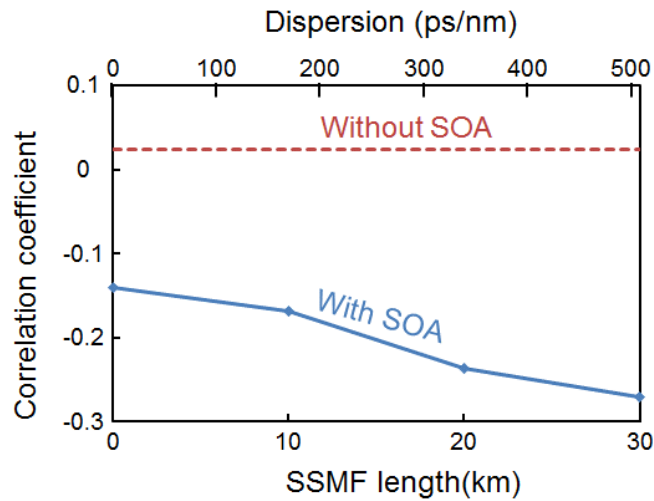


Figure 4.2 Measured correlation coefficient between the amplitude and frequency of the ultra-narrow SSIL as a function of SSMF length.

coefficient is measured to be 0.015. However, after EIN suppression using the gain-saturated SOA, it is changed to -0.14. The weak but distinct negative correlation should be attributed to self-phase modulation induced frequency chirp in the SOA. The intensity fluctuations of the SSIL induce temporal variations in the carrier density of the SOA and hence the refractive index changes [68]. Thus, the gain-saturated SOA induces frequency

chirp. The temporal waveform of the chirp can be decomposed into two components: one with its waveform almost identical to the output intensity waveform and the other which follows the time derivative of the output intensity waveform [68]. Figure 4.3(a) shows an example of the captured waveform of the amplitude and frequency at the output of the SOA. A negative correlation between the frequency and the amplitude of the SSIL at the output of the SOA is clearly observed. Figure 4.2 also shows that the negative correlation becomes stronger as the transmission distance increases. For example, the correlation coefficient is measured to be -0.28 after 30-km transmission over SSMF. This enhanced negative correlation in the presence of fiber dispersion can be explained as follows: the time derivative component of the instantaneous frequency waveform has blue- and red-shifted chirp at the rising and falling parts of the intensity waveform, respectively. This implies

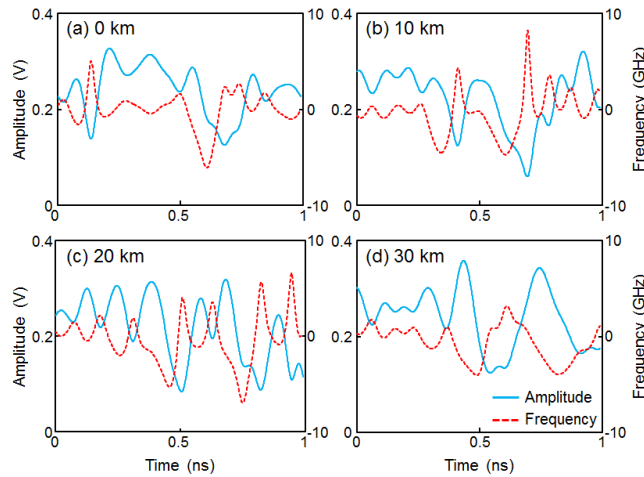


Figure 4.3 Captured amplitude and instantaneous frequency waveforms of the ultra-narrow SSIL after (a) 0-, (b) 10-, (c) 20-, and (d) 30-km transmission over SSMF.

that the peaks of red-shifted chirp follow the peaks of the intensity waveform (e.g., see Figure 4.3(a) at 0.6 ns).

On the other hand, red-shifted components of light in the anomalous dispersion medium travel slower than blue-shifted components. Thus, the anomalous dispersion of fiber makes the SOA output signal broadened in time and thus helps to align the peaks of red-shifted chirp with those of intensity waveform. Rising parts of the intensity waveform, which have blue-shifted chirp and travel faster than the other parts of the signal, also help to enhance the negative correlation. Examples of the captured waveforms in Figure 4.3 show the enhanced negative correlation between intensity and instantaneous frequency in the presence of fiber dispersion.

4.3 Impact of offset optical filtering on the performance of ultra-narrow SSIL

The frequency chirp is converted into optical intensity when the ultra-narrow SSIL signals pass through an optical frequency discriminator. The FM-to-AM-converted frequency waveform then produces destructive interference with the existing EIN, and finally suppresses the EIN. Owing to the negative correlation between amplitude and frequency of the ultra-narrow SSIL, the frequency discriminator should have a positive slope (i.e., the transmittance of the device increases with optical frequency). The frequency discrimination function can be readily implemented in a typical WDM-PON system without adding any additional components: the center wavelength of each channel is

located at the longer-wavelength edge of the AWG at the remote node. In SSIL-based WDM-PON systems, this offset optical filtering is simply achieved by slightly detuning the AWG to a longer wavelength.

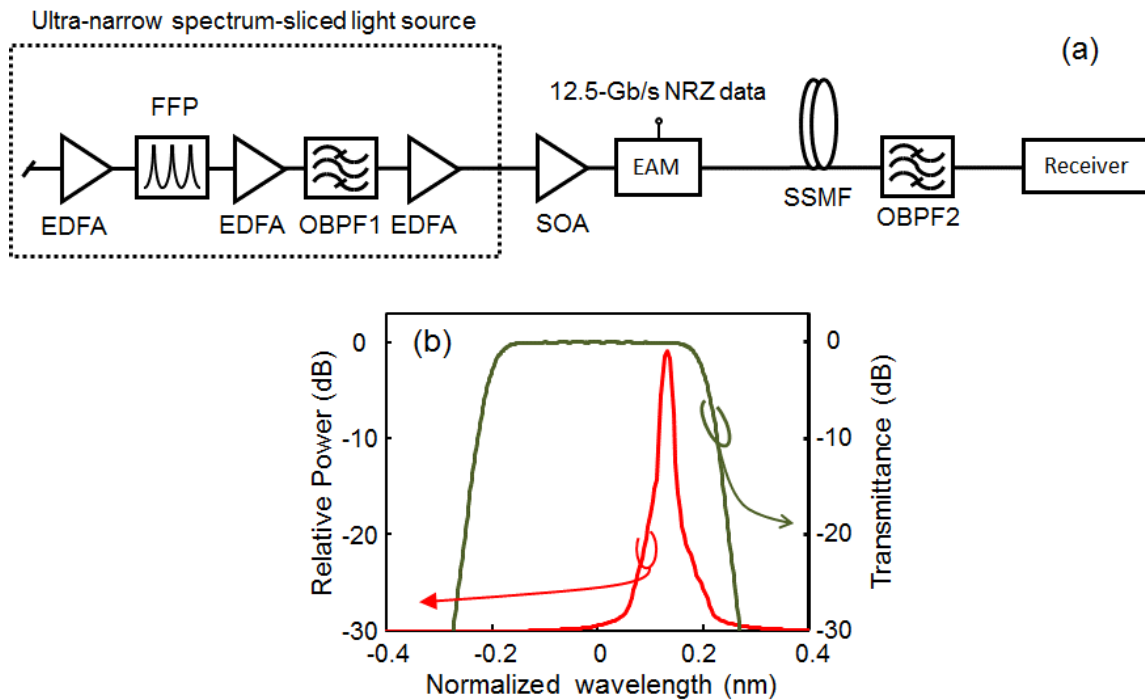


Figure 4.4 (a) Experimental setup to investigate the impact of offset optical filtering on the BER performance of the ultra-narrow SSIL. EAM: Electro-absorption modulator, (b) Transmittance of OBPF2 and the optical spectrum of the signal at SOA output with 0.12-nm optical offset.

Next, the impact of offset optical filtering on the performance of the ultra-narrow SSIL signals is investigated. Figure 4.4(a) shows the experimental setup for the BER measurement. Unpolarized ultra-narrow SSIL at 1542.14 nm is first generated using EDFAs, OBPF1, and the FFP filter, and then intensity-smoothed by using a gain-saturated SOA. The optical injection power into the SOA is kept to 5 dBm, which could be lowered

by utilizing an SOA with a low saturation power. It is worth to note that the cost of the additional EDFAs and FFP can be shared among optical network units in a multi-channel WDM-PON system [43]. For data modulation, a polarization-insensitive EAM is employed, which is driven by a 12.5-Gb/s NRZ signal (PRBS length is $2^{31}-1$). The extinction ratio of the signal is measured to be 10 dB. After transmission over SSMF, the signals are fed to OBPF2, which emulates the AWG at the remote node. Figure 4.4(b) shows the transmittance of OBPF2. The optical filter is based on a bulk diffraction grating and has flat-top passband with a full-width at half maximum of 0.4 nm. For offset optical filtering, the wavelength of the SSIL source is detuned without touching OBPF2. Figure 4.4(b) also shows the optical spectrum of the optical signal at SOA output with 0.12-nm optical offset. The signals are detected by the PIN receiver. BERs are measured by using an error detector.

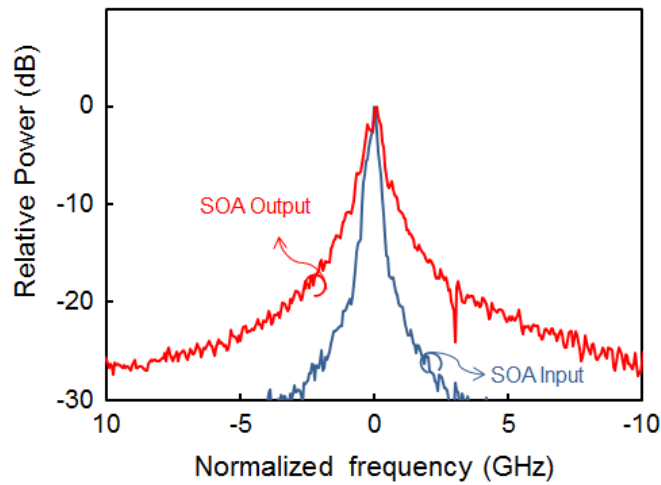


Figure 4.5 Optical spectra of the ultra-narrow SSIL.

Figure 4.5 shows the optical spectra of the ultra-narrow SSIL at the input and output of the SOA. For this measurement, the ultra-narrow SSIL is mixed with the output of an external cavity tunable laser and then detected with a photo-detector (bandwidth is 50 GHz) followed by an RF spectrum analyzer. Before the EIN suppression, the 3- and 20-dB linewidths of the light source are measured to be 400 MHz and 1.9 GHz, respectively. After the EIN suppression using the SOA, however, they are increased to 600 MHz and 7.4 GHz, respectively. This spectral broadening should be ascribed to phase modulation induced chirp and FWM inside the SOA [54, 17].

Figure 4.6 shows the measured variance of the EIN versus the SSMF length. Data modulation is not applied, and the optical power of the detected signal is kept unchanged throughout this measurement. The figure shows that the EIN variance increases with SSMF

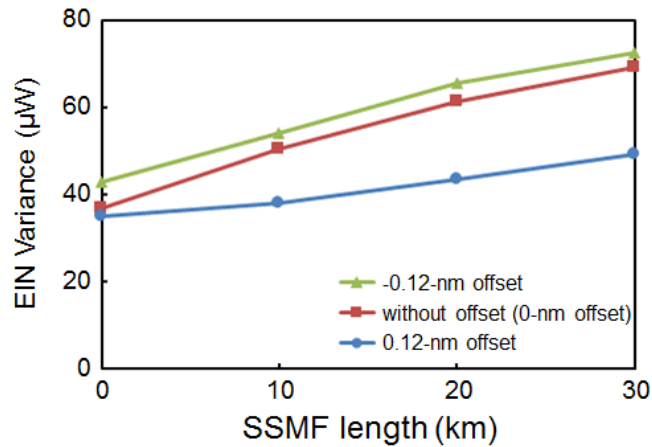


Figure 4.6 Measured EIN variance of the ultra-narrow SSIL as a function of SSMF length. For 0.12-nm offset filtering, a 0.12-nm detuning of the SSIL source is applied to OBPF2 longer wavelength edge.

length. This EIN increase can be explained as follows: when a gain-saturated SOA is employed to suppress the EIN of the SSIL source, the SOA creates a strong intensity correlation between different wavelength components of the light [17]. For example, intensity fluctuations at certain wavelength components are (partially) canceled by out-of-phase intensity fluctuations at other wavelength components, and consequently, this intensity correlation suppresses the overall EIN. However, this intensity correlation is sensitive to wavelength-dependent optical phenomena such as fiber dispersion. Chromatic dispersion serves to break the intensity correlation between different wavelength components of the SSIL and negates the EIN suppression achieved by using the SOA [20]. Figure 4.6 shows that the 0.12-nm offset filtering lowers the EIN variances compared to the case of no offset filtering (i.e., the offset is 0 nm). Thanks to the negative correlation between amplitude and frequency, offset optical filtering produces the destructive interference with the EIN and thus reduces the noise variance. On the other side, the -0.12-nm offset filtering increases the noise variance by producing the constructive interference with the existing EIN.

To have a better understanding of this offset filtering effect, the EIN spectra is also measured. The relative intensity noise (RIN) spectra are next measured for the ultra-narrow SSIL source to investigate the effect of offset optical filtering on the EIN spectrum. In this measurement, no data modulation is applied to detect the noise spectra only. Figure 4.7 shows the RIN spectra measured after 0-and 30-km transmission. The increase in EIN after transmission over dispersive medium is clearly observed in this figure. As explained in the previous paragraph, fiber dispersion enhances the EIN by breaking the intensity correlation between the different wavelength components of the SSIL. In particular, fiber dispersion

increases high-frequency EIN because the high-frequency components undergo a significant phase difference for a given temporal walk-off induced by dispersion [20]. The results also clearly show that offset optical filtering helps to lower the high-frequency EIN. For example, the EIN after 30-km transmission is lowered by 2 dB at 10 GHz, compared to the case of no offset filtering. One of the significant findings in this measurement is that offset optical filtering suppresses the high-frequency EIN. The cause of the negative correlation between amplitude and instantaneous frequency of the SSIL is frequency chirp induced by intensity fluctuations of the light. Therefore, a significant portion of the correlation occurs at fast-varying high-frequency components of the intensity waveform rather than slowly varying low-frequency ones. When offset optical filtering converts the

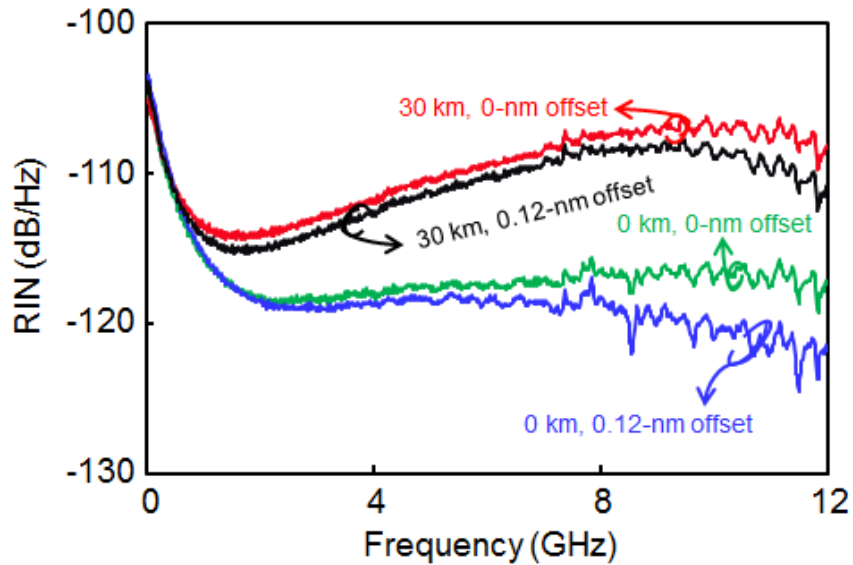


Figure 4.7 Measured RIN spectra of the ultra-narrow SSIL. Data modulation is not applied to this measurement.

frequency waveform into amplitude, the high-frequency EIN components, which have a relatively strong correlation, are efficiently suppressed.

Figure 4.8 shows the BER performance of the 12.5-Gb/s signals as a function of the filter offset measured at the received signal power of -15 dBm. The BERs are raised from 10^{-4} to 10^{-3} as the transmission distance increases. When the ultra-narrow SSIL is externally modulated by high-speed data (e.g., 12.5 Gb/s), the EIN residing mainly at low frequencies (e.g., less than 1 GHz) spreads all over the spectral contents of the data (e.g., up to about

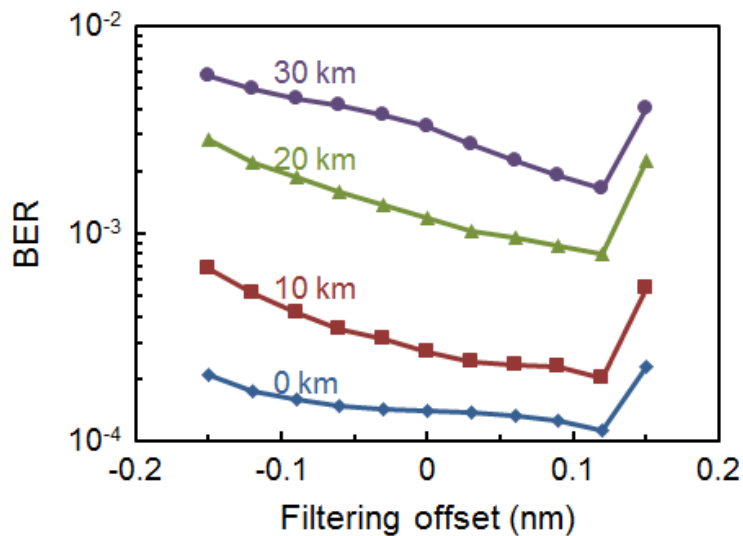


Figure 4.8 Measured BER performance of 12.5-Gb/s ultra-narrow SSIL signals versus the offset filtering. The received signal power is set to be -15dBm.

12.5 GHz in the 12.5-Gb/s modulation). As explained in the previous paragraph, chromatic dispersion increases the high-frequency EIN and deteriorates the BER performance after transmission. Figure 4.8 shows that despite the symmetric transmittance profile of OBPF2

[as see in Figure 4.4(b)], the BER performance is asymmetric on the filter offset. In particular, the BER performance is poorer when the signal wavelength is tuned to the shorter-wavelength edge of OBPF2 than when aligned with the longer-wavelength edge of the filter. This performance difference is because the FM-to-AM-converted signal produces constructive interference with the EIN to increase the EIN. The results also show that the BER improvement by offset filtering increases with the SSMF length, as expected from Figure 4.6. For example, there is only a marginal BER improvement at the back-to-back, but the BER is lowered by a factor of 2 after 30-km SSMF. This BER improvement near FEC threshold can be translated into more than five orders of magnitude improvement in corrected BER after FEC decoding for super-FEC codes such as RS(2720, 2550) [69].

It is worth noting that the offset optical filtering technique increases the link loss and consequently reduces the power budget of the system. In the demonstration, this system suffers from a loss increase by less than 1 dB when the offset is set to 0.12 nm. However, the proposed offset filtering improves BER floors, which are not improved by increasing the optical power at the receiver. The small reduction in power budget can be readily overcome by slightly increasing the fiber launch power.

4.4 Conclusion

The offset optical filtering technique has been proposed and demonstrated to reduce the EIN of the ultra-narrow SSIL source. This chapter has shown that there exists a negative correlation between amplitude and frequency of the light and it becomes stronger as the transmission distance over SSMF increases. This chapter also finds that offset optical

filtering converts the frequency waveform into amplitude and produces destructive interference with the EIN to reduce the noise. The proposed scheme can be implemented simply by detuning the wavelength of the AWG at the remote node, without incurring additional costs or adding new components in WDM-PON systems.

Chapter 5

Upstream Transmission Using Ultra-narrow SSIL in WDM-PON Systems

5.1 Introduction

With the benefits of high capacity, strong tolerance to optical dispersion and optical filtering effect, the ultra-narrow SSIL has been regarded as a promising light source in WDM-PONs [43]. However, the ultra-narrow linewidth of the SSIL would deteriorate the signal tolerance to the in-band crosstalk (e.g. Rayleigh backscattering).

Thus, in this chapter, the upstream transmission of 10-Gb/s incoherent light signals are first experimentally demonstrated, which are generated by using an ultra-narrow SSIL over a loopback-configured 20-km SSMF link. The performance limitation of the signals operating is first analyzed at two different FEC-rated line rates (i.e., 10.7 and 12.5 Gb/s) over three distinct link configurations. Then, the 25-nm wavelength operation of the 10-Gb/s/channel signals is demonstrated.

To improve the cost-effectiveness of the upstream transmission, this chapter is also investigated using RSOA for the EIN suppression as well as the data modulation. The upstream transmission of 5.35-Gb/s SSIL-seeded RSOA signals is transmitted over a 20-

km loopback configured SSMF. To the best of our knowledge, 5.35-Gb/s is the highest data rate ever achieved by using an SSIL-seeded RSOA or FP-LD.

5.2 10 Gb/s/channel upstream transmission using ultra-narrow SSIL source

5.2.1 Introduction

Recently, the ultra-narrow SSIL source has been proposed and demonstrated to improve the capacity and tolerance to optical dispersion effect in the WDM-PON systems. However, the performance improvement of the ultra-narrow linewidth comes at the expense of the tolerance of the in-band crosstalk and increasing spectrum-slicing loss.

To investigate the feasibility of the upstream transmission using ultra-narrow SSIL, the upstream transmission of 10-Gb/s ultra-narrow SSIL light signals is first experimentally demonstrated. This chapter first analyze the performance limitation of the signals operating at two different FEC-rated line rates (i.e., 10.7 and 12.5 Gb/s) over three distinct link configurations. Finally, the 25-nm wavelength operation of the signals is demonstrated.

5.2.2 Experimental setup

Figure 5.1(a) shows the experimental setup. A wideband ASE is first generated by an EDFA with no input signal and then spectrum-sliced by an FFP filter, which has a 3-dB

bandwidth of 700 MHz. The ultra-narrow incoherent light is amplified by another EDFA, and one of the FFP modes at 1542.1 nm is selected by two optical bandpass filters, OBPF1 and OBPF2, which emulate the AWG at the central office. The 3-dB bandwidth of the OBPFs is 0.4 nm. After transmission over 20-km SSMF, the incoherent light is fed to an optical circulator followed by a gain-saturated SOA for EIN suppression. The small signal gain and saturation input power of the SOA at 1542 nm and biased at 200 mA are 22 dB and -15 dBm, respectively. The EIN-smoothed ultra-narrow SSIL is sent to a polarization-

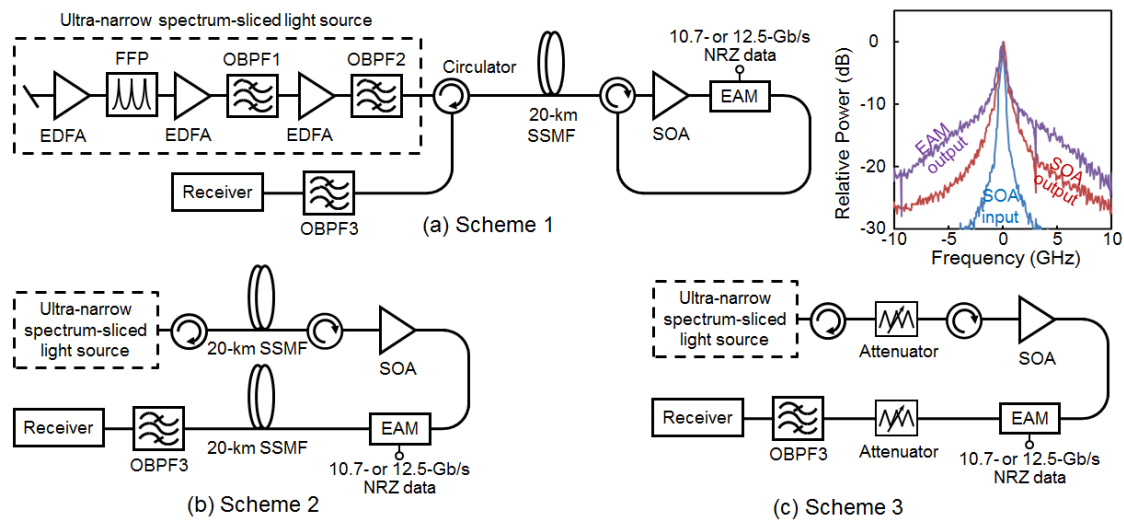


Figure 5.1 Experimental setup of (a) scheme 1 (upstream transmission), (b) scheme 2 (without in-band crosstalk), and (c) scheme 3 (without dispersion). The inset shows the optical spectra of the signal at the SOA input, SOA output, and EAM output.

insensitive EAM driven by a PRBS (length is $2^{31}-1$) for upstream transmission. The line rate is set to be 10.7 and 12.5 Gb/s, taking into account the 7% and 25% overheads of FEC, respectively. The ONU transmitter, which is composed of the circulator, SOA, and EAM

in the demonstration, could be replaced with a reflective EAM-SOA for low-cost implementation of the customer unit [75, 76]. After transmission over the SSMF, the 10-Gb/s signals pass through an OBPF3 and detected by a PIN receiver. The 3-dB bandwidth of the OBPF3 is 0.4 nm.

This chapter first optimizes the fiber launch power of the light source in the setup. The best BER performance can be achieved when the fiber launch power is 7.3 dBm. When the fiber launch power is low, the SOA cannot operate in a saturation mode to sufficiently suppress the EIN. On the other hand, the large fiber launch power reduces the signal-to-Rayleigh backscattering ratio at the receiver. This is because the received signal power levels off when the fiber launch power is large and the SOA is gain-saturated. At the fiber launch power of 7.3 dBm, the SOA input power of the source is measured to be 2.3 dBm, which is large enough to saturate the SOA. The inset in Figure 5.1 shows the optical spectrum of the ultra-narrow spectrum-sliced light at the SOA input. The 3- and 20-dB bandwidths are 0.4 and 1.8 GHz, respectively. After the EIN suppression by the SOA, the spectrum is broadened by FWM and phase-modulation-induced chirp inside the gain-saturated SOA, as shown in the inset of Figure 5.1. The 3- and 20-dB bandwidths are measured to be 0.6 and 7.5 GHz, respectively. It is worth noting that this bandwidth is still narrower than the bandwidth expanding, which is induced by the modulation at 10 Gb/s. Thus, the signal spectrum after the EAM is mainly determined by the modulation. This phenomenon is clearly observed in the optical spectrum of the signal measured at the EAM output (see Figure 5.1 inset).

5.2.3 Results and discussion

The BER performance of the 10-Gb/s signals is measured. Figure 5.2 shows the BER results of 10.7- and 12.5-Gb/s signals considering the different FEC overheads. As shown in the results, the BER is improved with the received signal power up to -18 dBm in both

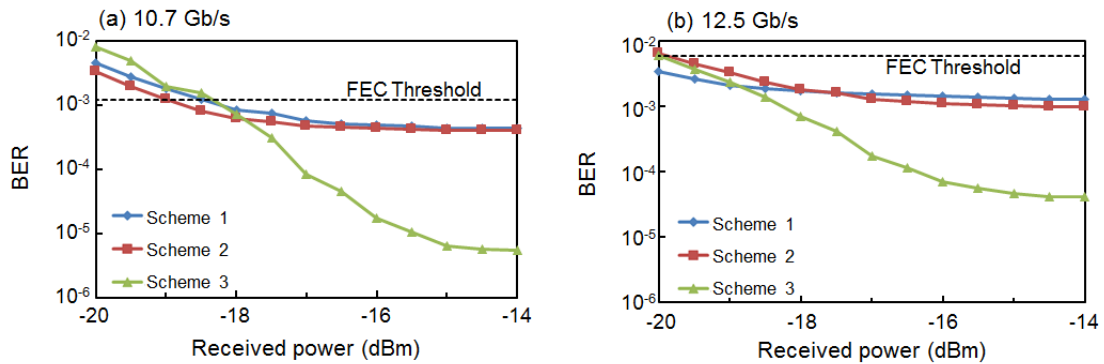


Figure 5.2 Measured BER as a function of the optical received power in three different configurations when the data rate is (a) 10.7 and (b) 12.5 Gb/s.

cases. However, error floors are observed at around 4×10^{-4} and 10^{-3} at 10.7 and 12.5 Gb/s, respectively. To investigate the primary cause of these error floors, the setup is modified as shown in Figure 5.1(b) and (c). In Scheme 2 of Figure 5.1(b), two separate fibers are utilized, one for seed light and the other for upstream transmission. This scheme is to exclude the effects of in-band crosstalk such as Rayleigh backscattering. The BER performance in Figure 5.2 shows a marginal difference between Scheme 2 and Scheme 1. Thus, it implies that the consequences of the Rayleigh backscattering are insignificant. It is interesting to note that the signal-to-Rayleigh-scattering ratio is measured to be 20 dB.

However, when the Scheme 2 replaces the transmission fibers with optical attenuators, as shown in Figure 5.1(c) (i.e., Scheme 3), the error floors are greatly improved. For example, error floors at 6×10^{-6} and 5×10^{-5} can be achieved for signals at 10.7 and 12.5 Gb/s, respectively. Thus, the error floors observed in the loopback-configured network (i.e., Scheme 1) are due to fiber dispersion. Not only does the fiber dispersion distort the signal waveforms, but it also breaks the intensity correlation created by the gain-saturated SOA (between the SSIL components at different wavelengths) [20].

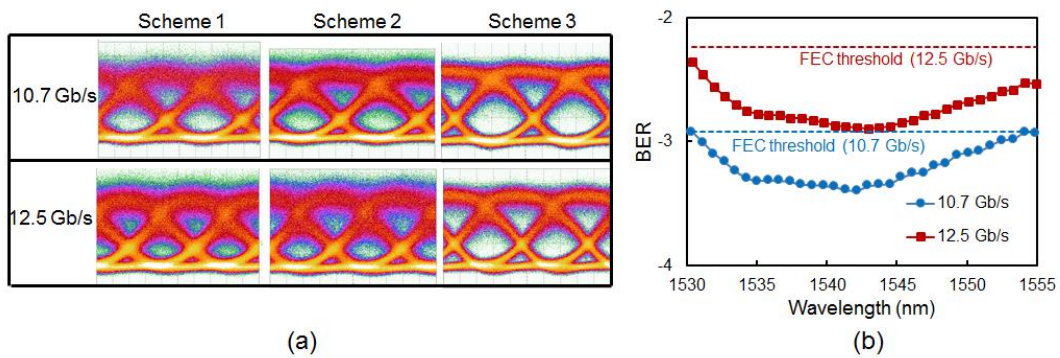


Figure 5.3 (a) Measured eye diagrams of the signals in three schemes at different data rates. The receiver signal power is -15dBm. (b) BER performance versus the center wavelength of the SSIL source.

The optical eye diagrams of the signals in Figure 5.3 (a) also substantiate the conclusion: eye closure of the signal as well as increased EIN for Scheme 1 and 2 are observed. Nevertheless, the BER performance can be better than FEC thresholds of 1.2×10^{-3} and 5.8×10^{-3} for the signals at 10.7 and 12.5 Gb/s, respectively.

Figure 5.3(b) shows the measured BER versus the center wavelength of the SSIL sources on the 100-GHz ITU-T grid when the received signal power is set to -15 dBm. Since the FSR of the FFP used is slightly larger than 100 GHz, the wavelength of the FFP is tuned to the grid every time the wavelength is changed. The results show that the 25 nm of operation range for both 10.7- and 12.5-Gb/s signals can be achieved. Owing to the non-white characteristics of the EIN, the 12.5-Gb/s signal outperforms the 10.7-Gb/s one.

5.2.4 Summary

The upstream transmission of 10-Gb/s signal generated is demonstrated by using an ultra-narrow SSIL light source in a loopback configured 20-km SSMF link. This section also shows 25-nm wavelength operation of the 10-Gb/s signals to demonstrate the feasibility of 320-Gb/s capacity in C-band using an SSIL.

5.3 5-Gb/S Upstream Transmission Using an RSOA Seeded by Ultra-narrow SSIL

5.3.1 Introduction

SSIL sources have long been considered as one of the promising candidates for light sources of WDM-PONs [11, 12]. The capability to simultaneously generate multiple WDM channels is particularly attractive for cost-effective implementation of upstream transmission for WDM-PON systems. RSOAs or FP-LD are typically used in conjunction

with the SSIL for the color-free operation of upstream WDM-PON systems [70, 71]. In this system, a broadband ASE is first sent from the central office, spectrum-sliced by an AWG at the remote node, and fed to RSOAs or FP-LDs located at the customer premises. Direct modulation of the optoelectronic devices imposes upstream information onto the seeded incoherent light, which is then sent back to the CO for detection.

However, major technical hurdles of these systems include the limited modulation bandwidth and poor dispersion tolerance. The maximum modulation bandwidth of RSOAs and FP-LDs is limited by the carrier lifetime and is typically less than 2 GHz [72, 73]. Thus, the previous experimental demonstrations using an SSIL-seeded RSOA or FP-LD transmitter are all, to our knowledge, performed at ≤ 2.5 Gb/s [70-74, 19]. On the other hand, the transmission performance of the SSIL-seeded RSOA or FP-LD system is limited by the wide linewidth of the seed light. When a wide-linewidth SSIL (e.g., linewidth wider than 0.1 nm) is used as a seed light, it primarily determines the spectral width of the RSOA- or FP-LD-modulated signal. Then, it can limit the maximum transmission distance over a dispersion-uncompensated link. For example, the dispersion-induced pulse broadening of a 2.5-Gb/s NRZ signal can exceed one-third the bit duration after 20-km transmission over SSMF when a 0.4-nm SSIL is used as a seed light. The broad linewidth of the SSIL also sets the minimum channel spacing of the WDM system and thus the maximum system capacity.

The ultra-narrow spectrum slicing technique has been proposed drastically to reduce the linewidths of SSIL signals [43]. Using this light source, the transmission of 10-Gb/s NRZ signal is successfully demonstrated over 20-km SSMF without any dispersion compensation. In this demonstration, however, the modulation was carried out by an

electro-absorption modulator, which would not be suitable for an upstream transmitter due to its large insertion loss. Moreover, an extra gain-saturated SOA was necessary for EIN suppression before data modulation.

This section demonstrates an upstream transmission of 5.35-Gb/s SSIL-seeded RSOA signals over a 20-km loopback configured SSMF link. To the best of our knowledge, 5.35-Gb/s is the highest data rate ever achieved by using an SSIL-seeded RSOA or FP-LD. The use of an RSOA for both data modulation and EIN suppression substantially simplifies the customer unit for cost-effective implementation of SSIL-based upstream WDM-PON systems. Two key techniques are adopted in our demonstration. The transmitter de-emphasis is exploited to accommodate the 5.35-Gb/s NRZ signal in the 1.4-GHz-bandwidth RSOA. The EIN noise, which remains after EIN suppression through the gain saturation of an RSOA, is mitigated by using the offset optical filtering technique [38]. Owing to the narrow linewidth of the seeded light, the uncorrected BER can be achieved lower than 10^{-3} after transmission over 20-km loopback configured SSMF link without dispersion compensation.

5.3.2 Experimental setup

Figure 5.4 shows the experimental setup. A broadband ASE emitted from an EDFA is first spectrum-sliced by using an FFP filter, which has a 3-dB bandwidth of 700 MHz and an FSR of 102 GHz. After boosting the SSIL, one of the wavelength modes at 1542.31 nm is selected through an OBPF (i.e. OBPF1 in Figure 5.4). In real systems, OBPF1, and the two EDFAs after the FFP should be replaced with a high-power EDFA. In such a case, the

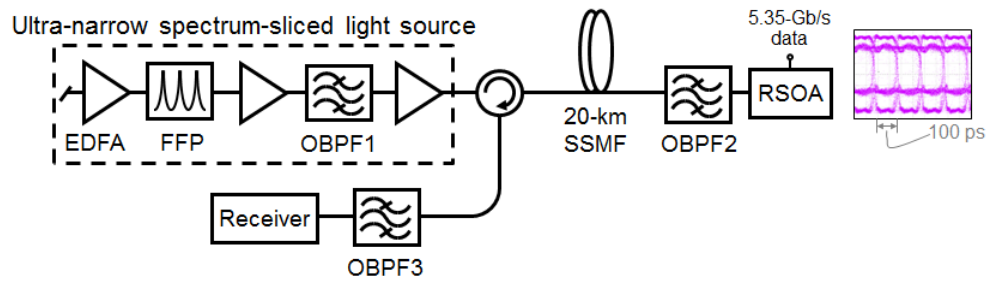


Figure 5.4 Experimental setup of 5-Gb/s RSOA-based upstream transmission.

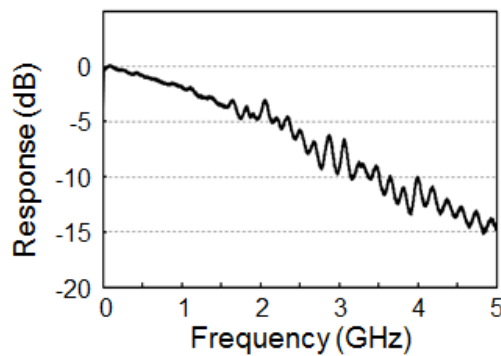


Figure 5.5 Measured E/O response of the RSOA used in the demonstration.

mode selection would be made by an AWG located at the RN. After transmission over 20-km SSMF, the ultra-narrow SSIL is fed to OBPF2, which emulates an AWG at the RN. The 3-dB bandwidth of OBPF2 is 0.4 nm. The unmodulated seed light is then injected into an RSOA for upstream modulation. The RSOA used in this experiment is an uncooled device housed in a transistor-outline can package. The bias current and saturation input

power of this optoelectronic device are 34 mA and -17 dBm, respectively. When the injection power is -10.3 dBm, the optical gain of the RSOA is measured to be 12.6 dB. Figure 5.5 shows the measured E/O response of the RSOA. The 3-dB bandwidth is measured to be 1.4 GHz. However, the frequency response of this device has a moderate slope up to 5 GHz, and the 10-dB modulation bandwidth reaches 3.5 GHz. The RSOA is directly modulated by a 5.35-Gb/s NRZ signal (PRBS length is $2^{31}-1$) integrated with a two-tap de-emphasis signal condition to boost high-frequency components of the signal which suffer more loss than low-frequency ones. The 1st post-tap de-emphasis emphasizes the first bit immediately after the transition and de-emphasizes the remaining bits. The de-emphasis is quantified through the amplitude of the emphasized signal (V_1) and the de-emphasized signal (V_2) as the following equation:

$$De - emphasis\ level\ (dB) = 20\log\left(\frac{V_1}{V_2}\right) \quad (13)$$

Here, the V_1 is the amplitude of emphasized signal (i.e. the bit immediately after transition); V_2 is the amplitude of the de-emphasized signal (i.e. the remaining bits). The inset in Figure 5.4 shows the eye diagram of the electrical signal driving the RSOA. It is assumed that an FEC with 7% overhead is used [69]. Finally, the 5.35-Gb/s modulated upstream signal traverses the 20-km SSMF back to the CO to be detected by a PIN receiver.

The de-emphasis ratio is first optimized by measuring the BER performance. The results are shown in Figure 5.6(a). In this measurement, the RSOA injection power, and optical power at the receiver are kept to be -10.3 and -15 dBm, respectively. An offset optical filtering of 0.17 nm is applied, the effect of which will be explained later. In this plot, the BERs are measured while changing the de-emphasis ratio. The RSOA bias current

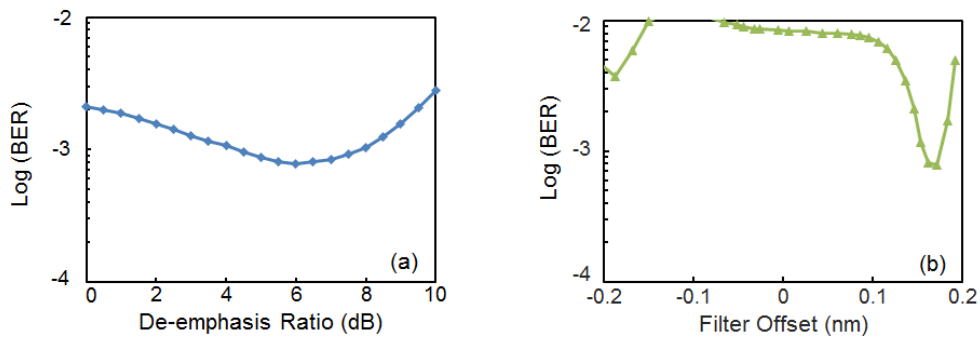


Figure 5.6 Measured BERs (a) as a function of the de-emphasis ratio, and (b) as a function of filter offset. The RSOA injection power and the signal received power are kept to be -10.3 and -15 dBm, respectively.

is adjusted at each point to ensure that the RSOA driving current (i.e., AC-coupled data plus DC bias) is always kept positive. The results show that the best BER performance is obtained when the de-emphasis ratio is 6 dB. The eye diagrams in Figure 5.7 confirm the performance improvement when the de-emphasis is employed. The optimum de-emphasis ratio would be determined by the frequency response of the system, which is mainly governed by the frequency response of the RSOA in the demonstration. Among modulation data patterns that drive the RSOA, alternating bit patterns such as '101010' contain the highest frequency components. In the experiment, these patterns are mainly composed of a 2.675 GHz (which is half of 5.35 GHz) tone and its harmonics. In Figure 5.5, the RSOA at 2.675 GHz exhibits 6 to 7 dB lower E/O conversion efficiency than DC component, which agrees well with the optimized de-emphasis ratio of 6 dB in Figure 5.6(a).

Next, the effect of offset optical filtering on the BER performance is investigated. Figure 5.6(b) shows the measured BER as a function of the filter offset between the light

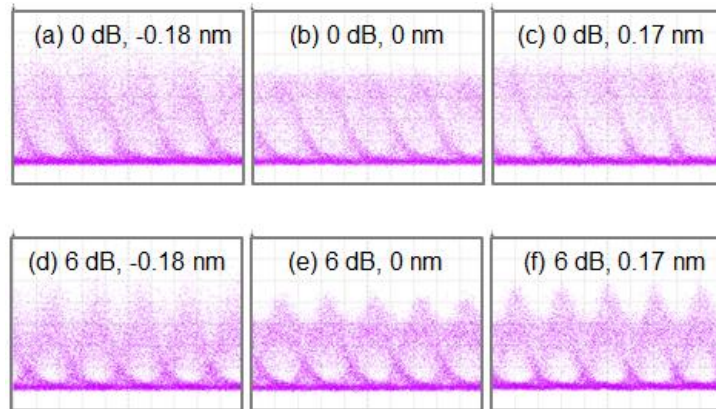


Figure 5.7 The eye diagrams measured at the receiver with (a) no de-emphasis and -0.18-nm offset filtering (b) no de-emphasis and no offset filtering, (c) no de-emphasis and 0.17-nm offset filtering, (d) 6-dB de-emphasis and -0.18-nm offset filtering, (e) 6-dB de-emphasis and no offset filtering, (f) 6-dB de-emphasis and 0.17-nm offset filtering. The RSOA injection power and received power are kept to be -10.3 and -15dBm, respectively.

source and OBPF2. In this measurement, the offset is adjusted by tuning the wavelength of the SSIL source. A 6-dB de-emphasis is applied to the signal driving the RSOA. Recently, [38] has shown that the offset optical filtering reduces the EIN of the ultra-narrow SSIL. A negative correlation is created between the amplitude and frequency of the ultra-narrow SSIL when a gain-saturated SOA is employed to suppress the EIN. The offset optical filtering then converts the frequency modulation into amplitude modulation to produce destructive interference with the existing EIN. This offset filtering can be readily realized by either locating the source wavelength at the longer-wavelength of the AWG at

the RN or detuning the wavelength of the AWG to a shorter side with the light wavelength fixed. A positive slope (i.e., increasing transmittance with optical frequency) of the filter converts the frequency waveform into amplitude waveform without changing the sign of the negative correlation. Figure 5.6(b) shows that a BER is improved more than an order of magnitude when the offset is 0.17 nm. At this filtering offset, the BER is improved to be less than 8×10^{-4} . It is interesting to note that offset filtering with a negative slope (i.e., at the shorter-wavelength edge of the filter) inverts the frequency waveform during the frequency-to-amplitude conversion and produces constructive interference with the EIN. Thus, the EIN noise grows at negative filter offsets, compared to center filtering. For example, the BER is measured to be poorer than 10^{-2} when the offset ranges from -0.08 to -0.15 nm. The electrical eye diagrams in Figure 5.7(a) and (d) clearly show the increase in EIN after negative offset filtering. One noticeable feature of Figure 5.6(b) is that a BER improvement can be achieved when the offset filtering is around -0.18 nm. This is attributed to the fact that offset optical filtering also serves to compensate for the limited bandwidth of the RSOA. This can be explained as follows. Due to the changes of refractive index in RSOA, blue- and red-shifted chirps are generated at the trailing and leading edges of the RSOA output signal [68]. A negative offset filtering helps to improve the rising time of the leading edges by giving them a higher transmittance whereas a positive offset filtering shortens the falling time of the trailing edges [77, 78]. It is worth noting that the offset filtering increases the total link loss. In the experiment, the received power is reduced by 2.4 dB at 0.17-nm offset filtering. However, the offset filtering improves BER floors, which are not improved by increasing the optical power at the receiver. The small reduction

in power budget should be overcome by slightly increasing the fiber launch power from the CO.

5.3.3 Results and discussion

Figure 5.8(a) shows the BER performance of the 5.35-Gb/s signal in the loopback configured link. It indicates that there exists an error floor at around 8×10^{-4} after upstream transmission over 20-km SSMF. To investigate the cause of this error floor, the BER curve is measured at the back-to-back operation. In this case, the transmission fiber is replaced with an optical attenuator with the same loss to keep the seed power into the RSOA

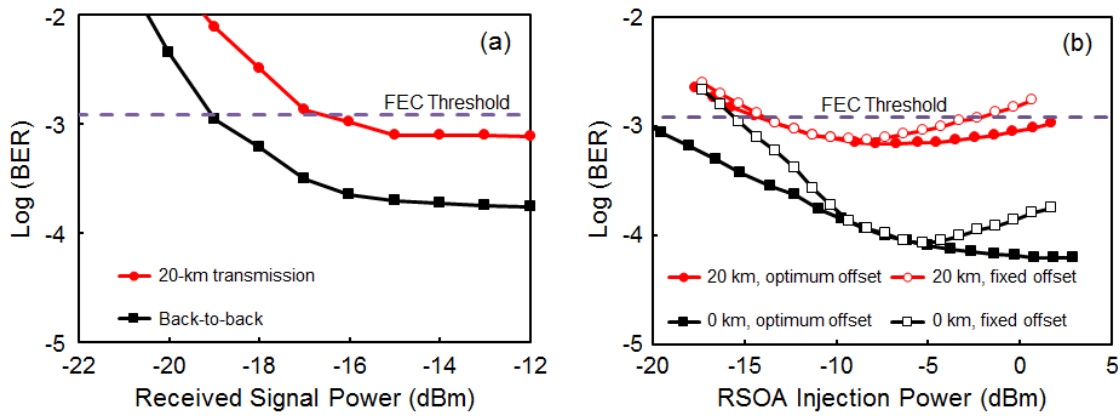


Figure 5.8 (a) BER curves measured at the back-to-back and after 20-km transmission with 0.17-nm offset filtering. (b) Measured BER as a function of the RSOA injection power at the back-to-back and after 20-km transmission. The optical power at the receiver is set to be -15dBm. The de-emphasis of 6dB is employed for both measurements.

unchanged. The results show that compared to the 20-km transmission, the error floor is improved to around 10^{-4} . Since the signal-to-Rayleigh-scattering ratio is measured to be 25.7 dB in the 20-km link and this scattering ratio turns out to have a negligible effect on the BER performance, it can be concluded that the error floor observed after transmission should be ascribed to fiber dispersion effects. When a gain-saturated SOA is employed to suppress the EIN of the SSIL source, a strong intensity correlation is created between wavelength components of the light source [17]. Fiber chromatic dispersion induces temporal walk-off between the wavelength components and serves to break the intensity correlation [20]. Consequently, the EIN suppression achieved by the SOA is negated, and the EIN increases with the accumulated fiber dispersion. Nevertheless, a decent receiver sensitivity (at an uncorrected BER of 1.2×10^{-3}) of -16.6 dBm can be obtained after upstream transmission.

Lastly, the acceptable range of RSOA injection power is measured which can achieve BERs lower than the FEC threshold. Figure 5.8(b) shows the BER measured at the received power of -15 dBm as a function of RSOA injection power. The injection power is adjusted by controlling the fiber launch power of the ultra-narrow SSIL source. The figure shows that the BER after 20-km transmission exhibits a bathtub curve with its minimum at the RSOA injection power of -7 dBm when the filter offset is set to be optimum for each point. This behavior of the BER curve can be explained as follows. When the RSOA injection power is low, the system will suffer from insufficient EIN suppression by the RSOA. On the other hand, when the RSOA injection power becomes high (by increasing the fiber launch power), the system performance is deteriorated by low signal-to-Rayleigh-scattering ratio. This is because Rayleigh-back-scattered light increases with the fiber

launch power but high RSOA injection power leads to a low optical gain of RSOA and thus reduced the signal-to-Rayleigh-scattering ratio. This section also finds that the optimum filtering offset moves to a longer wavelength as the RSOA injection power decreases. For example, the optimum filter offset shifts from 0.17 to 0.15 nm as the RSOA injection power increases from -17.3 to 7.8 dBm. This is because the slope of the filter should be increased to cancel the EIN when the RSOA injection power is low and thus, the EIN suppression is not sufficient. In multi-channel WDM-PON systems, fiber launch power may vary from channel to channel due to the non-flat spectral profile of the ASE source. In this case, the filtering offset cannot be optimized according to the RSOA injection power. This is because the filtering offset should be identical all over the WDM channels in SSIL-seeded WDM-PON systems. Therefore, the acceptable range of RSOA injection power is also measured with the filtering offset fixed to 0.17 nm. Figure 5.8(b) shows that the measured BERs after 20-km transmission are lower than the FEC threshold when the RSOA injection power ranges from -2.3 to -13.3 dBm. It implies the seed power variation of 11 dB is acceptable in multi-channel WDM-PON systems. The acceptable range can be increased when the transmission distance is shorter than 20 km. The back-to-back measurement in Figure 5.8(b) shows that successful upstream transmission can be achieved as long as the RSOA injection power is larger than -15 dBm.

5.3.4 Summary

The upstream transmission of 5.35-Gb/s signals generated from the RSOA seeded by ultra-narrow SSIL is measured. The light source can generate an incoherent comb signal

with narrow-linewidth teeth, each being demultiplexed at the remote node to be used as a wavelength-specific seed light for RSOAs at the customer premises. The single-port semiconductor optoelectronic device not only suppresses the EIN inherent in the incoherent light but also impose upstream data through direct modulation. Thus, the demonstrated system can be implemented in a cost-effective manner for upstream WDM-PON systems. Thanks to de-emphasis, offset optical filtering ultra-narrow linewidth of the source, a BER lower than 10^{-3} can be achieved after transmission over 20-km loopback configured SSMF link without any dispersion compensation. This section also shows that the demonstrated system can tolerate an 11-dB variation of the ASE power from channel to channel.

5.4 Conclusion

This chapter first demonstrates the upstream transmission of 10-Gb/s signal generated by using an ultra-narrow SSIL in a loopback configured 20-km SSMF link. The 25-nm wavelength operation of the 10-Gb/s signals is also demonstrated to confirm the feasibility of 320-Gb/s capacity in C-band window using the ultra-narrow SSIL source.

To further improve the cost effectiveness, the upstream transmission of 5.35-Gb/s signals generated from the RSOA has been demonstrated, which is seeded by ultra-narrow SSIL. The single-port RSOA not only suppresses the EIN inherent in the incoherent light source but also impose upstream data through direct modulation. The 6-dB de-emphasis and offset optical filtering are applied to accommodate the 5.35-Gb/s signal in the 1.4-GHz-bandwidth RSOA and suppress the EIN, respectively. Also, the offset optical filtering is exploited to reduce the existing EIN, which remains after EIN suppression using the

gain-saturated SOA. With the benefits of these two techniques and ultra-narrow linewidth of the source, the BER is achieved to be lower than 10^{-3} after transmission over 20-km loopback configured SSMF link without any dispersion compensation. Thus, the demonstrated system can be implemented in a cost-effective manner for upstream WDM-PON systems.

Chapter 6

Downstream Transmission Using Ultra-narrow SSIL in WDM-PON Systems

6.1 Introduction

The SSIL source offers many advantages to cost-effective implementation of WDM-PON systems, such as simultaneous generation of multiple wavelength channels and high robustness against optical reflection. Thus, the SSIL sources have long been considered as one of the promising candidates for light sources of WDM-PONs [11-13]. However, the biggest drawback of this light source is the significant EIN (EIN), which is originated by the spontaneous-spontaneous beating between different wavelength components of the spectrum-sliced light. The EIN bandwidth is governed by the optical bandwidth of the light source B_o . A large B_o extends the EIN over high frequencies at the receiver and consequently lowers the power spectral density of the noise which distorts the signal quality. Thus, the SNR of the SSIL signal is limited by B_o/B_e , where B_e is the electrical bandwidth of the receiver. The conventional way of reducing the deleterious effects of this EIN and increasing the data rate is to broaden B_o [11, 15]. This is to maintain the SNR of the signal even though B_e is increased to accommodate the higher data rate signal. However, this approach imposes many problems: not only this approach is unhelpful to

improve the capacity of the system, but it also makes the signal susceptible to optical filtering and fiber dispersion. Therefore, previously reported 10-Gb/s transmission experiments using SSIL sources are all demonstrated with the help of dispersion-shifted fiber or using DCMs.

This chapter investigates the available performance of the signal using the ultra-narrow SSIL in downstream transmission. The reach extension of a 10-Gb/s SSIL signal using EDC is first experimentally demonstrated. It is the first time the EDC is utilized for an incoherent light signal. By using a DFE having a 3-tap transversal filter and 7-tap feedback filter; the 10-Gb/s signal over 50-km SSMF is successfully transmitted. 50-km is the longest transmission distance over dispersion-uncompensated SSMF link ever achieved by using a 10-Gb/s SSIL signal.

Furthermore, a 25-Gb/s/channel SSIL-seeded WDM-PON system, for the first time to the knowledge, is experimentally demonstrated in this chapter. An ultra-narrow SSIL is employed to make the 25-Gb/s signal robust against the CD and optical filtering. However, the SSIL source having an ultra-narrow linewidth suffers from significant EIN. To suppress this noise, a gain-saturated SOA and the offset optical filtering are exploited [33, 38]. The waveform distortions caused by CD are mitigated by using the EDC. With the aid of these techniques, the 25-Gb/s OOK signal can be transmitted over 20-km SSMF. To the best of the knowledge, this is the first time that the signal using SSIL source could provide the transmission at rate higher than 10 Gb/s/channel.

6.2 50-km Transmission of 10-Gb/s SSIL signals using EDC

6.2.1 Introduction

Cost-effective implementation and maintenance of wavelength-specific light sources have long been a major stumbling block to widespread deployment of WDM-PONs. An SSIL source has attracted a significant amount of attention as a solution to this issue. The biggest drawback of SSIL sources, compared to conventional wavelength-specific distributed feedback lasers, is the significant EIN created by the spontaneous-spontaneous beating between different wavelength components of the spectrum-sliced light [11].

Even though the low-frequency (typically less than 2 GHz) EIN can be suppressed by using an FFNR circuit [24] or a gain-saturated SOA [30], the conventional approach to relieving this adverse EIN was to increase the optical linewidth of the source, B_o . This phenomenon is because that the SNR of the unpolarized SSIL is governed by B_o/B_e , where B_e is the electrical bandwidth of the receiver [11]. However, a large B_o not only reduces the spectral efficiency of the SSIL system but it also makes the optical signal vulnerable to fiber dispersion and optical filtering. Therefore, previously reported 10-Gb/s transmission experiments using an SSIL source are all performed over dispersion-shifted fiber or using DCMs.

This section demonstrates through experiment the reach extension of a 10-Gb/s SSIL signal using EDC without any costly optical dispersion compensation techniques. It is the first time the EDC is utilized for an incoherent light signal. By using a DFE having a 3-tap

transversal filter and 7-tap feedback filter; the 10-Gb/s signal is successfully transmitted over 50-km SSMF. 50-km is the longest transmission distance over dispersion-uncompensated SSMF link ever achieved by using a 10-Gb/s SSIL signal.

6.2.2 Experimental setup

The experimental setup is depicted in Figure 6.1. An EDFA with no input signal first generates an unpolarized wideband ASE, which is then spectrally sliced by using an FFP filter. The 3-dB bandwidth and FSR of the filter are 400 MHz and 102 GHz, respectively. After optical amplification, one of the FFP modes located at 1542 nm is selected by an AWG (bandwidth is 0.4 nm). The ultra-narrow spectrum-sliced light is then sent to an SOA for EIN suppression. The SOA used is biased at 200 mA and provides an optical gain of 6.1 dB at this bias current when the input power is 5.3 dBm. The saturation input power of the SOA is -15 dBm, and hence, the SOA operates in a deep saturation mode. The EIN-suppressed incoherent light is fed to a polarization-insensitive EAM driven at a 12.5-Gb/s NRZ pseudo-random bit sequence (length is $2^{15}-1$). It is assumed that a concatenated FEC

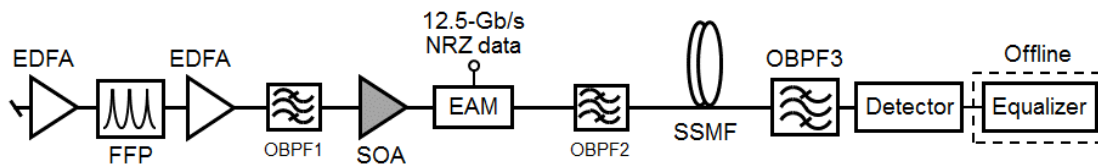


Figure 6.1 Experimental setup of 12.5-Gb/s SSIL-based transmission. Electronic equalizer is utilized to extend the transmission distance.

with an overhead of 25% is utilized. For example, the concatenated RS(255, 129) + convolutional self-orthogonal code (n_0/k_0 is 7/6, J is 8) can achieve a BER of 10^{-12} for signals with an uncorrected BER of 5.8×10^{-3} . The modulated incoherent signal is amplified to 5 dBm and launched to SSMF. At the end of the transmission fiber, the signal is sent to an optical bandpass filter, which emulates an AWG at the remote node. Then, the signal is detected with a 50-Gsample/s real-time oscilloscope after the optical-to-electrical conversion of a PIN-FET detector. Electrical equalization and direct error counting are performed offline using 10 million samples of data.

6.2.3 Results and discussion

This section first investigates the impact of fiber chromatic dispersion on the ultra-narrow SSIL signal. It has been shown that the GS-SOA suppresses the intensity noise by creating the intensity correlation between the components of the output light at different wavelengths [20, 17]. However, wavelength-dependent optical phenomena such as fiber dispersion and narrow optical filtering break this correlation and consequently undo the EIN suppression [20, 17]. To isolate the waveform distortions from the EIN increase caused by relationship breakdown, eye diagrams is constructed using averaged waveforms of the signal, as shown in Figure 6.2. Thus, the eye closure in these eye diagrams is mainly

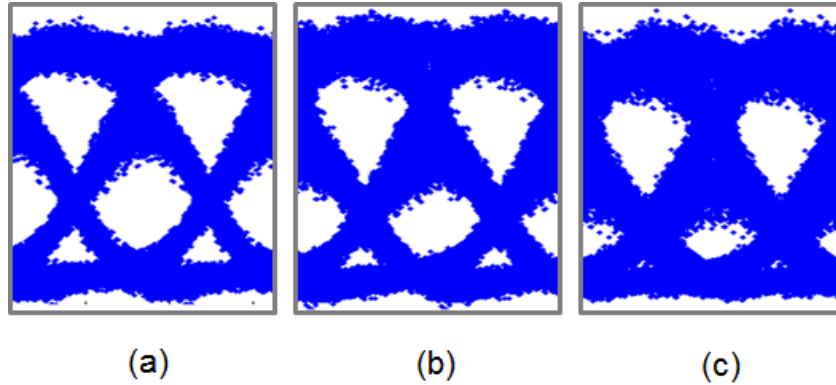


Figure 6.2 Eye diagrams constructed from averaged waveforms of the signal at (a) 0 km, (b) 20 km, and (c) 50 km.

caused by dispersion-induced waveform distortions rather than the EIN of the light source. Without the SSMF (i.e. back-to-back operation), some eye closure exists due to the limited bandwidth of the EAM and photo-detector. As the transmission distance increases, one noticeable feature of the eye diagrams is that the eye closure mainly comes from reduced amplitude of isolated marks. As the fiber dispersion increases, isolated marks fast lose their localized energy.

Next, the Q-factor of the isolated mark in ‘000010000’ patterns is measured to investigate the effect of fiber dispersion on the EIN increase. Figure 6.3 shows the results. The Q-factor is calculated to be $(I_1 - I_0)/\sigma_1$. The term I_1 is the average photocurrent of the isolated mark, I_0 is the average photocurrent of the spaces, and σ_1 is the standard deviation of the isolated mark. It clearly shows that the fiber dispersion serves to break the EIN created by the gain-saturated SOA even though the optical linewidth of the proposed

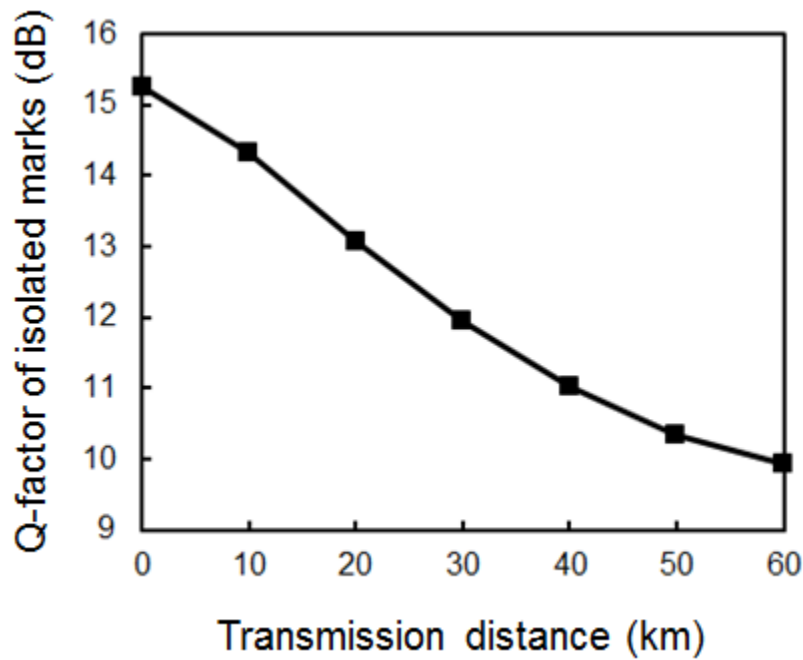


Figure 6.3 Q-factor of the isolated mark in '00001000' pattern versus the transmission distance over SSMF.

light source is measured to be about 1 GHz only. This is because the spectral expansion produced by the 12.5-Gb/s data modulation makes the signal susceptible to wavelength-dependent optical phenomena including fiber dispersion. From Figure 6.2 and 6.3, it can be concluded that the transmission performance of ultra-narrow spectrum-sliced light signals would be limited by a poor SNR of isolated marks, which comes from both the reduced amplitude of the separate marks and the EIN increased by correlation breakdown.

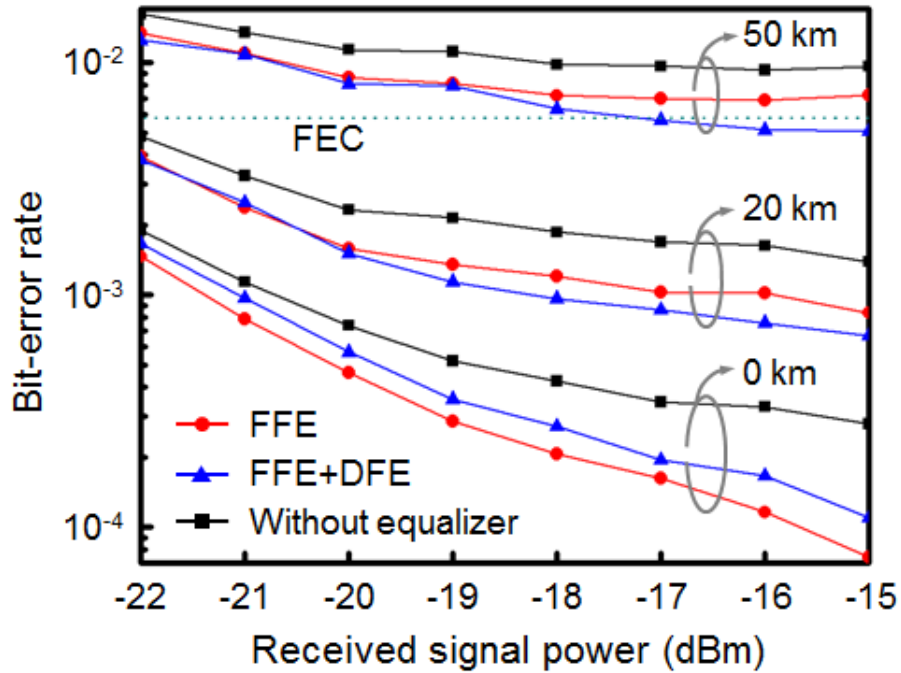


Figure 6.4 Measured BER curves after 0-, 20-, and 50-km transmission.

Figure 6.4 shows the BER curves. For post-detection electronic equalization, an electronic equalizer composed of either feedforward equalizer (FFE) or FFE plus DFE is exploited. The tap coefficients of the equalizer are determined according to the least mean square algorithm. The structure of the FFE and DFE is illustrated in Appendix B. At the back-to-back operation, the receiver sensitivity (at a BER of 5.8×10^{-3}) is measured to be better than -22 dBm without any equalization. An error floor is observed to be at around 3×10^{-4} . The error level rises as the transmission distance increases. For example, the receiver sensitivities at -15 dBm received signal power are measured to be 1.6×10^{-3} and

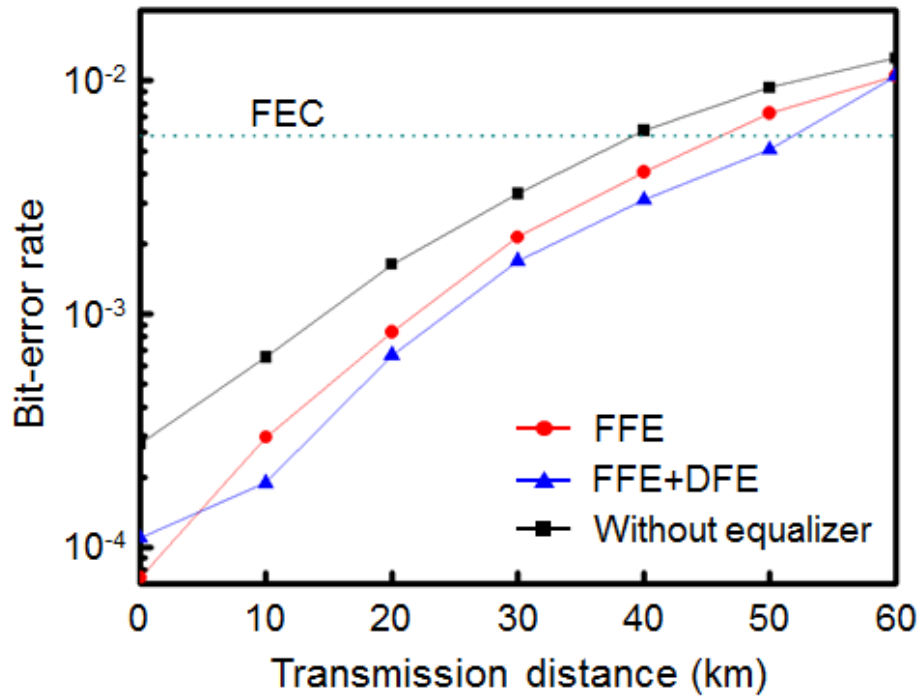


Figure 6.5 BER performance versus transmission distance.

9×10^{-3} after 20- and 50-km transmission, respectively. This degradation should be attributed to the reduced amplitude of isolated marks and the increased EIN, as analyzed in the previous paragraph. The electronic equalization enhances the amplitude of isolated marks and thus the BER performance. For example, the BER is improved by up to a factor of 4 at the back-to-back operation when a 6-tap FFE is employed. EDC also enhances the BER after transmission. The BER performance versus the transmission distance is summarized in Figure 6.5. In this plot, the received signal power is -15 dBm. Since the significant performance improvement is achieved by using low-tap number equalizers, the

maximum number of taps is limited to 7. The figure shows that the longest transmission distance without EDC is less than 40 km. With the FFE only, however, it is available to bridge up to 40 km over SSMF. With 3-tap FFE+7-tap DFE, the transmission distance can be further improved up to 50 km, beyond which would be limited by the increased EIN.

It is worth noting that bit errors mostly occur at the isolated marks in the system and thus single-bit errors overwhelmingly dominate over consecutive errors. Therefore, it is expected that the FEC designed for non-burst random noise (e.g., additive white Gaussian noise) would work for the system.

6.2.4 Summary

This section has demonstrated through experiment the Transmission of 10-Gb/s ultra-narrow SSIL signal over 50-km SSMF using electronic equalization. Ultra-narrow linewidth of the light source makes the signal less susceptible to fiber dispersion than the conventional spectrum-sliced light signal and also allows us to utilize the EDC. Owing to the EIN increase caused by correlation breakdown, the reach extension achieved by using electrical equalization is limited to about 25%.

6.3 25-Gb/s/per-channel WDM-PON Using SSIL sources

6.3.1 Introduction

WDM-PONs, thanks to their high capacity, future-proof upgradability, and secure privacy, have been regarded as a promising solution for broadband optical access networks. However, the widespread deployment of such systems has been hindered mainly by relatively expensive WDM components including wavelength-specific light sources [3]. To lower the implementation, operation, and maintenance costs of WDM-PON systems, extensive attention has been paid to cost-effective colorless transmitters such as SSIL seeded optical transmitters [11, 43, 36, 37, 18]. In WDM-PON systems based on these optical transmitters, a broadband ASE light is spectrum-sliced by an AWG and fed as seed lights to colorless optical modulators including RSOAs and electro-absorption modulators. Thus, these WDM-PON systems could be implemented cost-effectively without requiring costly wavelength-specific optical transmitters. The WDM-PON systems based on SSIL-seeded optical transmitters have been approved by ITU-T as an international standard for PONs providing 1.25-Gb/s/channel data services [13].

However, the potential of the SSIL-seeded optical transmitters to offer greater than 10-Gb/s/channel services is very unclear. This is because that the performance of these optical transmitters is limited by the spontaneous-spontaneous beat noise of the incoherent ASE light. The SNR of the SSIL-seeded optical transmitter is governed by B_o/B_e , where B_o is the optical linewidth of the SSIL source and B_e is the receiver electrical bandwidth

[11]. The use of a gain-saturated SOA has been proposed to suppress the beat noise [54], but a large B_o should be still exploited to accommodate high-speed signals [36, 37]. For example, it is necessary to have B_o greater than 0.5 nm to accommodate 10-Gb/s data rate. However, a large B_o makes the signal susceptible to fiber chromatic dispersion and optical filtering (by AWGs in the network), and more importantly it limits the total capacity of WDM-PON system [43]. For these reasons, all the previously demonstrated SSIL-seeded WDM-PON systems were limited to 10 Gb/s/channel.

This chapter experimentally demonstrates, for the first time to our knowledge, a 25-Gb/s/channel SSIL-seeded WDM-PON system. To make the 25-Gb/s signal robust against the CD and optical filtering, the ultra-narrow-linewidth SSIL [43] is exploited. However, the SSIL source having an ultra-narrow linewidth suffers from significant EIN. To suppress this noise, a gain-saturated SOA and offset optical filtering [33, 38] are utilized. The waveform distortions caused by CD are mitigated by using the EDC. With the aid of these techniques, the 25-Gb/s OOK signal can be transmitted over 20-km SSMF.

6.3.2 Experimental setup

Figure 6.6 (a) shows the experimental setup. A wideband ASE generated from an EDFA with no input signal is first spectrum-sliced by an FFP filter. The FFP filter used in this experiment has a 3-dB bandwidth of 0.005 nm (is 700 MHz) and an FSR of 0.82 nm. This ultra-narrow spectrum pre-slicing localizes the optical power of the SSIL-seeded light at around the center of the passbands of AWGs in the network. Thus, it not only minimizes

the power loss of the signal incurred by the AWGs in the network but also greatly improves the energy consumption of the SSIL source [18]. Due to the periodicity of the passbands

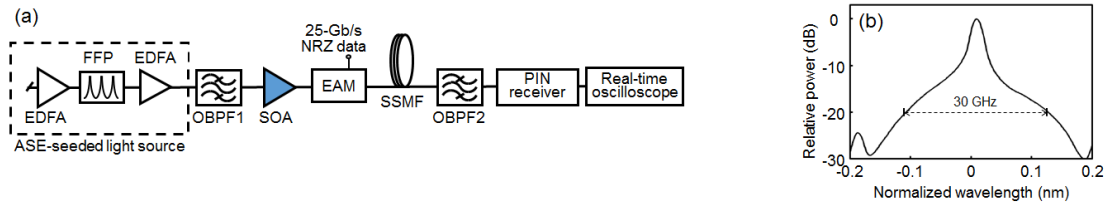


Figure 6.6 (a) Experimental setup of 25-Gb/s/channel SSIL-seeded transmission (b) The optical spectrum of the 25-Gb/s OOK signal measured at the output of the modulator.

of the FFP, only one FFP filter is required for the generation of multiple WDM lights. One of the periodic passbands of the spectrum pre-sliced ASE is selected by using an optical bandpass filter, which emulates an AWG at the central office. The ultra-narrow SSIL at 1542.37 nm is then sent to a gain-saturated SOA for the suppression of the beat noise inherent in the incoherent ASE light. The SOA has a small signal gain of 22 dB and a saturation input power of -15 dBm when biased at 200 mA. The optical power of the SSIL into the SOA is set to be 1.5 dBm. Thus, the SOA operates in the saturation regime. For data modulation, the SSIL is fed to an EAM driven by a 25-Gb/s non-return-to-zero signal. The modulation bandwidth of the EAM is measured to be 15 GHz. Figure 6.6(b) shows the optical spectrum of the signal measured at the output of the EAM. Due to the ultra-narrow linewidth of the SSIL, the spectral width of the signal is determined by data modulation and its 20-dB spectral width is measured to be 30 GHz. This signal can be fit into a dense WDM grid with a 50-GHz channel spacing. The 25-Gb/s OOK signal is launched into

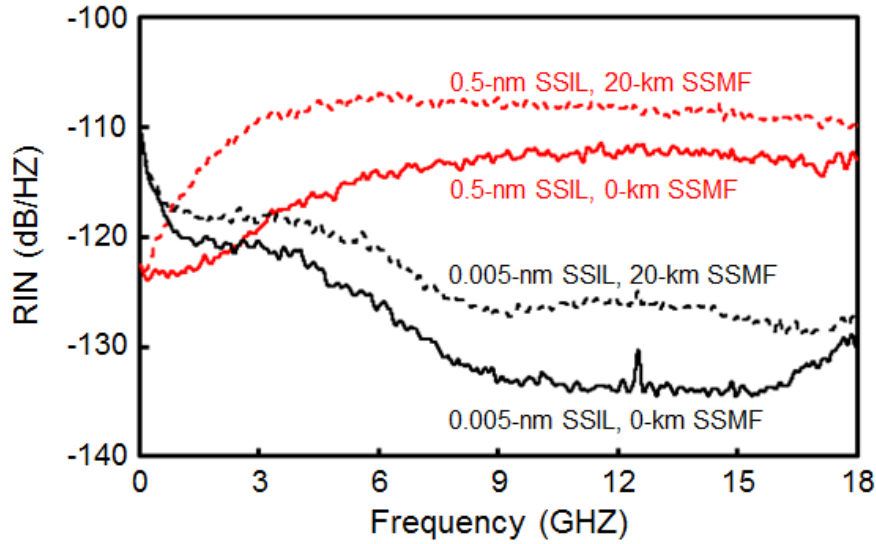


Figure 6.7 RIN of the SSIL sources with two different linewidths measured at the output of the SOA.

SSMF and then fed to OBPF2 (passband center equals 1542.14nm, 3-dB bandwidth is 0.64 nm) before direct detection. This optical filter emulates an AWG located at the remote node. The detected signal is sampled by using a 100-Gsample/s oscilloscope and processed off-line. To compensate for the CD and band-limitation of the modulator, a half-symbol-spaced 4-tap FFE followed by a 2-tap DFE is employed. The tap coefficients of the equalizer are determined by the minimum mean-square error criterion.

6.3.3 Results and discussion

This section first shows the efficacy of the use of ultra-narrow-linewidth SSIL. Figure 6.7 shows the RIN of the two SSILs having different linewidths measured at the output of

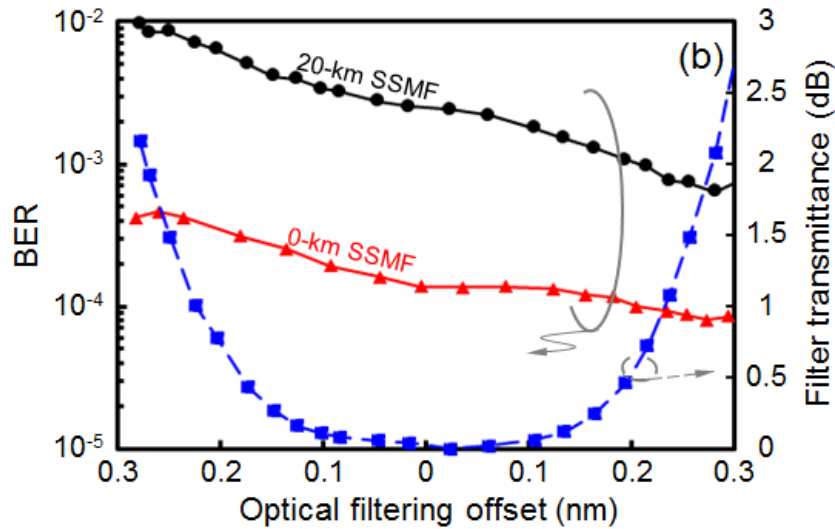


Figure 6.8 Measured BER performance of the 25-Gb/s OOK signal as a function of the optical filtering offset. Also plotted is the power loss incurred by offset filtering.

the SOA. No data modulation is applied to observe the RIN only. When the linewidth of the SSIL is 0.5 nm, the RIN is lower than -120 dB/Hz below 3 GHz. The RIN increases to higher than -113 dB/Hz beyond 9 GHz since the high-frequency RIN is not suppressed by the SOA. After transmission over 20-km SSMF, the RIN rises considerably since the spontaneous-spontaneous beat noise suppressed by the SOA is restored by CD [20]. The SOA suppresses the beat noise by creating an intensity correlation between different wavelength components of the SSIL. However, this correlation is vulnerable to wavelength-dependent phenomena and thus can be broken by CD [20]. On the other hand, the SSIL having a 0.005-nm linewidth has much lower RIN than the wide-linewidth SSIL.

Except at the frequencies lower than 1 GHz, the measured RIN is lower than -120 dB/Hz. Owing to the ultra-narrow linewidth of the SSIL sources, this RIN is also kept relatively low after 20-km transmission. Thus, the ASE seed light with an ultra-narrow linewidth outperforms the wide-linewidth SSIL regarding RIN and tolerance to CD and consequently is more suitable for 25-Gb/s transmission.

Next, the BER improvement produced by the offset optical filtering is investigated. Figure 6.8 displays the BER performance of the signal as a function of the wavelength offset between the SSIL and OBPF2. The offset optical filtering is achieved by tuning the passbands of the FFP filter without touching OBPF2. Thus, this offset filtering technique does not increase the complexity of the WDM-PON system. The results clearly show that the BER is improved when the SSIL is detuned to longer wavelengths. For example, the BER measured after 20-km transmission is reduced from 2.4×10^{-3} to 7.5×10^{-4} when the wavelength of the SSIL shifts from 1542.14 to 1542.37 nm (i.e., 0.23-nm offset). This performance improvement should be attributed to the fact that a gain-saturated SOA creates a correlation between amplitude and frequency (or chirp) of the SSIL and then the offset optical filtering converts the chirp into amplitude to produce destructive interference with the existing beat noise of the SSIL [38]. Although 0.23-nm offset filtering increases the link loss by 1.1 dB, it could be readily compensated by slightly increasing fiber launch power. The optimum amount of filtering offset remains unchanged regardless of the transmission distance.

Figure 6.9 shows the measured receiver sensitivity (when the BER is 10^{-3}) of the 25-Gb/s OOK signal as a function of the transmission distance. Without using the EDC and offset optical filtering, a receiver sensitivity of -15.7 dBm is achieved, but after 6-km

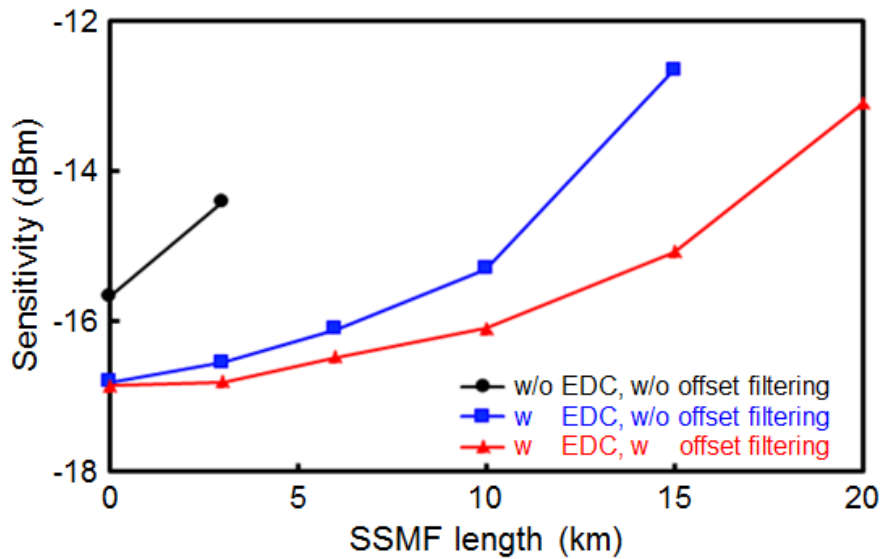


Figure 6.9 Measured sensitivity (BER is 10^{-3}) versus the transmission distance.

transmission an error floor at around 1.8×10^{-3} is observed. In the presence of EDC at the receiver, the receiver sensitivity is improved by 1.1 dB in the back-to-back condition since the EDC compensates for the band-limitation of the modulator. The EDC also compensates for the waveform distortions caused by CD and enables us to transmit the 25-Gb/s signal up to 15-km-long SSMF. Figure 6.9 shows that the efficacy of offset optical filtering is improved as the transmission distance increases. This is because the correlation between amplitude variation and the chirp of the seed light is enhanced with the transmission distance [38]. With the aid of the EDC and offset filtering, the 25-Gb/s signal can be transmitted over 20-km-long SSMF.

Figure 6.10 shows the measured BER curves of the 25-Gb/s OOK signal. The 0.23-nm offset filtering is employed, and the EDC is used at the receiver. In the back-to-back condition, the receiver sensitivity is measured to be -16.8 dBm. After transmission over 20-km-long SSMF, the receiver sensitivity is degraded to -12.8 dBm, but BERs lower than the forward error correction threshold of 10^{-3} can be achieved. The penalty after the transmission is caused by the enhanced spontaneous-spontaneous beat noise, as explained

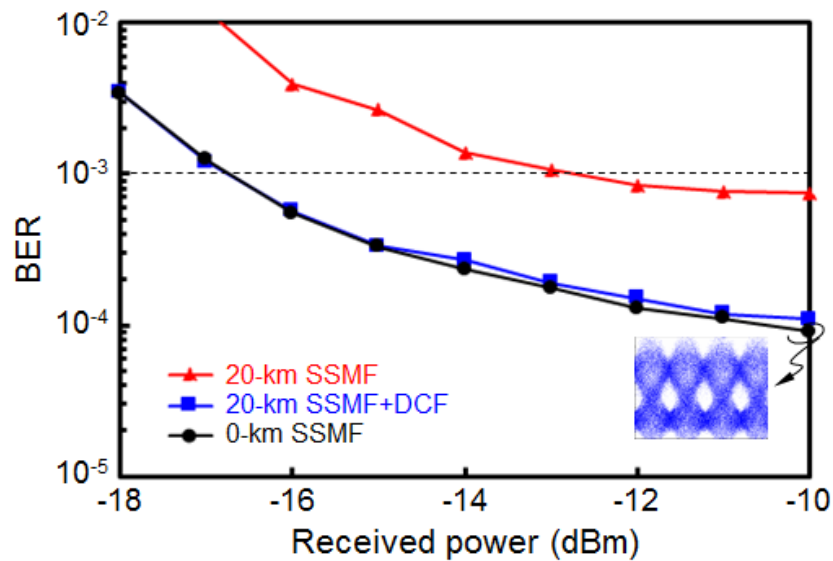


Figure 6.10 Measured BER as a function of received power. The inset is the eye diagram of the signal at the output of the EDC.

in the previous page. Thus, the BER performance after transmission can be considerably improved by using optical dispersion compensation. Figure 6.10 also shows the measured BER curve when a dispersion compensating fiber is inserted into the network. The amount

of dispersion and insertion loss of the DCF are -400 ps/ nm and 3.0 dB, respectively. The result shows that when the fiber CD is compensated, the performance after 20-km transmission is almost the same as the back-to-back performance. Thus, in WDM-PON systems having a large number of channels, a DCF module could be used in the systems to compensate for the fiber dispersion all over the WDM channels.

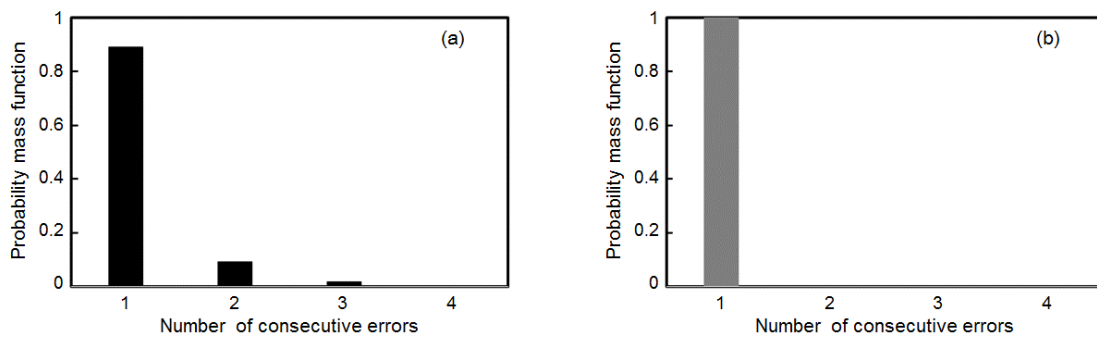


Figure 6.11 (a) Measured PMF of the number of consecutive errors in the back-to-back operation (BER is 10^{-4}) (b) The PMF of the number of consecutive errors of the signal with Gaussian noise.

6.3.4 FEC selection

In previous studies, the FEC coding is utilized to relax the BER requirement from 10^{-12} to 1.2×10^{-3} or 5.8×10^{-3} at the expense of 7% or 12.5% overhead, respectively. To further investigate the suitable FEC code for the ultra-narrow SSIL utilized with a gain-saturated SOA, the statistical characteristics of the error occurrences is firstly identified. The EIN of the SSIL source is not solely Gaussian-like noise [47]. With sufficient noise suppression of GS SOA, this EIN would exhibit

Gaussian distribution and the actual distribution would change with the transmission distance as well as the transmission capacity.

The probability mass function (PMF) of the number of consecutive errors (BER is 10^{-4}) is measured in Figure 6.11 (a). This figure demonstrates that there exist the consecutive errors (i.e., burst errors), and the majority of the burst error have a length of 2 bits. This is in contrast to the case of Gaussian noise, where the probability of burst error is minuscule as shown in Figure 6.11 (b). Therefore, to obtain the better BER improvement, the FEC is required to correct the relatively short burst errors as well as the random errors. To correct the burst errors, the FEC codes can be

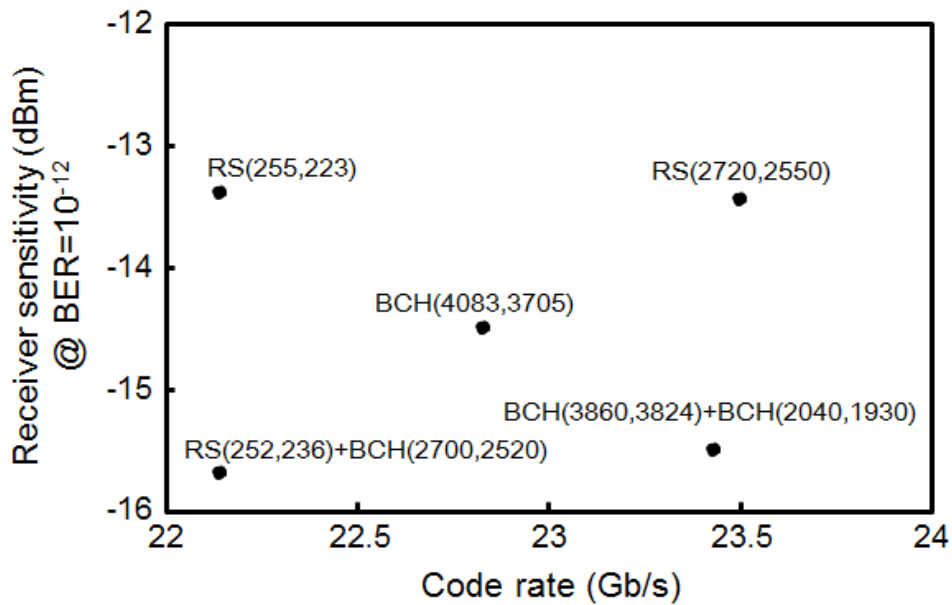


Figure 6.12 Measured receiver sensitivity versus code rate (without FEC overhead) for various FEC codes.

utilized, which are based on non-binary Galois fields (e.g. interleaved Bose-Chaudhuri-Hocquenghem codes (BCH codes) or RS codes) [55, 79].

Moreover, to relax the BER threshold, an FEC code with higher FEC coding/decoding complexity and larger overhead is typically expected to obtain a larger net coding gain. To evaluate the impact of FEC complexity and overhead, the receiver sensitivity (at FEC corrected BER equals 10^{-12}) is measured as a function of the code rate for FEC codes with various overhead. The SOA optical injection power was fixed to be 1.5 dBm.

The line rate is set to be 25 Gb/s (including the overhead of FEC codes). Hence, the horizontal axis shows the code rate without considering the FEC overheads. The vertical axis shows the required optical received power after transmission over 20-km SSMF. Increasing the FEC overhead (i.e. lower code rate) could always obtain higher coding gain [80]. However, Figure 6.12 shows that higher FEC code overhead cannot necessarily improve the receiver sensitivity. This was because that increasing the FEC complexity could improve the coding gain with lower FEC overhead [80].

Thus, it is necessary to utilize an efficient FEC (i.e. high coding gain with small overhead) for the SSIL-seeded WDM-PON systems. Among the FEC codes evaluated in Figure 6.12, the Reed-Solomon codes and Bose-Chaudhuri-Hocquenghem codes are investigated, such as RS(255, 223), RS(2720,2550), BCH(4083, 3705), the concatenated scheme using RS(252,236) as outer and BCH(2700,2520) as inner code and another concatenated scheme using BCH(3860, 3824) as outer code and BCH(2040, 1930) as inner code. Both of these codes could reduce the error floor and extend the reach distance up to 20 km.

Moreover, as previously discussed, the EIN would result in some burst errors, which would slightly change the coding gain of FEC codes [81]. Although RS codes and BCH codes are based on non-binary Galois fields and could correct the burst error, it is necessary to do the practical experiments to confirm the effectiveness of the FEC codes in the SSIL-seeded WDM-PONs.

6.3.5 Summary

This section has experimentally demonstrated a 25-Gb/s/channel WDM-PON system based on SSIL-seeded light sources. Thanks to the spectrum pre-slicing by using an ultra-narrow FFP filter, offset optical filtering, and EDC, a 25-Gb/s OOK signal over 20-km SSMF is successfully transmitted at BER lower than 10^{-3} .

6.4 Conclusion

This chapter has demonstrated the available performance using ultra-narrow SSIL source in downstream transmission. Thanks to the strong tolerance to optical dispersion of the ultra-narrow SSIL, the 10-Gb/s signal could be transmitted over 35-km at BER threshold (i.e. 5.8×10^{-3}) without any dispersion compensation. With the assistance of simple electronic equalization (i.e. 3 tap FFE + 7-tap DFE), the reach extension could be larger than 25%.

Furthermore, through the offset optical filtering and electronic equalization, a 25-Gb/s/channel WDM-PON system has been successfully experimentally demonstrated based on SSIL-seeded light sources at BER lower than 10^{-3} . To the best of our knowledge, this is the first time that the SSIL-seeded light sources could transmit signals at a data rate higher than 12.5 Gb/s/channel.

Chapter 7

Conclusions and Future Works

7.1 Conclusions

Chapter 3 has conducted the experimental and simulation studies on the optimum linewidth of SSIL source using a GS-SOA (as an EIN suppressor) for the maximum capacity and longest transmission distance. The BER performances of the 10-Gb/s OOK signal generated by using the SSIL source are evaluated over a wide range of source linewidth. Chapter 3 has found out that there are two windows of linewidth for high-speed operation of the SSIL source: very broad (i.e., the linewidth is much wider than the receiver bandwidth) and ultra-narrow (i.e., the linewidth is much narrower than the receiver bandwidth) and. However, when the SSIL linewidth is very broad, the fiber chromatic dispersion and narrow optical filtering serve to break the intensity correlation created by the GS-SOA, and consequently, the BER performances of the 10-Gb/s signal are considerably deteriorated after transmission. Thus, the optimum linewidth for capacity and transmission distance is found to be ultra-narrow. For example, as shown in the simulation, by using ultra-narrow SSIL sources with a 200-MHz linewidth, it is possible to transmit the 10-Gb/s OOK signal over 60-km long dispersion-uncompensated SSMF. Moreover, the channel spacing can be reduced as narrow as 13.2 GHz for the 10-Gb/s signals and thus it is feasible to implement an ultra-dense WDM system with the spectral efficiency of 0.75

b/s/Hz. However, these benefits come at the expense of large spectrum-slicing loss and immense optical input power into the SOA. It has been shown that the ultra-narrow optical filtering of a wideband ASE induces a significant spectrum-slicing loss. The SOA input power of the SSIL required to suppress the EIN sufficiently is also increased when the linewidth of the SSIL is ultra-narrow. However, these enhanced requirements of optical power could be readily satisfied by using high-gain and/or high-power optical amplifiers. The cost of these optical amplifiers can be shared by multiple channels and thus becomes insignificant as the number of WDM channels increases. It has also been demonstrated that the use of ultra-narrow SSIL sources makes the signal susceptible to in-band crosstalk possibly caused by Rayleigh backscattering and optical reflection in WDM-PON systems. Nevertheless, the experimental and simulation results show that the 10-Gb/s OOK signal generated by using the ultra-narrow SSIL source with a 700-MHz linewidth is robust against in-band crosstalk as large as -14 dB on the signal. Therefore, the ultra-narrow SSIL sources could be used to implement high-capacity WDM-PON systems cost-effectively.

Chapter 4 have proposed and demonstrated the offset optical filtering technique cooperated with the gain-saturated SOA to reduce the existing EIN of the ultra-narrow SSIL source. It has been shown that a negative correlation exists between amplitude and frequency of the light and it becomes stronger as the transmission distance over SSMF increases. It is also found that offset optical filtering converts the frequency waveform into amplitude and produces destructive interference with the EIN to reduce the noise. The proposed scheme can be implemented simply by detuning the wavelength of the AWG at the remote node, without neither incurring additional costs nor adding new components in WDM-PON systems. In the demonstration, the system suffers from a loss increase by less

than 1 dB when the offset is set to 0.12 nm. However, the proposed offset filtering improves BER floors, which are not improved by increasing the optical power at the receiver. The small reduction in power budget can be readily overcome by slightly increasing the fiber launch power.

Chapter 5 first demonstrates the upstream transmission of 10-Gb/s signal generated by using an ultra-narrow SSIL in a loopback configured 20-km SSMF link. The 25-nm wavelength operation of the 10-Gb/s signals is also shown to demonstrate the feasibility of 320-Gb/s capacity in C-band using an SSIL. To further improve the cost-effectiveness and simplify the implementation, an RSOA is utilized as a direct modulator as well as an EIN suppressor. This chapter has successfully demonstrated an upstream transmission of 5.35-Gb/s ultra-narrow SSIL signals using an RSOA over a loopback-configured 20-km link. The key enablers are offset optical filtering and de-emphasis. a BER lower than 1.2×10^{-3} is achieved with the RSOA injection power as low as -13.3 dBm.

Chapter 6 experimentally demonstrated a 25-Gb/s/channel WDM-PON system based on SSIL-seeded light sources. Thanks to the spectrum pre-slicing by using an ultra-narrow FFP filter, offset optical filtering, and EDC, a 25-Gb/s OOK signal is successfully transmitted over 20-km SSMF at BER lower than 10^{-3} . This is the first time, to the best of our knowledge, SSIL could provide service greater than 10-Gb/s/channel. This chapter also demonstrated through experiment the transmission of 10-Gb/s ultra-narrow SSIL signal over 50-km SSMF using simple electronic equalization. Ultra-narrow linewidth of the light source makes the signal less susceptible to fiber dispersion than the conventional spectrum-sliced light signal and also allows us to utilize the EDC. Owing to the EIN increase caused

by correlation breakdown, the reach extension achieved by using electrical equalization is limited to about 25%.

The findings of this thesis can help implementing WDM-PONs in a cost-effective way by utilizing ultra-narrow SSILs with efficient EIN-suppression techniques and FEC codes. The use of ultra-narrow SSILs is beneficial for cost-sensitive access applications since it could provide high-speed service (i.e. transmission rate larger than 25 Gb/s/channel) with narrow channel spacing and without the costly optical dispersion compensation techniques.

7.2 Future works

7.2.1 FEC

The explosive development of high-speed DSP and ADC processors have accelerated the utilization of more and more signal processing techniques in optical communication systems. Especially, the forward error correction coding greatly improves the tolerance of fiber distortion as well as the channel capacity [80-82]. Conventionally, 7% overhead is employed for the FEC coding to achieve limited performance improvement [69, b80-82]. At the expense of higher overhead ratio (e.g. 25%), the system performance can be further improved. More importantly, the third-generation FEC (e.g. soft-decision decoding low-density parity-check (LDPC) codes) [83-86] and Turbo codes [87-91] could increase the BER limitation from 10^{-3} to higher than 10^{-2} . Thus, practical FEC experiment in the optical communication system using ultra-narrow SSIL could further improve the system performance.

7.2.2 Feedforward noise reduction with ultra-narrow SSIL source

The FFNS technique has been applied to reduce the EIN of the SSIL-seeded WDM system [24]. Moreover, it has been demonstrated that this technique could work constructively with the GS-SOA method at 10-Gb/s/channel WDM system. Conventionally, the SSIL has linewidth much larger than the electrical receiver bandwidth and the EIN also has a bandwidth greater than the electrical receiver bandwidth. Thus, the FFNS performance depends on the characteristics of its feedforward noise-reduction circuits, which dramatically increases the system complexity and implementation cost. However, the EIN of ultra-narrow SSIL source is mainly located within the low-frequency band (less than 3 GHz). Hence, the FFNS can be utilized associated with the ultra-narrow SSIL, and the FFNS circuit could be independent of the data rate.

Appendix A:

SNR of Optical Signal Using SSIL

This section illustrates the derivation of (4) in details.

This derivation process is based on [59, 92]. To simplify this question, the optical amplifier is assumed to have unity gain G and uniform coupling efficiency over an optical bandwidth B_o . The input optical power is set to be P_{in} at optical frequency ω , which is centered at the optical passband B_o .

Then the optical amplifier would generate spontaneous emission power at the optical passband B_o . The power is given as below [94]

$$P_{sp} = N_{sp}(G - 1)h\nu B_o \quad (\text{A1})$$

The $h\nu$ is the photon energy, N_{sp} is the spontaneous emission factor, G is the amplifier gain, B_o is the optical bandwidth and P_{sp} is the spontaneous emission power.

In the electronic field, the spontaneous emission could be represented as E_{sp} , which is a sum of cosine terms as shown below:

$$E_{sp}(t) = \sum_{k=(-\frac{B_o}{2\delta\nu})}^{\frac{B_o}{2\delta\nu}} \sqrt{2N_{sp}(G - 1)h\nu\delta\nu} \cdot \cos((\omega_o + 2\pi k\delta\nu)t + \Phi_k) \quad (\text{A2})$$

$$N_{sp}(G - 1)h\nu = N_o \text{ and } \frac{B_o}{2\delta\nu} = M \quad (\text{A3})$$

This Φ_k denotes the random phase of the k^{th} component of the spontaneous emission. The M is the number of frequency components; each component has $\delta\nu$ bandwidth. Moreover, N_o represents the spontaneous emission noise power at the amplifier output.

Therefore, at the amplifier output, the total electrical field can be expressed as

$$E(t) = \sqrt{2GP_{in}} \cos(\omega_o t) + \sum_{k=-M}^M \sqrt{2N_o \delta v} \cdot \cos((\omega_o + 2\pi k \delta v)t + \Omega_k) \quad (A4)$$

Assuming this photodetector has unity quantum efficiency, then the photocurrent $i(t)$ is proportional to the optical intensity as shown below

$$i(t) = \overline{E^2(t)} \frac{e}{h\nu} \quad (A5)$$

The bar represents the time averaging over optical frequencies. Then the photocurrent can be expressed as

$$i(t) = GP_{in} \frac{e}{h\nu} + \frac{4e}{h\nu} \sum_{k=-M}^M \sqrt{GP_{in} N_o \delta v} \cdot \cos(\omega_o t) \cos((\omega_o + 2\pi k \delta v)t + \Phi_k) + \left[\sum_{k=-M}^M \cos((\omega_o + 2\pi k \delta v)t + \Phi_k) \right]^2 \quad (A6)$$

The three terms in (A6) indicate the signal, signal-spontaneous beating noise, and spontaneous-spontaneous beating noise, respectively [59].

Signal-Spontaneous Beating Noise

Firstly, simplify the signal-spontaneous beating noise.

$$i_{sig-sp}(t) = \frac{4e}{h\nu} \sum_{k=-M}^M \sqrt{GP_{in} N_o \delta v} \cdot \cos(\omega_o t) \cos((\omega_o + 2\pi k \delta v)t + \Phi_k) = \frac{2e}{h\nu} \sqrt{GP_{in} N_o \delta v} \sum_{k=-M}^M \cos(2\pi k \delta v t + \Phi_k) \quad (A7)$$

According to (A7), each frequency $2\pi k\delta\nu$ has two components and a random phase. Thus, the power spectrum of $i_{sig-sp}(t)$ is uniform within the frequency range $[0, B_o/2]$ and has density as

$$\begin{aligned} N_{sig-sp} &= \frac{4e^2}{(h\nu)^2} GP_{in}N_o \cdot \frac{1}{2} \cdot 2 \\ &= \frac{4e^2}{h\nu} P_{in}N_{sp}(G-1)G \quad (A8) \end{aligned}$$

Spontaneous-Spontaneous Beating Noise

Derived from the (A6), the spontaneous-spontaneous beating noise can be expressed as

$$\begin{aligned} i_{sp-sp}(t) &= 2N_o \frac{\delta\nu e}{h\nu} \left[\sum_{k=-M}^M \cos((\omega_o + 2\pi k\delta\nu)t + \Phi_k) \right]^2 \\ &= 2N_o \frac{\delta\nu e}{h\nu} \left[\sum_{k=-M}^M \cos(\beta_k) \sum_{j=-M}^M \cos(\beta_j) \right] \quad (A9) \end{aligned}$$

where $\beta_k = ((\omega_o + 2\pi k\delta\nu)t + \Phi_k)$ and $\beta_j = ((\omega_o + 2\pi j\delta\nu)t + \Phi_j)$ A(10)

The (A10) can be simplified as

$$i_{sp-sp}(t) = 2N_o \frac{\delta\nu e}{h\nu} \left[\sum_{k=-M}^M \sum_{j=-M}^M \frac{1}{2} \cos(\beta_k - \beta_j) + \frac{1}{2} \cos(\beta_k + \beta_j) \right] \quad (A11)$$

In (A11), the terms in $\cos(\beta_k + \beta_j)$ have frequencies at $2\omega_o$. Due to the limited response of the photodetector, the average of the terms in $\cos(\beta_k + \beta_j)$ is zero [59]. Thus, (A11) can be further simplified as

$$i_{sp-sp}(t) = \frac{N_o \delta v e}{h\nu} \left[\sum_{k=0}^{2M} \sum_{j=0}^{2M} \cos((k-j)2\pi\delta v t) + (\Phi_k - \Phi_j) \right] \quad (\text{A12})$$

Thus, in (A12), there are $2M$ average terms, which are obtained at $k = j$, and the average terms can be written as

$$I_{sp}^{dc} = \frac{N_o \delta v e 2M}{h\nu} = N_{sp} (G - 1) e B_o \quad (\text{A13})$$

Moreover, the power of the average components are

$$P_{sp}^{dc} = I_{sp}^{dc2} = [N_{sp} (G - 1) e B_o]^2 \quad (\text{A14})$$

Moreover, according to (A14), the terms number at different frequencies could be obtained

Frequency	Terms number
$-(2M - 1)\delta v$	1
$-(2M - 2)\delta v$	2
\vdots	\vdots
$-n\delta v$	$2M - n$
\vdots	\vdots
$n\delta v$	$2M - n$
\vdots	\vdots
$(2M - 1)\delta v$	1

Hence, the spontaneous-spontaneous beating noise has power density near dc as

$$N_{sp-sp} = \frac{(2N_o e)^2 \delta v}{h\nu^2} \left(\frac{B_o}{\delta v} - 1 \right) \cdot \frac{1}{2} = 2N_{sp}^2 (G - 1)^2 e^2 B_o \quad (\text{A15})$$

Usually, the optical bandwidth of ASE, B_o is much larger than the electrical bandwidth of the receiver B_e . Thus, the power of spontaneous-spontaneous beating noise within the electrical bandwidth (extract the average components) can be derived as

$$P_{sp}^{ac} = B_e \cdot N_{sp-sp} = 2N_{sp}^2 (G - 1)^2 e^2 B_o B_e \quad (A16)$$

In the SSIL signal, the average terms of the spontaneous-spontaneous beating are considered as the signal components while the variance terms of the spontaneous-spontaneous beating are taken as the EIN. Thus, according to (A15) and (A16), the SNR of the SSIL signal can be expressed as

$$SNR = \frac{P_{sp}^{dc}}{P_{sp}^{ac}} = \frac{B_o}{B_e} \quad (A17)$$

Appendix B:

Electronic Equalization

This section illustrates the structure of the electronic equalization, which is utilized in the upstream transmission using ultra-narrow SSIL in WDM-PON systems (i.e. Chapter 5) and downstream transmission using ultra-narrow SSIL in WDM-PON systems (i.e. Chapter 6).

In principle, all of the linear impairments could be sufficiently compensated through the digital filters [93]. The adaptive equalizer can handle everything including laser phase noise, time-varying chromatic dispersion as well as the polarization-mode dispersion. Thus, to hand the time-varying optical dispersion and other slow linear distortion effects, in the systems, the fractional DFE is utilized, which could automatically adjust its tap coefficients to compensate for the chromatic dispersion and optimize the system performance. The algorithm and structure of this equalizer are illustrated as below.

Linear equalizer: feedforward equalizer

The structure of the linear feedforward equalizer is shown in figure B.1. In the tap and delay equalizer, the interval between two adjacent taps is T . And the criterion of minimization of the mean square error (MMSE) is utilized to determine the coefficients $\{c_k\}$ of the equalizer taps.

Through the iterative algorithm, the MMSE could be eventually obtained after successive corrections of the tap weights. The principle of LMS equalizer could be illustrated by the following equations:

$$y(n) = \vec{w}^{(n)H} \cdot \vec{x}(n) \quad (\text{B1})$$

$$e(n) = d(n) - y(n) \quad (\text{B2})$$

$$\vec{w}^{(n+1)} = \vec{w}^{(n)} + \mu \vec{x}(n) \cdot e^*(n) \quad (\text{B3})$$

Here $y(n)$ is the output signal of the equalizer. $\vec{w}^{(n)} = [w[0], w[1], \dots, w[N-1]]$ is the vector of the equalizer taps' weights, and N is the tap length of the equalizer. $\vec{x}(n) = [x[n-1], x[n-2], \dots, x[n-N]]$ is the vector of the received signal samples, n is the number of the received symbol. μ is the step size of this iterative algorithm which determines the convergence of the tap weights. $e(n)$ is the error between the desired symbol and the equalized signal.

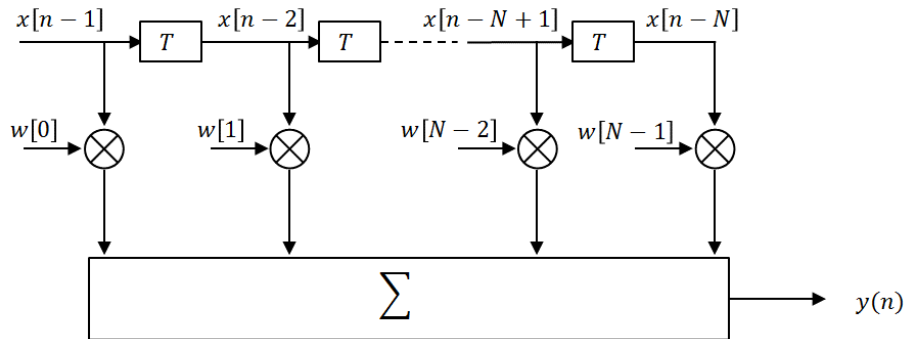


Figure B.1 Structure of symbol-spaced FFE [93].

In the above illustration, the receiver is assumed to have the knowledge of the error between the desired signal and the equalized output signal. Thus, a training sequence is utilized to initialize the equalizer's tap coefficients to be converged. In the training stage, the pre-defined training sequence is utilized as the desired signal in the receiver. After the equalizer's tap weight is converged, the receiver turns to the receiving stage.

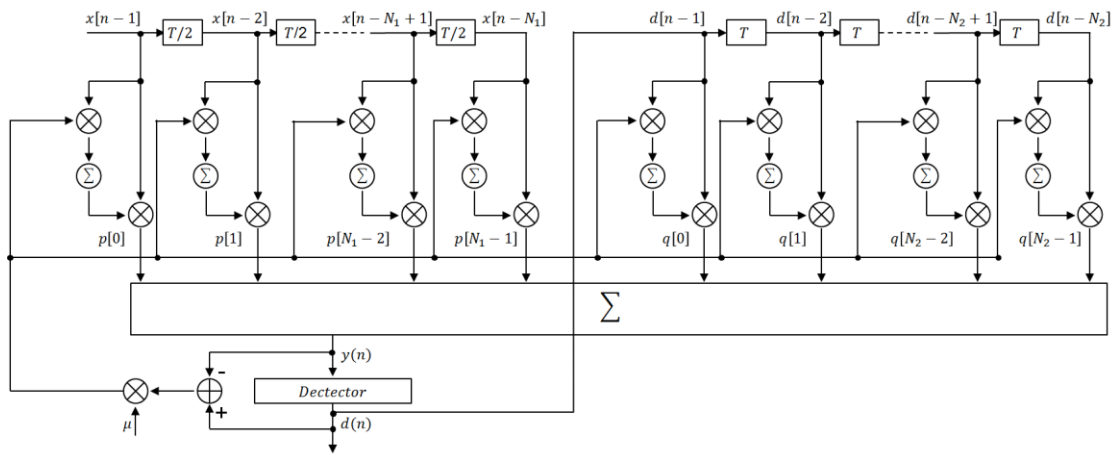


Figure B.2 Structure of half-symbol-spaced DFE [93].

Linear equalizer: feedforward equalizer

However, the feedforward equalizer would amplify the noise and crosstalk. Thus, adding the nonlinear equalizer (e.g. DFE) could help to flatten the channel response. The structure of the FFE + DFE is displayed in figure B.2. As shown in Figure B.2, the fractionally spaced equalizer is utilized, which has half-symbol spaced tap interval. Compared to the symbol-spaced equalizer (i.e. tap interval = symbol duration), fractionally spaced equalizer satisfies the Nyquist requirement, and the performance would not be degraded by the aliasing effect.

To initialize the tap weights, the pre-defined sequence is first utilized. Upon the convergence of the tap coefficients (i.e. MMSE), we can switch to a directed decision where the decision output are used to form the error signal $e[n]$ and fed to the feedback.

The principle of this equalizer could be expressed as below

$$y(n) = \vec{w}(n)^H \cdot \begin{bmatrix} \vec{x}(n) \\ d(n) \end{bmatrix} \quad (B4)$$

$$e(n) = d(n) - y(n) \quad (B5)$$

$$\vec{w}(n+1) = \vec{w}(n) + \mu \begin{bmatrix} \vec{x}(n) \\ d(n) \end{bmatrix} \cdot e^*(n) \quad (B6)$$

$$\vec{x}(n) = [x[n-1], x[n-2], \dots, x[n-N_1]] \quad (B7)$$

$$\vec{d}(n) = [d[n-1], d[n-2], \dots, d[n-N_2]] \quad (B8)$$

$$w(n) = [p[0], p[1], \dots, p[N_1-1], q[0], q[1], \dots, q[N_2-1]] \quad (B9)$$

Where N_1 is the tap length of the FFE and N_2 is the tap length of the DFE.

Bibliography

- [1] P. W. France, *Local Access Network Technologies*, UK: Institution of Engineering and Technology, 2004.
- [2] J. Zheng and H. T. Mouftah, "Media access control for Ethernet passive optical networks: an overview," *IEEE Communication Magazine*, vol. 43, no. 2, pp.145-150, 2005.
- [3] C.-H. Lee, W. V. Sorin, and B. Y. Kim, "Fiber to the home using a PON infrastructure," *IEEE/OSA Journal of Lightwave Technology*, vol. 24, no. 12, pp. 4568-4583, Dec. 2006.
- [4] F. Saliou et al., "WDM PONs based on colorless technology," *Optical Fiber Technology*, 26, pp.126-134, 2015.
- [5] C.-H. Lee and H.-K. Lee, "WDM-PON Architectures and Technologies," *OptoElectronics and Communications Conference (OECC) 2010*, paper 6A2-1, 2010.
- [6] J. Campbell, "Coarse WDM makes waves in metro/access markets," *WDM Solutions*, Nov. 2000.
- [7] B. Whitman, "Fibre Access Deployment Worldwide: Market Drivers, Politics and Technology Choices," *OptoElectronics and Communications Conference (OECC)*, pp. 6–9, 2004.

- [8] K. Akimoto, J. Kani, M. Teshima, and K. Iwatsuki, "Spectrum-sliced 25-GHz spaced, 155 Mbps \times 32 channel WDM access," Conference of Lasers and Electro-Optics (CLEO), Baltimore, MD, 2001, pp. II-556-II-557.
- [9] D. Manandhar, H. H. Kim, C. H. Kim, and J. S. Lee, "25-GHz spaced spectrum-sliced WDM PON using 50-GHz AWGs," IEEE Photonics Technology Letters, vol. 27, no. 13, pp. 1383-1386, Apr. 2015.
- [10] K. Akimoto, J. Kani, M. Teshima, and K. Iwatsuki, "Super-dense WDM transmission of spectrum-sliced incoherent light for wide-area access network," IEEE/OSA Journal of Lightwave Technology, vol. 21, no. 11, pp. 2715-2721, Nov. 2003.
- [11] J. S. Lee, Y. C. Chung, and D. J. DiGiovanni, "Spectrum-sliced fiber amplifier light source for multi-channel WDM applications," IEEE Photonics Technology Letters, vol. 5, no. 12, pp. 1458-1461, 1993.
- [12] D. Jung, S. K. Shin, C. Lee, and Y. C. Chung, "Wavelength-division-multiplexed passive optical network based on spectrum-slicing technique," IEEE Photonics Technology Letters, vol. 10, no. 9, pp. 1334-1336, Sep. 1998.
- [13] Multichannel seeded DWDM applications with single-channel optical interfaces, ITU-T G.698.3, 2012.
- [14] J. S. Lee, Y. C. Chung, T. H. Wood, J. P. Meester, C. H. Joyner, C. A. Burrus, J. Stone, H. M. Presby, and D. J. DiGiovanni, "Spectrum-sliced fiber amplifier light source with a polarization-insensitive electroabsorption modulator," IEEE Photonics Technology Letters, vol. 6, no. 8, pp. 1035-1037, Aug. 1994.

- [15] D. D. Sampson and W. T. Holloway, "Transmission of 622 Mbit/s spectrum-sliced WDM channel over 60 km of nondispersion-shifted fiber at 1550 nm," *Electronics Letter*, vol. 30, no. 21, pp. 1767–1768, 1994.
- [16] G. J. Pendock and D. D. Sampson, "Transmission performance of high bit rate spectrum-sliced WDM systems," *IEEE/OSA Journal of Lightwave Technology*, vol. 14, no. 10, pp. 2141-2148, 1996.
- [17] A. D. McCoy, P. Horak, B. Thomsen, M. Ibsen, and D. J. Richardson, "Noise suppression of incoherent light using a gain-saturated SOA: implications for spectrum sliced WDM systems," *IEEE/OSA Journal of Lightwave Technology*, vol. 23, no.8, pp: 2399-2409, 2005.
- [18] H. H. Lee et al., "Demonstration of performance enhanced pre-spectrum sliced seed light for low-cost seeded WDM-PON architecture," *Optical Fiber Technology*, 19, pp. 126-131, 2015.
- [19] S.-H. Cho, J.-H. Lee, J.-H. Lee, E.-G. Lee, H.-H. Lee, E.-S. Jung, B.-S. Choi, D.-C. Kim, O-K. Kwon, and S. S. Lee, "Demonstrations of RSOA based loop-back WDM-PON with 100 Gb/s (80 x 1.25 Gb/s) capacity employing spectrum sliced incoherent light injection," *OptoElectronics and Communications Conference (OECC)*, pp. 1–3, 2010.
- [20] H. Kim, S. Kim, S. Hwang, and Y. Oh, "Impact of dispersion, PMD, and PDL on the performance of spectrum-sliced incoherent light sources using gain-saturated semiconductor optical amplifiers," *IEEE/OSA Journal of Lightwave Technology*, vol. 24, no. 2, pp: 775-784, 2006.

- [21] A. D. McCoy, B. C. Thomsen, M. Ibsen, and D. J. Richardson, "Filtering effects in a spectrum-sliced WDM system using SOA-based noise reduction," *IEEE Photonics Technology Letters*, vol. 16, no. 2, pp. 680–682, 2004.
- [22] J.-Y. Kim, S.-R. Moon, S.-H. Yoo, and C.-H. Lee, "Mitigation of filtering effect in an injection seeded WDM-PON," *OptoElectronics and Communications Conference (OECC)*, Busan, Korea, Paper 6A2–2, 2012.
- [23] H. H. Lee, M. Y. Park, S. H. Cho, J. H. Lee, J. H. Yu, and B. W. Kim, "Filtering effects in a spectrum-sliced WDM-PON system using a gain-saturated reflected-SOA," *Optical Networking and Communication Conference and Exhibition (OFC)*, paper JWA72, 2009.
- [24] A. J. Keating, W. T. Holloway, and D. D. Sampson, "Feedforward noise reduction of incoherent light for spectrum-sliced transmission at 2.5 Gb/s," *IEEE Photonics Technology Letters*, vol. 7, no. 12, pp: 1513–1515, Dec. 1995.
- [25] Y. S. Jang and Y. C. Chung, "Four-wave mixing of incoherent light in a dispersion shifted fiber using a spectrum-sliced fiber amplifier light source," *IEEE Photonics Technology Letters*, vol. 10, no. 2, pp. 218-220, Feb. 1998.
- [26] S. J. Kim, J. H. Han, J. S. Lee, and C. S. Park, "Intensity noise suppression in spectrum-sliced incoherent light communication systems using a gain-saturated semiconductor optical amplifier," *IEEE Photonics Technology Letters*, vol. 11, pp. 1042–1044, 1999.
- [27] Y. Katagiri, K. Suzuki, and K. Aida, "Intensity stabilisation of spectrum-sliced Gaussian radiation based on amplitude squeezing using semiconductor optical amplifiers with gain saturation," *Electronics Letter*, vol. 35, pp. 1362–1364, 1999.

- [28] M. Zhao, G. Morthier, R. Baets, and J. Dekoster, "Investigation of the intensity noise reduction using a saturated semiconductor optical amplifier in spectrum sliced WDM systems," Conference of Lasers and Electro-Optics (CLEO), pp. 383–384, 2001.
- [29] M. Zhao, G. Morthier, and R. Baets, "Analysis and optimization of intensity noise reduction in spectrum-sliced WDM systems using a saturated semiconductor optical amplifier," IEEE Photonics Technology Letters, vol. 14, pp. 390–392, 2002.
- [30] S. Kim, J. Han, J. Lee, and C. Park, "Suppression of intensity noise in 10Gbit/s spectrum-sliced incoherent light channel using gain-saturated semiconductor optical amplifiers," Electronics Letter, vol. 35, no. 12, pp:1000–1001, June 1999.
- [31] T.-Y. Kim, "Intensity noise suppression of 2.5 Gb/s spectrum-sliced incoherent signal using a gain-saturated SOA injected by broadband light," OptoElectronics and Communications Conference (OECC), pp. 46–47, 2004.
- [32] Q. Hu, C. Yu, P.Y. Kam and H. Kim, "Optimum linewidth of spectrum-sliced incoherent light source using a gain-saturated semiconductor optical amplifier," IEEE/OSA Journal of Lightwave Technology, vol. 33, no.17, pp: 3744-3750, 2015.
- [33] F.Koyama, T.Yamatoya, and K. Iga, "Highly gain-saturated GaInAsP/InP SOA modulator for incoherent spectrum-sliced light source," Conference of Indium Phosphide and Related Materials, Williamsburg, VA, 2000, pp. 439–442.
- [34] A. D. McCoy, P. Horak, B. C. Thomsen, M. Ibsen, and D. J. Richardson, "Improving signal quality in a spectrum-sliced WDM system using SOA-based noise reduction," IEEE Photonics Technology Letters, vol. 17, no. 1, pp. 241–243, Jan. 2005.

- [35] T. Yamatoya and F. Koyama, "Optical preamplifier using optical modulation of amplified spontaneous emission in saturated semiconductor optical amplifier," IEEE/OSA Journal of Lightwave Technology, vol. 22, pp. 1290-1295, 2004.
- [36] J.-Y. Kim et al., "400 Gb/s (40×10 Gb/s) ASE injection seeded WDM-PON based on SOA-REAM," Optical Networking and Communication Conference and Exhibition (OFC), OW4D.4, 2013.
- [37] J.-Y. Kim, S.-R. Moon, Y. S.-Hwa, C.-H. Lee, "800 Gb/s (80×10Gb/s) capacity WDM-PON based on ASE injection seeding," Optics Express, vol. 22, no. 9, pp. 10359-10365, 2014.
- [38] Q. Hu, and H. Kim, "Performance improvement of ultra-narrow spectrum sliced incoherent light using offset filtering," IEEE Photonics Technology Letters, vol. 26, no. 9, pp. 870-873, 2014.
- [39] F. Koyama, "High power superluminescent diodes for multi-wavelength light source," IEEE Lasers and Electro-Optics Society (LEOS) Annual Meeting, San Francisco, CA, pp. 333–334, paper TuY2, 1999.
- [40] M.H. Reeve, A.R. Hunwicks, W. Zhao, S.G. Methley, L.Bickers, and S. Hornung, LED spectral slicing for single-mode local loop applications. Electronics Letters, vol. 24, no.7, pp.380-390, 1988
- [41] S. S. Wagner, T. E. Chapuran, "Broadband high-density WDM transmission using superluminescent diodes," IEEE/OSA Journal of Lightwave Technology, vol. 26, no.11, pp: 696-697, 1990.

- [42] S.-H. Yoo, S.-R. Moon, M. Kye, and C.-H. Lee, "Pulsed-SSIL-seeded DWDM optical system with interferometric noise suppression," *Optics Express*, 22, pp. 8790-8797, 2014.
- [43] Z. Al-Qazwini and H. Kim, "Ultra-narrow spectrum-sliced incoherent light source for 10-Gb/s WDM PON," *IEEE/OSA Journal of Lightwave Technology*, vol. 30, no. 19, pp: 3157–3163, 2012.
- [44] P. A. Humblet and M. Azizoglu, "On the bit error rate of lightwave system with optical amplifiers," *IEEE/OSA Journal of Lightwave Technology*, vol. 9, no. 11, pp. 1576–1582, Nov. 1991.
- [45] J. W. Goodman, "Statistical Optics". New York, NY, USA: Wiley, 1985, pp. 246.
- [46] J.-S. Lee, "Signal-to-noise ratio of spectrum-sliced incoherent light sources including optical modulation effects," *IEEE/OSA Journal of Lightwave Technology*, vol. 14, no. 10, pp. 2197–2201, Oct. 1996.
- [47] S.-R. Moon, S.-H. Yoo, M. Kye, C.-H. Lee, "Feedforward Noise Suppression for SSIL-seeded WDM Systems," *IEEE/OSA Journal of Lightwave Technology*, vol. 34, no. 9, pp. 2297-2303, 2016.
- [48] J. Han, J. W. Ko, J. S. Lee, and S. Y. Shin, "0.1-nm narrow bandwidth transmission of a 2.5-Gb/s spectrum-sliced incoherent light channel using an all-optical bandwidth expansion technique at the receiver," *IEEE Photonics Technology Letter*, vol. 10, pp. 1501–1503, 1998.
- [49] F. Ohman, S. Bischoff, B. Tromborg, and J. Mork, "Noise and regeneration in semiconductor waveguides with saturable gain and absorption," *IEEE Journal of Quantum Electronics*, vol. 40, pp. 245–255, 2004.

- [50] T. Viviero, N. Calabretta, I. Tafur, Monroy, G. Carvalho, Kassar, F. Ohman, K. Yvind, A. Gonzalez-Marcos, and J. Mork, "10 Gb/s-NRZ optical 2R-regeneration in two-section SOA-EA chip," IEEE Lasers and Electro-Optics Society (LEOS) Annual Meeting, pp. 806–807, 2007.
- [51] K. Sato and H.Toba, "Reduction of mode partition noise by using semiconductor optical amplifiers," IEEE Journal of Selected Topics in Quantum Electronics, vol. 7, pp. 328–333, 2001.
- [52] A. Keating and D. Sampson, "Reduction of excess intensity noise in spectrum-sliced incoherent light for WDM applications," IEEE/OSA Journal of Lightwave Technology, vol. 15, no. 1, pp. 53-61, 1997.
- [53] D. Derickson, "Fiber optic test and measurement," Prentice-Hall, 1998, appendix A.
- [54] M. Munroe, J. Cooper, and M. G. Raymer, "Spectral broadening of stochastic light intensity-smoothed by a saturated semiconductor optical amplifier," Journal of Quantum Electronics, vol. 34, pp. 548-551, 1998.
- [55] S. Kaneko, J.-I. Kani, K. Iwatsuki, A. Ohki, M. Sugo, and S. Kamei, "Scalability of spectrum-sliced DWDM transmission and its expansion using forward error correction," IEEE/OSA Journal of Lightwave Technology, vol. 24, no. 3, pp. 1295-1301, 2006.
- [56] W. Mathlouthi, F. Vacondio, and L. A. Rusch, "High-bit-rate dense SS-WDM PON using SOA-based noise reduction with a novel balanced detection," IEEE/OSA Journal of Lightwave Technology, vol. 27, no. 22, pp. 5045-5055, 2009.
- [57] S.-H. Cho, J. H. Lee, J. H. Lee, E.-G. Lee, H.-H. Lee, E.-S. Jung, and S. S. Lee, "Improving transmission performance in EIN limited 2.5-Gb/s spectral slicing

- loopback WDM-PON based on RSOA employing the dispersion management,” International Conference on Optical Internet (COIN), pp. 2159-6395, 2010.
- [58] V. Arya and I. Jacobs, “Optical preamplifier receiver for spectrum-sliced WDM,” IEEE/OSA Journal of Lightwave Technology, vol. 15, pp. 576–583, 1997.
- [59] N. A. Olsson, “Lightwave systems with optical amplifiers,” IEEE/OSA Journal of Lightwave Technology, vol. 14, pp. 955 - 966, 1989.
- [60] S.-R. Moon, S.-H. Yoo, and C.-H. Lee, “Effect of noise distribution in a WDM system seeded by a spectrum-sliced ASE,” IEEE/OSA Journal of Lightwave Technology, vol. 32, no. 12, pp. 2271-2276, 2014.
- [61] M. Shtaif, B. Tromborg, and G. Eisenstein, "Noise spectra of semiconductor optical amplifiers: Relation between semiclassical and quantum descriptions," IEEE Journal of Quantum Electronics, vol. 34, pp. 869-878, 1998.
- [62] J. S. Lee, Y. C. Chung, and C. S. Shim, “Bandwidth optimization of a spectrum-sliced amplifier light source using an angle-tuned Fabry-Perot filter and a double-stage structure,” IEEE Photonics Technology Letters, vol. 6, no. 10, pp. 1197-1199, 1994.
- [63] Q. Hu and H. Kim, “10-Gbps upstream transmission of ultra-narrow spectrum-sliced incoherent light signal,” OptoElectronics and Communications Conference (OECC) 2014, paper TU5A-4, 2014.
- [64] Q. Hu, C. Yu, and H. Kim, “5-Gb/s upstream transmission using an RSOA seeded by ultra-narrow spectrum-sliced incoherent light,” Optical Fiber Technology, vol. 21, pp. 137-140, 2015.

- [65] Y. C. Chung, J. M. Wiesenfeld, G. Raybon, U. Koren, and Y. Twu, "Intermodulation distortion in a multiple-quantum-well semiconductor optical amplifier," *IEEE Photonics Technology Letters*, vol. 3, no. 2, pp. 130–132, Feb. 1991.
- [66] Y. S. Jang, C.-H. Lee, and Y. C. Chung, "Effects of crosstalk in WDM systems using spectrum sliced light sources," *IEEE Photonics Technology Letters*, vol. 11, no. 6, pp. 715–717, 1999.
- [67] H. Kim, H. C. Ji, and C. H. Kim, "Effects of intraband crosstalk on incoherent light using SOA-based noise suppression technique," *IEEE Photonics Technology Letters*, vol. 18, no. 14, pp. 1542–1544, 2006.
- [68] G. Agrawal and N. Anders Olsson, "Self-phase modulation and spectral broadening of optical pulses in semiconductor laser amplifiers," *IEEE J. Quantum Electron.*, vol. 25, no. 11, pp. 2297-2306, 1989.
- [69] Forward error correction for high bit-rate DWDM submarine systems, 2004ITU-T G.975.1, 2004.
- [70] H. D. Kim, S. G. Kang, and C. H. Lee, "A low-cost WDM source with an ASE injected Fabry-Perot semiconductor laser," *IEEE Photonics Technology Letters*, vol. 12, pp. 1067–1069, 2000.
- [71] P. Healey, P. Townsend, C. Ford, L. Johnston, P. Townley, I. Lealman, L. Rivers, S. Perrin, and R. Moore, "Spectral slicing WDM-PON using wavelength-seeded reflective SOAs," *Electronics Letter*, vol. 37, pp. 1181–1182, 2001.
- [72] S.-H. Cho, S. S. Lee, and D. W. Shin, "Transmission performance enhancement for EIN limited 2.5 Gbit/s RSOA-based WDM-PON by using dispersion management," *Electronics Letter*, vol. 46, pp. 636-638, 2010.

- [73] H.-K. Lee, H.-S. Cho, J.-Y. Kim, and C.-H. Lee, "A WDM-PON with an 80 Gb/s capacity based on wavelength-locked Fabry-Perot laser diode," *Optics Express*, vol. 18, pp. 18077-18085, 2010.
- [74] J.-Y. Kim, S.-R. Moon, S.-H. Yoo, and C.-H. Lee, "DWDM-PON at 25 GHz channel spacing based on ASE injection seeding," *Optics Express*, vol. 20, B45-B51, 2012.
- [75] H. S. Kim, D. C. Kim, K. S. Kim, B. S. Choi and O. K. Kwon, "10 Gb/s REAM-SOA for low cost WDM-PON," *Optical Networking and Communication Conference and Exhibition (OFC)*, Paper JThA23, 2011.
- [76] D. C. Kim, H.-S. Kim, K. S. Kim, B.-S. Choi, J.-S. Jeong, and O.-K. Kwon, "10 Gbps SOA-REAM using Monolithic Integration of Planar Buried-Hetero structure SOA with Deep-Ridge Waveguide EA Modulator for Colourless Optical Source in WDM-PON," *European Conference on Optical Communication (ECOC)*, paper Tu.5.LeSaleve.5, 2011.
- [77] Y. Liu, E. Tangdionga, Z. Li, S. Zhang, H. De Waardt, G. Khoe, and H.J.S. Dorren, "Error-free all-optical wavelength conversion at 160 Gb/s using a semiconductor optical amplifier and an optical bandpass filter," *IEEE/OSA Journal of Lightwave Technology*, vol. 24, pp. 230-236, 2006.
- [78] H. Kim, "A dual-detector optical receiver for WDM PON utilizing directly modulated RSOAs and delay interferometers," *IEEE Photonics Technology Letters*, vol. 23, pp. 1733-1735, 2011.
- [79] K. Y. Cho, A. Agata, Y. Takushima, and Y. C. Chung, "Performance of forward-error correction code in 10-Gb/s RSOA-based WDM PON," *IEEE Photonics Technology Letters*, vol. 22, no. 1, pp. 57-59, 2010.

- [80] A. Tychopoulos, O. Koufopavlou, and I. Tomkos, "FEC in optical communications," *IEEE Circuits and Systems Magazine*, pp. 79-86, 2006.
- [81] A. Agata and N. Edagawa, "Performance analysis of forward error correction codes for various degradation factors in optical transmission system," *European Conference on Optical Communication (ECOC)*, Copenhagen, Denmark, 2002.
- [82] K. Y. Cho, A. Agata, Y. Takushima, and Y. C. Chung, "FEC optimization for 10-Gb/sWDM PON implemented by using bandwidth-limited RSOA," *Optical Networking and Communication Conference and Exhibition (OFC)*, San Diego, CA, Paper OMN5, 2009.
- [83] I. B. Djordjevic, S. Sankaranarayanan, and B. Vasic, "Irregular low-density parity-check codes for long-haul optical communications," *IEEE Photonics Technology Letters*, vol. 16, no. 1, pp. 338-340, 2004.
- [84] I. B. Djordjevic, O. Milenkovic, and B. Vasic, "Generalized low-density parity-check codes for optical communication systems," *IEEE/OSA Journal of Lightwave Technology*, vol. 23, no. 5, pp. 1939-1946, 2005.
- [85] I. B. Djordjevic and B. Vasic, "Iteratively decodable codes from orthogonal arrays for optical communication systems," *IEEE Communication Letter*, vol. 9, no. 10, pp. 924-926, 2005.
- [86] S. Sankaranarayanan, I. B. Djordjevic, and B. Vasic, "Iteratively decodable codes on nm flats for WDM high-speed long-haul transmission," *IEEE/OSA Journal of Lightwave Technology*, vol. 23, no. 11, pp. 3696-3701, 2005.

- [87] O. A. Sab and V. Lemaire, "Block turbo code performances for long-haul DWDM optical transmission systems," Optical Networking and Communication Conference and Exhibition (OFC), Baltimore, MD, Paper ThS5, 2000.
- [88] M. Akita, H. Fujita, T. Mizuochi, K. Kubo, H. Yoshida, K. Kuno, and S. Kurahashi, "Third generation FEC employing turbo product code for long-haul DWDM transmission systems," Optical Networking and Communication Conference and Exhibition (OFC), Anaheim, CA, Paper WP2, Mar. 2002.
- [89] T. Mizuochi, K. Kubo, H. Yoshida, H. Fujita, H. Tagami, M. Akita, and K. Motoshima, "Next generation FEC for optical transmission systems," Optical Networking and Communication Conference and Exhibition (OFC), Atlanta, GA, Paper ThN1, 2003.
- [90] T. Mizuochi, K. Ouchi, T. Kobayashi, Y. Miyata, K. Kuno, H. Tagami, K. Kubo, H. Yoshida, M. Akita, and K. Motoshima, "Experimental demonstration of net coding gain of 10.1dB using 12.4 Gb/s block Turbo code with 3-bit soft decision," Optical Networking and Communication Conference and Exhibition (OFC), Atlanta, GA, Paper PD21, Mar. 2003.
- [91] T. Mizuochi, Y. Miyata, T. Kobayashi, K. Ouchi, K. Kuno, K. Kubo, K. Shimizu, H. Tagami, H. Yoshida, H. Fujita, M. Akita, and K. Motoshima, "Forward error correction based on block turbo code with 3-bit soft decision for 10 Gb/s optical communication systems," IEEE Journal of Selected Topics in Quantum Electronics, vol. 10, no. 2, pp. 376–386, Mar.–Apr. 2004.
- [92] H. S. Kim, R. P. H. Haaksman, T. P. Newson, and D. J. Richardson, "Noise properties and phase resolution of interferometer systems interrogated by

- narrowband fiber ASE sources,” *IEEE/OSA Journal of Lightwave Technology*, vol. 17, no. 11, pp. 2327-2335, Nov. 1999.
- [93] J. G. Proakis, *Digital Communications*, 4th edition, New York: McGraw-Hill, 2001.
- [94] T. Mukai, Y. Yamamoto, and T. Kimura, “S/N and error rate performance in AlGaAs semiconductor laser preamplifier and linear repeater systems,” *IEEE Transactions on Microwave Theory and Techniques*, vol. 30, pp. 1548-1554, 1982.
- [95] G. P. Agrawal, *Fiber-Optics Communication Systems*, 4th edition, Wiley, 2010.
- [96] R. Hui and M. O'Sullivan *Fiber optic measurement techniques*, 1st edition, Academic Press, 2008.
- [97] Y. C. Chung, J. M. Wiesenfeld, G. Raybon, U. Koren, and Y. Twu, “Intermodulation distortion in a multiple-quantum-well semiconductor optical amplifier,” *IEEE Photon. Technol. Lett.*, vol. 3, no. 2, pp. 130–132, Feb. 1991.